USE OF NATURAL SWITCHING IN THE BOUNDARY CONTROL OF DC/DC BUCK AND BOOST CONVERTERS

A THESIS SUBMITTED TO

THE GRADUATE SCHOOL OF ENGINEERING AND SCIENCE

OF BILKENT UNIVERSITY

IN PARTIAL FULFILLMENT OF THE REQUIREMENTS FOR

THE DEGREE OF

MASTER OF SCIENCE

IN

ELECTRICAL AND ELECTRONICS ENGINEERING

By

Yunus Emre Koç

August 2021

USE OF NATURAL SWITCHING IN THE BOUNDARY CONTROL OF DC/DC BUCK AND BOOST CONVERTERS
By Yunus Emre Koç
August 2021

We certify that we have read this thesis and that in our opinion it is fully adequate, in scope and in quality, as a thesis for the degree of Master of Science.

Ömer Morgül(Advisor)

Abdullah Atalar

İsmail Uyanık

Approved for the Graduate School of Engineering and Science:

Ezhan Karaşan
Director of the Graduate School

ABSTRACT

USE OF NATURAL SWITCHING IN THE BOUNDARY CONTROL OF DC/DC BUCK AND BOOST CONVERTERS

Yunus Emre Koç
M.S. in Electrical and Electronics Engineering
Advisor: Ömer Morgül
August 2021

DC-DC converters are extensively used in many power electronics applications such as photovoltaic systems, wind energy systems, DC motor drives, mobile devices, electric vehicles, etc. Fundamental performance criteria in these applications include tight line and load regulation, low output voltage ripple, high efficiency and fast response to load uncertainties. Also, the trade-off between high performance and component sizes must be considered. In order to meet these requirements, a boundary control method is developed for the resistive loaded buck and boost DC-DC converters. First, normalized plant models are obtained for both converters. The normalization generalizes the controller design by making it independent of the circuit parameters. Then, natural phase plane trajectories of the systems are derived in the normalized domain. Using the natural trajectories of the converters as switching surfaces, special boundary control laws are defined. Switches in the systems are driven by control inputs generated according to the control laws. Via this boundary control method, the fast dynamic response is provided by utilizing passive components that take up the most space, namely inductor and capacitor, at their theoretical limits. This allows the overall circuit size to be kept small. Finally, the control laws are altered by a small factor so that in steady state, finite and controlled frequency operation and known ripple magnitudes of system states are obtained. In this way, a common problem in boundary control applications called chattering is eliminated. It is shown via simulations that the proposed controllers manage to recover from load and start-up transients by single switching action for both converters.

Keywords: DC-DC buck converter, DC-DC boost converter, boundary control, natural switching surface, normalization, chattering effect.

ÖZET

DA/DA BUCK VE BOOST DÖNÜŞTÜRÜCÜLERİN SINIR KONTROLÜNDE DOĞAL ANAHTARLAMANIN KULLANILMASI

Yunus Emre Koç
Elektrik Elektronik Mühendisliği, Yüksek Lisans
Tez Danışmanı: Ömer Morgül
Ağustos 2021

DA-DA dönüştürücüler, fotovoltaik sistemler, rüzgar enerjisi sistemleri, DA motor sürücüleri, mobil cihazlar, elektrikli araçlar gibi birçok güç elektroniği uygulamasında yaygın olarak kullanılmaktadır. Bu uygulamalardaki temel performans kriterleri arasında düşük hat ve yük regülasyonu, düşük voltaj dalgalanması, yüksek verim ve yük belirsizliklerinde hızlı tepki yer almaktadır. Yüksek performans ve malzeme boyutları arasındaki ödünleşim de dikkate alınmalıdır. Bu gereksinimleri karşılamak amacıyla direnç yüklü buck ve boost tipi DA-DA dönüştürücüler için bir sınır kontrol yöntemi geliştirilmiştir. İlk olarak, her iki dönüştürücü için normalize edilmiş sistem modeli elde edilir. Normalleştirme, kontrolcü tasarımını devre parametrelerinden bağımsız hale getirerek genelleştirir. Sonra sistemlerin normalize edilmiş faz düzlemindeki doğal yörüngeleri türetilir. Dönüştürücülerin doğal yörüngelerinin anahtarlama yüzeyleri olarak kullanıldığı özel sınır kontrol yasaları tanımlanır. Sistemlerdeki anahtarlar, kontrol yasalarına göre üretilen kontrol sinyalleri ile sürülür. Bu sınır kontrol yöntemi ile en fazla yer kaplayan pasif bileşenler, yani bobin ve kapasitör teorik limitlerinde kullanılarak hızlı dinamik tepki sağlanır. Böylece toplam devre boyutunun küçük tutulmasına olanak sağlanır. Son olarak, kontrol yasalarında küçük bir değişiklik yapılarak kararlı durumda sonlu ve kontrollü bir anahtarlama frekansı ile sistem durumlarında belirli dalgalanma değerleri elde edilir. Bu sayede sınır kontrol uygulamalarında sık rastlanan "chattering" problemi ortadan kaldırılmış olur. Önerilen kontrolcülerin her iki dönüştürücü için tek bir anahtarlama ile yük ve başlatma geçici durumlarını atlatabildiği benzetim yöntemi ile gösterilmiştir.

Anahtar sözcükler: DA-DA buck dönüştürücü, DA-DA boost dönüştürücü, sınır kontrol, doğal anahtarlama yüzeyi, normalizasyon, chattering etkisi.

Acknowledgement

I would like to express my sincere gratitude to my advisor, Prof. Ömer Morgül, who guided me with his wisdom and experience throughout this study and did not refrain from his support. It is a great honor for me to have worked with such a successful yet modest academician. I will consider myself indebted to him for the rest of my life for everything he taught me.

I would like to thank the thesis committee members, Prof. Abdullah Atalar and Asst. Prof. İsmail Uyanık, for their kindness to examine this thesis and their valuable contributions.

I am grateful to my beloved wife, Şule İdacı Koç, for her unconditional love, support and understanding. I owe her so much as she always motivates me to move forward in life and gives me strength.

I would like to thank my friends, M. Kerem Kurban, Furkan and Nagehan Kökdoğan, Oğuzhan and Ayşegül Çalıkkasap, who accompanied me along this challenging journey at Bilkent and helped me keep my mood high. Especially, Furkan deserves special thanks for his intellectual contributions to my study.

I would also like to thank my dear mother, Berrin Koç, who was always there for me with her emotional support and prayers.

Finally, I would like to thank The Scientific and Technological Research Council of Turkey (TÜBİTAK) for providing financial support via BİDEB 2210-A Scholarship Program.

Contents

List of Figures

List of Tables

Chapter 1

Introduction

1.1 Motivation and Background

The field of power electronics is of great importance for humans in terms of both the ease of life they offer and the efficient use of energy resources in nature. Its applications ranging from micro-watt battery managements circuits to multi mega-watt power systems can be found in almost all types of electrical equipment nowadays. Switch-mode DC-DC converters are one of the most widely used and researched branches of power electronics. They provide great benefits over linear ones such as higher efficiency, lower weight and size [1]. Their function is to generate a stabilized DC voltage from an unregulated DC source as the name implies. The most fundamental two DC-DC converter topologies are buck converter which converts the input voltage to a lower level at the output and boost converter which steps up the input voltage. Their countless application areas include maximum power point tracking (MPPT) in photovoltaic (PV) power systems [2–4], fuel cell-powered electric vehicles (EV) [5,6], power factor correction of grid-connected systems, wind turbines [7] and mobile devices [8]. Another interesting application of buck converter is speed control of DC motor [9–11] which attracted attention in the literature due to its smooth start advantage.

In recent years, the growing energy demand and depletion rate of fossil fuels led to a great interest in renewable resources like solar energy and wind. Consequently, power electronic circuits like DC-DC converters that are utilized for regulating the outputs of these energy sources gained an increasing emphasis. Therefore, improvements in performance and efficiency of DC-DC converters as well as reduction in circuit size and cost have become one of the major pursues both in the control area and in the power electronics area.

Although DC-DC converters are non-linear systems due to their switching nature, linear control methods like proportional-integral-derivative (PID), voltage mode pulse width modulation (PWM) control and current mode PWM control are commonly used in industrial applications. However, these conventional linear control approaches show unsatisfactory dynamic performance under large-signal operating conditions since they are implemented based on small-signal models. The need for improving the conversion efficiency and dynamic performance of DC-DC converters in today's applications led to a search for control methods alternative to the industry-standard linear controllers. Various methods, including boundary control, sliding mode control and fuzzy logic control, have been presented. An extensive literature review on this topic will be provided in the following chapter.

1.2 Overview of the Thesis

The rest of the thesis is organized as follows:

- In Chapter 2, a literature review on various control methods that are used for DC-DC converters is provided with an emphasis on buck and boost topologies. First, traditional linear controllers are introduced, along with their advantages and drawbacks. Then, recent studies on non-linear control techniques are mentioned. The main difficulties which are still open to investigation in the field and some proposed solutions are discussed.

- In Chapter 3, a boundary control method is proposed for the resistive loaded buck converter. First, the system trajectories on the phase plane are derived. Then, the natural switching surface is obtained and a boundary control law is formulated by using the system trajectories. Under this control law, transient responses and steady state operation of the converter are analyzed in detail. Afterward, computer simulations and theoretical results are compared based on an example design. Finally, simulations are further elaborated for the discussion of possible discrepancies between theory and practical implementations.

- In Chapter 4, a work similar to the one in the previous chapter is carried out to obtain a controller for the resistive loaded boost converter. Analysis and simulations are also adapted to the boost topology.

- In Chapter 5, concluding remarks are made and ideas for future research directions are pointed out.

1.3 Main Contributions

The work presented herein has made the following contributions to the buck and boost converter control literature:

- The natural state-plane trajectories of the resistive loaded buck and boost converters for both switch ON and OFF states are derived in the normalized domain. Note that similar derivations were done in [12] for buck and in [13] for boost converters. However, these studies assumed constant current load and did not include the damping effect caused by load resistance in the analysis.

- For both converters, boundary control laws are proposed, which are expected to provide minimum time transient responses, zero chattering and fixed frequency steady state operation thanks to the use of natural switching surfaces.

- With the help of normalization, a theoretical foundation is established that enables calculation of loading, unloading and start-up transient recovery times along with the peak voltage and current deviations irrespective of the circuit parameters and operating conditions.

- Procedures to be followed to design buck and boost converters that satisfy specific performance requirements under the proposed control laws are given in pseudocode format.

Chapter 2

Problem Definition and Literature Review

2.1 Basic DC-DC Converter Topologies and the Control Problem

Buck and boost converters are the most basic two DC-DC converter topologies. Buck converters are used to generate a DC voltage at the output lower than the voltage of the source. The output voltage can be regulated at the desired reference value by controlling the ON and OFF times of $M1$ and $M2$ transistors shown in Figure 2.1. Note that the transistors are never simultaneously ON or OFF due to the control signals being inverse of each other. Energy is transferred from the source to the load when $M1$ is ON and $M2$ is OFF. Reversing the switch positions disrupts the energy transfer. So, a square waveform occurs at the common node of transistors. Passing it through an LC filter yields a voltage across the load that is ideally DC. Controlling the switch ON and OFF times determines how much energy is transferred to load at each cycle, hence the level of the output voltage.

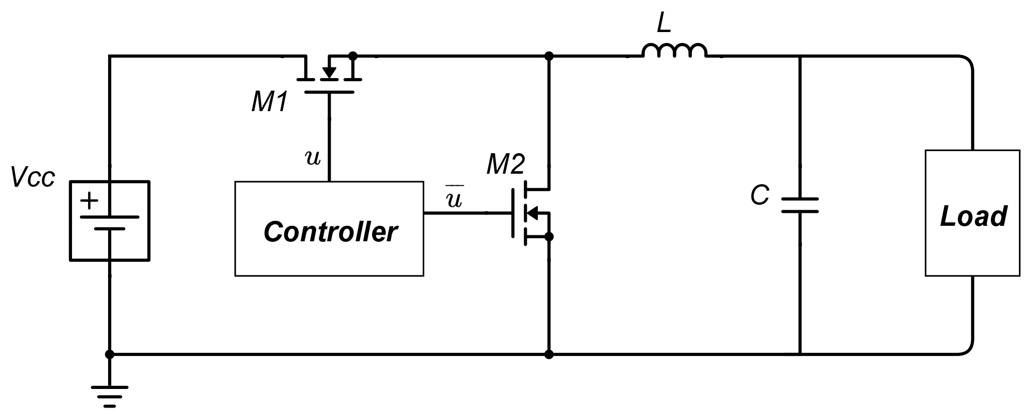

Figure 2.1: DC-DC Buck converter topology

The boost converter has a working principle similar to that of the buck converter. Its function is to convert the voltage of the source to a higher level at the output. When the transistor (M) given in Figure 2.2 is ON, energy builds up in the inductor. When it is OFF, the diode automatically turns ON, and the stored energy is transferred to the load side. The capacitor at the output is charged during this time, causing the voltage to rise above the source voltage. The longer the transistor is kept ON, the more energy is stored and transferred to the load. Therefore, the output voltage can be regulated to the desired value by driving the transistor in a controlled manner.

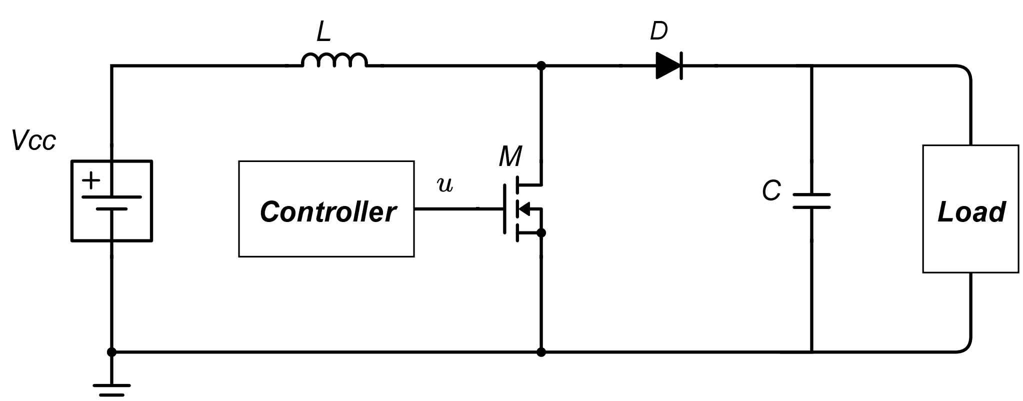

Figure 2.2: DC-DC Boost Converter topology

The main control problem of buck and boost DC-DC converters is to find a control rule for the switching signal that will stabilize the voltage on the load at the desired value for the given input voltage, filter elements and load. Controllers are expected to provide zero steady state error at the output under varying input voltage and loading conditions. Also, fast dynamic response to start-up (when the converter is first energized), input voltage and load transients must be provided so that the output voltage is regulated in a short time. Other controller performance criteria include high efficiency and fixed switching frequency operation. Detailed analysis of control problems will be given in Chapters 3 and 4.

2.2 Proportional-Integral-Derivative Control

Applications of numerous control techniques on DC-DC power converters is widely researched for nearly 50 years. One of the oldest techniques used for regulation of DC power is proportional-integral-derivative (PID) control. It is one of the most preferred control methods in industrial applications mainly because it is easy to comprehend and its implementation is simple. Also, methods like Ziegler-Nichols tuning make it easy to adjust the controller parameters so that optimal closed-loop performance is achieved [14]. In practical applications of DC-DC buck and boost converters, although it is needed for low settling time during transients, the derivative term is often omitted in order to avoid high sensitivity to measurement errors and interference [15] and PI controller is used. Conventional PID controllers are originally designed for controlling linear time-invariant (LTI) systems. However, buck and boost DC-DC converters are non-linear due to the semiconductor switches in the circuit. Moreover, due to the switching nature, they are time-varying systems as well. For these reasons, the PID control method is applied to these converters based on their averaged small-signal models [16]. Linearizing the behaviour of the converter around an operating point limits the optimal performance to a specific condition [17]. Therefore, these controllers exhibit poor dynamic performance in large-signal uncertainties such as load, source or parameter variations [18,19].

2.3 Voltage Mode and Current Mode Control

There are two other conventional control methods frequently used for DC-DC converters aside from PID. These are pulse width modulation (PWM) based methods, namely voltage mode control (VMC) and current mode control (CMC). VMC technique uses only one voltage feedback loop and generates a PWM signal according to the compensated output voltage error. Then, the duty cycle of the switch is controlled by this signal [20]. On the other hand, CMC typically has two feedback loops, one for output voltage and one for inductor current. This method is quite similar to VMC except that the PWM signal is generated using both feedbacks. CMC method is studied for boost and buck DC-DC converters in [21] and [22], respectively. CMC is generally preferred over VMC in practical applications because it provides an over-current protection feature and a greater bandwidth. Even though these two traditional methods show satisfactory performance for most applications, they suffer from the same slow dynamic response problem in large-signal operating conditions as mentioned for PID control because they employ PID controllers as compensators in their feedback loops [23]. Also, achieving a fast dynamic response in the control of boost converter using linear controllers is especially hard because it is a non-minimum phase system having an undesired right-half plane zero in its small-signal transfer function. Crossover frequency must be kept low by compensators for stability, which in return reduces the bandwidth. This problem is thoroughly investigated in [24]. Another problem caused by averaged modelling of DC-DC converters is sub-harmonic oscillations which can lead to chaotic behaviour. This phenomenon is studied for the current mode controlled boost converter in [1].

2.4 Boundary Control

2.4.1 Sliding Mode Control

It is known that DC-DC converters are variable structure systems (VSS) by their nature, meaning their configuration changes during the operation due to the ON-OFF switches. Sliding mode control (SMC) is considered a well-suited non-linear control method for these kinds of systems [25,26]. In recent years, a great amount of academic study has been conducted for the application of SMC techniques to DC-DC converters. This interest of researchers arises from the guaranteed stability of SMC as well as robustness against load and parameter uncertainties. Moreover, SMC has a simpler design procedure compared to other non-linear control methods due to its order reduction property [25]. The work in [27] shows that the SMC provides dynamic responses consistent with the design for a wider range of operating conditions than PWM-based linear control methods by comparing the SMC method with VMC for the buck converter and with CMC for the boost converter. SMC is used in the current feedback loop of CMC for boost converter in [28]. The design is simulated under input voltage, load resistance and reference voltage step changes and shown to be stable despite the non-minimum phase behaviour of boost converter. An application of SMC to buck converter is examined in [4] for photovoltaic (PV) systems. In this study, it is experimentally demonstrated that the insensitivity of SMC to changing input voltage is superior to the PI control.

2.4.2 Curved Switching Surfaces

Classical SMC is a type of boundary control that uses first-order switching surfaces in its control law. Although it provides good large-signal operation performance and stability, its transient response is not optimal [29]. To improve this, a second-order switching surface to be used for boundary control of buck converter is proposed in [30]. As a continuation of this study, a detailed comparison between use of first and second-order switching surfaces is presented in [29]. As a result, it is shown that the employment of curved switching surfaces in boundary control improves the dynamic response of the converter. Conventionally, switching surfaces are defined on a state plane where inductor current and capacitor voltage are selected as system states. In [31], a second-order switching surface is defined on a state-energy plane formed by inductor current and total instantaneous energy stored in the system. Using this surface for control of boost converter provided a fast dynamic response to transients at the expense of implementation complexity. Another application of curved switching surfaces is presented in [32] for buck and boost converters. In this study, switching surfaces that provide theoretically minimum transient recovery time are calculated and stored in a digital memory as lookup tables. In [13], a curved switching surface is defined by using the natural dynamics of a constant current loaded boost converter with the help of a normalization technique. It is shown via a geometrical comparison that this method outperforms first and second-order switching surface boundary control applications in start-up and load transient responses. An approach similar to [13] is adopted in [12] for boundary control of buck converter. Moreover, physical limits to start-up and load transient performances are laid out as functions of system parameters so that benchmarking of any buck converter can be done. Likewise, the work in [13] is further extended in [33] to provide a transient performance benchmarking tool for the boost converter.

2.4.3 Studies on Chattering Reduction

One of the main drawbacks of using SMC for DC-DC converters is the so-called chattering phenomenon [34–36]. It is in the form of high (ideally infinite) frequency switching that may cause adverse effects such as low control accuracy and low efficiency [36]; even burnout may occur due to overheating of components. Another downside of SMC is variable frequency operation which may lead to electromagnetic interference (EMI) problems, as stated in [27, 37]. Therefore, in practical applications of SMC for DC-DC converters, it is necessary to keep the switching frequency constant or at least limited to an upper level.

Hysteresis modulation is the most widely used technique for alleviating the chattering problem in SMC. It defines a hysteresis band around the sliding surface and enables the control of switching frequency by the width of this band [27]. The study in [38] uses hysteresis modulation to obtain a finite switching frequency operation for the buck converter. Similarly, in [39], using hysteresis provides a finite and controlled operating frequency for the start-up transient of the boost converter. The width of the hysteresis band can be varied during operation in order to obtain an almost constant frequency, as presented in [40]. Aside from variable hysteresis width, different control methods that provide fixed-frequency operation for DC-DC converters are compared in [37]. Since the chattering is a result of discontinuous control action (utilization of signum function) in SMC, researchers managed to eliminate chattering by developing a continuous control strategy in [41]. This strategy is successfully applied to buck converter in [42]. As an alternative method for chattering reduction, disturbance observer based SMC is utilized for controlling buck and boost converters in [43] and [44], respectively. The work in [45] achieves a chattering-free operation for both buck and boost converters via an uncertainty and disturbance estimator based SMC method.

2.5 Other Control Methods

In order to improve the dynamic response to large-signal transients, a hybrid controller is proposed in [46] for boost converters. The method is a combination of CMC, which is used for steady state operation and a non-linear, state-plane based control that copes with the load changes while maintaining a maximum voltage deviation. On the other hand, fuzzy logic control methods that can adapt to non-linear behaviours of the DC-DC converters are being developed as an alternative to PI control. The work in [15] presents a comprehensive comparison of fuzzy logic control and PID/PI control for both buck and boost converters. The experimental results for boost converter in this work showed that fuzzy logic control provides a significant performance increase in terms of settling time and overshoot during large-signal transients compared to PID/PI control. However, the results of the two control methods are comparable in the case of the buck converter. Another interesting application of fuzzy logic control for a buck converter is given in [47]. In this work, stability is ensured with zero load regulation under constant power load, which is the case when the main converter supplies a point of load (POL) converter. A digital implementation of adaptive CMC is used for buck converter in [48]. Parameters of PI compensator in the voltage feedback loop is altered adaptively according to changing resistive load with the help of a lookup table. As a result, a faster transient response compared to the classical constant parameter PI controller is achieved. The study in [49] shows that the transient performance of PI-controlled buck converter can be improved by handling load transients via a model predictive control (MPC) method. Alternatively, an artificial neural network (ANN) is used in conjunction with the PID controller for the purpose of improving the transient response of buck converter and providing robustness against circuit parameter uncertainties in works [50] and [51], respectively. The ANN-based control method is also applied to boost converter in [52] for regulating the output voltage in case of input voltage variations encountered in PV arrays.

2.6 The Proposed Method

The control method proposed for buck and boost converters in this study is a boundary control scheme in which natural dynamics of the system are utilized. Behaviours of the converters under resistive load are investigated in the normalized domain to form a switching boundary on the state plane. Then, special control rules are proposed for both converters to generate the switching signals. Designed controllers achieve fast transient response to start-up and load step changes, two fundamental performance measures in DC-DC converters. In Chapters 3 and 4, detailed explanations of the proposed method and its performance evaluation are presented.

Chapter 3

Boundary Control of DC-DC Buck Converter

3.1 Normalization and Modelling

A simplified circuit diagram of the DC-DC buck converter is given in Figure 3.1. Since the two transistors in buck converter topology are only used as on-off switches and are never simultaneously on or off, they are represented by a single pole double throw switch in the diagram. The system is considered lossless for the analysis. In other words, parasitic elements such as DC resistance of the inductor, equivalent series resistance (ESR) of the capacitor and on-state resistances ($R_{ds(on)}$) of transistors are ignored. Also, the inductor and capacitor values are assumed constant. Throughout this chapter, the circuit configuration is called on-state when the switch is in the "ON" position and off-state when it is in the "OFF" position, as shown in the diagram. Modelling is done with the help of a normalization technique [13] to provide generality of analysis and cover all possible combinations of system parameters. The utilization of this technique also facilitates the derivation of natural trajectories of the system.

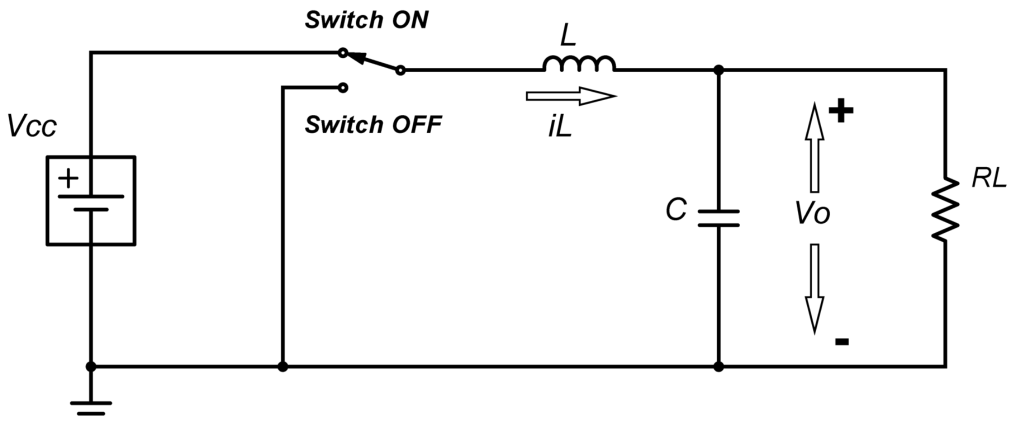

Figure 3.1: Simplified buck converter circuit diagram

The normalization is performed by using

$$V_{ref},\ Z_0 = \sqrt{L/C} \text{ and } f_0 = \frac{1}{2\pi\sqrt{LC}}, \tag{3.1}$$

where V_{ref} is the reference value of the output voltage, Z_0 is the characteristic impedance and f_0 is the natural frequency of L and C values.

Normalized versions of all circuit parameters are denoted by adding "n" to their subscripts. They are defined as

$$v_{on} = \frac{v_o}{V_{ref}},\ V_{ccn} = \frac{V_{cc}}{V_{ref}},\ i_{Ln} = \frac{i_L\ Z_0}{V_{ref}},\ R_{Ln} = \frac{R_L}{Z_0},\ f_n = \frac{f}{f_0},\ t_n = f_0\ t, \tag{3.2}$$

where v_o is the output voltage across the load resistor, V_{cc} is the input voltage, i_L is the inductor current and R_L is the load resistance. The switching frequency, f and the time, t are also normalized.

3.1.1 Switch On-state Model

The control signal which turns the switch on and off is called u. When a resistive loaded buck converter is in on-state ($u = 1$), its dynamics are described by the following two differential equations in the normalized domain:

$$\begin{aligned}\frac{di_{Ln}}{dt_n} &= 2\pi(V_{ccn} - v_{on})\\ \frac{dv_{on}}{dt_n} &= 2\pi(i_{Ln} - \frac{v_{on}}{R_{Ln}}).\end{aligned} \tag{3.3}$$

In order to move the equilibrium of this system to the origin, new coordinates can be defined as

$$\begin{aligned}\hat{i}_{Ln} &= i_{Ln} - \frac{V_{ccn}}{R_{Ln}}\\ \hat{v}_{on} &= v_{on} - V_{ccn}.\end{aligned} \tag{3.4}$$

Using (3.4) in (3.3) gives

$$\begin{aligned}\frac{d\hat{i}_{Ln}}{dt_n} &= -2\pi\hat{v}_{on}\\ \frac{d\hat{v}_{on}}{dt_n} &= 2\pi\left(\hat{i}_{Ln} - \frac{\hat{v}_{on}}{R_{Ln}}\right).\end{aligned} \tag{3.5}$$

Note that (3.5) can be written in matrix form as follows:

$$\begin{bmatrix}\frac{d\hat{i}_{Ln}}{dt_n}\\ \frac{d\hat{v}_{on}}{dt_n}\end{bmatrix} = \underbrace{\begin{bmatrix}0 & -2\pi\\ 2\pi & -\frac{2\pi}{R_{Ln}}\end{bmatrix}}_{A}\begin{bmatrix}\hat{i}_{Ln}\\ \hat{v}_{on}\end{bmatrix}. \tag{3.6}$$

Next, we will derive the analytic solutions of (3.5). The eigenvalues of A can be found as the roots of the following characteristic polynomial:

$$\det(\lambda I - A) = \lambda^2 + \frac{2\pi}{R_{Ln}}\lambda + 4\pi^2. \tag{3.7}$$

The roots of the system can be written as

$$\lambda_{1,2} = -\alpha \pm j\beta, \tag{3.8}$$

where

$$\alpha = \frac{\pi}{R_{Ln}} \text{ and } \beta = \frac{\pi}{R_{\mathrm{Ln}}}\sqrt{4R_{\mathrm{Ln}}^2 - 1}. \tag{3.9}$$

Note that we have

$$\alpha^2 + \beta^2 = 4\pi^2. \tag{3.10}$$

$4R_{Ln}^2 > 1$ is assumed for complex roots. This assumption introduces an upper limit for the load current that can be supplied by the converter for which the theory herein applies.

Next, we evaluate the eigenvectors of A, which are the solutions of the following equation:

$$A\underline{v} = \lambda\underline{v}. \tag{3.11}$$

Since eigenvalues are complex conjugate of each other, so are the eigenvectors. For the eigenvalue $\lambda = -\alpha + j\beta$, the corresponding eigenvector v can be found from (3.11) as follows:

$$v = \begin{pmatrix} 2\pi \\ \alpha \end{pmatrix} + j\begin{pmatrix} 0 \\ -\beta \end{pmatrix}. \tag{3.12}$$

Note that v is one of the infinitely many eigenvectors. For the state matrix A, cv is also an eigenvector $\forall c \in \mathbb{C}$ such that $c \neq 0$.

To find the analytical solutions of (3.6), we first perform a coordinate change by using the following similarity transformation:

$$\begin{bmatrix} \hat{i}_{Ln} \\ \hat{v}_{on} \end{bmatrix} = \begin{bmatrix} 2\pi & 0 \\ \alpha & -\beta \end{bmatrix} \begin{bmatrix} z_1 \\ z_2 \end{bmatrix}, \tag{3.13}$$

where z_1 and z_2 are the new variables. By using (3.13) in (3.6), we obtain:

$$\begin{bmatrix} \dot{z}_1 \\ \dot{z}_2 \end{bmatrix} = \begin{bmatrix} -\alpha & \beta \\ -\beta & -\alpha \end{bmatrix} \begin{bmatrix} z_1 \\ z_2 \end{bmatrix}. \tag{3.14}$$

If we use polar coordinates for z_1 and z_2 such that

$$\begin{aligned} z_1 &= r\cos\theta \\ z_2 &= r\sin\theta, \end{aligned} \tag{3.15}$$

then (3.14) becomes:

$$\begin{aligned}\dot{r} &= -\alpha r \\ \dot{\theta} &= -\beta.\end{aligned} \tag{3.16}$$

Solutions of (3.16) can easily be given as follows:

$$\begin{aligned}r(t) &= r_0\ e^{-\alpha t} \\ \theta(t) &= \theta(0) - \beta t.\end{aligned} \tag{3.17}$$

To find the equations for state trajectories, we need to eliminate time. By using (3.17), we obtain:

$$t = \frac{\theta(0) - \theta}{\beta}. \tag{3.18}$$

By using (3.18) in (3.17), we obtain:

$$r = r_0\ e^{\left(-\frac{\alpha}{\beta}(\theta(0) - \theta)\right)}. \tag{3.19}$$

Taking the square of (3.19) and switching back to z coordinates gives

$$z_1^2 + z_2^2 = \left(z_{10}^2 + z_{20}^2\right) e^{\left(-\frac{2\alpha}{\beta}(\theta(0) - \theta)\right)}, \tag{3.20}$$

where $z_{10} = z_1(0)$, $z_{20} = z_2(0)$ and

$$\begin{aligned}\theta(0) &= \tan^{-1}\frac{z_{20}}{z_{10}} \\ \theta &= \tan^{-1}\frac{z_2}{z_1}.\end{aligned} \tag{3.21}$$

To express the solutions in original variables, we could use (3.13) as follows:

$$\begin{aligned}z_1 &= \frac{\hat{i}_{Ln}}{2\pi} \\ z_2 &= \frac{\alpha z_1 - \hat{v}_{on}}{\beta} = \frac{\alpha}{2\pi\beta}\hat{i}_{Ln} - \frac{1}{\beta}\hat{v}_{on}.\end{aligned} \tag{3.22}$$

Substituting (3.22) into (3.20) results in

$$\frac{\hat{i}_{Ln}^2}{4\pi^2} + \left(\frac{\alpha\hat{i}_{Ln}}{2\pi\beta} - \frac{\hat{v}_{on}}{\beta}\right)^2 = r_0^2\ e^{\left(-\frac{2\alpha}{\beta}(\theta(0) - \theta)\right)}, \tag{3.23}$$

where

$$r_0^2 = \frac{\hat{i}_{Ln}(0)^2}{4\pi^2} + \left(\frac{\alpha \hat{i}_{Ln}(0)}{2\pi\beta} - \frac{\hat{v}_{on}(0)}{\beta}\right)^2, \tag{3.24}$$

$$\theta(0) = \arctan\left(\frac{\left(\frac{\alpha \hat{i}_{Ln}(0)}{2\pi\beta} - \frac{\hat{v}_{on}(0)}{\beta}\right)}{\frac{\hat{i}_{Ln}(0)}{2\pi}}\right), \tag{3.25}$$

$$\theta = \arctan\left(\frac{\left(\frac{\alpha \hat{i}_{Ln}}{2\pi\beta} - \frac{\hat{v}_{on}}{\beta}\right)}{\frac{\hat{i}_{Ln}}{2\pi}}\right), \tag{3.26}$$

which is the solution of (3.5). As a final step, the solution of (3.3) can be obtained by reverting the coordinate change in (3.4) and re-writing (3.23). However, it would only shift the origin of the state plane from $(0, 0)$ to $(i_{Ln} = \frac{V_{ccn}}{R_{Ln}}, v_{on} = V_{ccn})$. Since dynamics are the same, the solution is not repeated.

The family of phase plane trajectories defined by (3.23) is named λ_{on}, which is given below:

$$\lambda_{on}(\hat{v}_{on}, \hat{i}_{Ln}, \hat{v}_{on}(0), \hat{i}_{Ln}(0)) = \frac{\hat{i}_{Ln}^2}{4\pi^2} + \left(\frac{\alpha \hat{i}_{Ln}}{2\pi\beta} - \frac{\hat{v}_{on}}{\beta}\right)^2 - r_0^2 e^{\left(-\frac{2\alpha}{\beta}(\theta(0) - \theta)\right)}. \tag{3.27}$$

Note that for a given initial condition $\hat{i}_{Ln}(0)$ and $\hat{v}_{on}(0)$, the solution trajectory of (3.3) can be found from (3.27) as $\lambda_{on} = 0$, where various coefficients are given in equations (3.9) and (3.24)-(3.26). Notation for dependence on variables will be omitted for convenience unless they are evaluated at a constant. As an example, λ_{on} is used to express $\lambda_{on}(\hat{v}_{on}, \hat{i}_{Ln}, \hat{v}_{on}(0), \hat{i}_{Ln}(0))$. This applies to all other functions that will be defined.

Some of infinitely many trajectories in the λ_{on} family are plotted in Figure 3.2 for randomly selected initial conditions. As shown by the figure, the on-state natural trajectories of buck converter are in the forms of decaying spirals with an equilibrium point at $(i_{Ln} = \frac{V_{ccn}}{R_{Ln}}, v_{on} = V_{ccn})$. One of these trajectories is specially named as σ_{on} and highlighted with green color in the figure. It corresponds to the state trajectory which passes through the target point. Since the solutions of (3.3) are unique, this trajectory is unique as well.

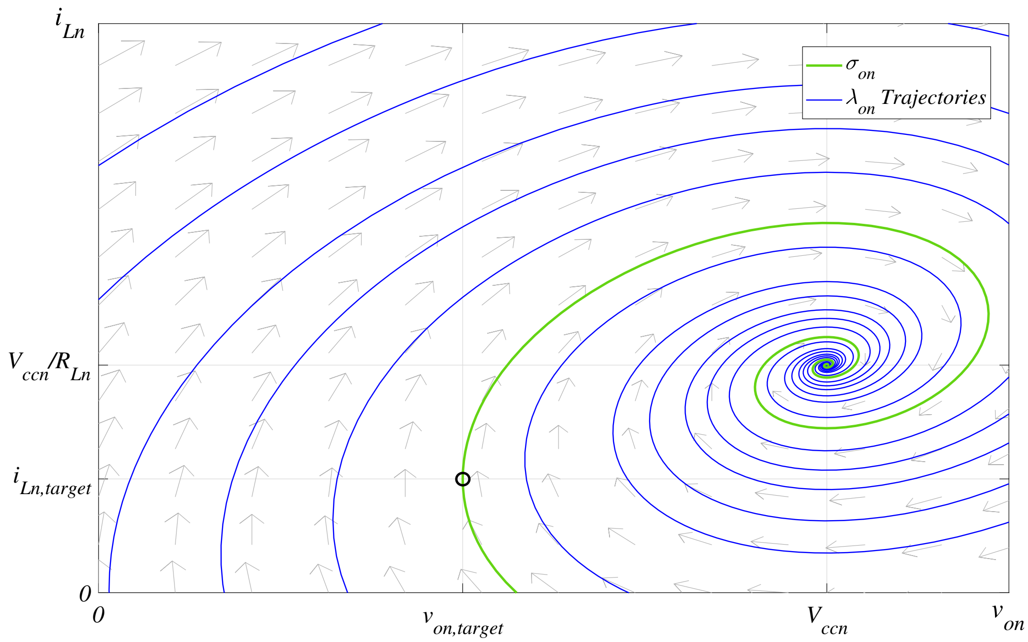

Figure 3.2: Buck converter on-state natural trajectories

3.1.2 Switch Off-state Model

Governing differential equations for a resistive loaded buck converter when it is in off-state ($u = 0$) can be written in the normalized domain as

$$\begin{aligned} \frac{di_{Ln}}{dt_n} &= -2\pi v_{on} \\ \frac{dv_{on}}{dt_n} &= 2\pi(i_{Ln} - \frac{v_{on}}{R_{Ln}}). \end{aligned} \tag{3.28}$$

It can be seen that the equilibrium of (3.28) is already at the origin. Also, the equations are exactly the same as the shifted versions of on-state equations given in (3.5). Therefore, (3.23) can be used as off-state solutions of buck converter by substituting $\hat{i}_{Ln}$ with i_{Ln} and $\hat{v}_{on}$ with v_{on}. Omitting intermediate steps, the solution is directly obtained as

$$\frac{i_{Ln}^2}{4\pi^2} + \left(\frac{\alpha i_{Ln}}{2\pi\beta} - \frac{v_{on}}{\beta}\right)^2 = r_0^2\, e^{\left(-\frac{2\alpha}{\beta}(\theta(0) - \theta)\right)}, \tag{3.29}$$

where

$$r_0^2 = \frac{i_{Ln}(0)^2}{4\pi^2} + \left(\frac{\alpha i_{Ln}(0)}{2\pi\beta} - \frac{v_{on}(0)}{\beta}\right)^2, \tag{3.30}$$

$$\theta(0) = \arctan\left(\frac{\left(\frac{\alpha i_{Ln}(0)}{2\pi\beta} - \frac{v_{on}(0)}{\beta}\right)}{\frac{i_{Ln}(0)}{2\pi}}\right), \tag{3.31}$$

$$\theta = \arctan\left(\frac{\left(\frac{\alpha i_{Ln}}{2\pi\beta} - \frac{v_{on}}{\beta}\right)}{\frac{i_{Ln}}{2\pi}}\right), \tag{3.32}$$

Equation (3.29) describes the family of buck converter off-state natural trajectories which are called λ_{off} and given below:

$$\lambda_{off}(v_{on}, i_{Ln}, v_{on}(0), i_{Ln}(0)) = \frac{i_{Ln}^2}{4\pi^2} + \left(\frac{\alpha i_{Ln}}{2\pi\beta} - \frac{v_{on}}{\beta}\right)^2 - r_0^2\, e^{\left(-\frac{2\alpha}{\beta}(\theta(0) - \theta)\right)}. \tag{3.33}$$

To find a solution trajectory of (3.28) for a given initial condition $i_{Ln}(0)$ and $v_{on}(0)$, the equation (3.33) can be used as $\lambda_{off} = 0$, where related coefficients are given in equations (3.9) and (3.30)-(3.32).

As in the on-state case, some randomly selected λ_{off} trajectories are illustrated in Figure 3.3. Solutions are in spiral form with the equilibrium point located at $(i_{Ln} = 0, v_{on} = 0)$. The trajectory passing through the target point is specially named σ_{off} and featured by red color in the figure. It is worth noting that the solutions of (3.28) are unique; consequently, so is this trajectory.

3.2 Control Law Definition

There are two main objectives to be achieved by designing a controller for the buck converter. The first one is to keep the converter's output voltage in regulation, meaning $v_o = V_{ref}$. The second is to maintain the output power equal to the input power ($P_{out} = P_{in}$) for reaching maximum theoretical efficiency. Using these conditions, a target operating point on the normalized state plane is determined.

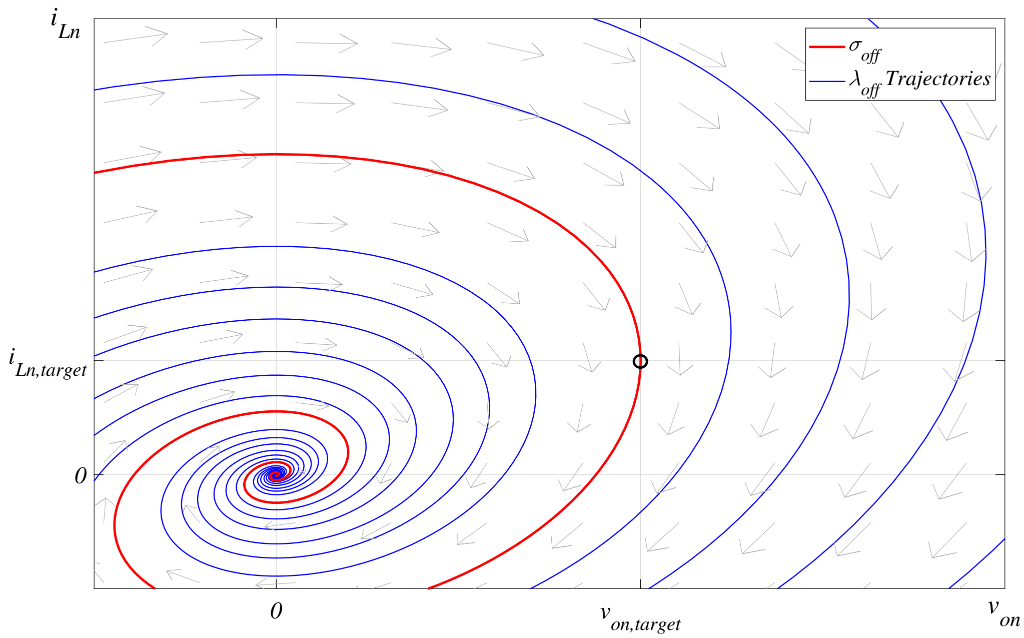

Figure 3.3: Buck converter off-state natural trajectories

Since at the target we have $v_0 = V_{ref}$, by using (3.2), we obtain its normalized value as:

$$v_{on} = 1. \tag{3.34}$$

In steady state, the second condition ($P_{out} = P_{in}$) yields

$$\frac{v_o^2}{R_L} = V_{cc}\, i_L \frac{v_o}{V_{cc}}. \tag{3.35}$$

If we make the cancellations in (3.35) and then normalize it by using (3.2), we get the i_{Ln} at the target as:

$$i_{Ln} = \frac{v_{on}}{R_{Ln}}. \tag{3.36}$$

So, the target operating point can be written as:

$$\begin{aligned} v_{on,target} &= 1 \\ i_{Ln,target} &= \frac{1}{R_{Ln}}. \end{aligned} \tag{3.37}$$

In the design of the control law, the on-state and off-state natural trajectories that cross through the target operating point are used. These two particular trajectories are named on-state switching curve σ_{on} and off-state switching curve σ_{off} which are shown in Figures 3.2 and 3.3, respectively.

The equation for σ_{on} can be obtained as follows:

$$\sigma_{on}(\hat{v}_{on}, \hat{i}_{Ln}) = \lambda_{on}\left(\hat{v}_{on}, \hat{i}_{Ln}, \hat{v}_{on}(0) = 1 - V_{ccn}, \hat{i}_{Ln}(0) = \frac{1 - V_{ccn}}{R_{Ln}}\right), \tag{3.38}$$

where λ_{on} is given by (3.27). Note that (3.37) is substituted into λ_{on} as an initial condition.

Similarly, the σ_{off} equation can be found as:

$$\sigma_{off}(v_{on}, i_{Ln}) = \lambda_{off}\left(v_{on}, i_{Ln}, v_{on}(0) = 1, i_{Ln}(0) = \frac{1}{R_{Ln}}\right), \tag{3.39}$$

where λ_{off} is given by (3.33) and (3.37) is used as an initial condition.

The controller must drive the states of the system from any initial point to the target operating point on the state plane. For this purpose, a control law is defined as follows:

$$\begin{aligned} &\text{when} \quad i_{Ln} < \frac{v_{on}}{R_{Ln}}, \quad \text{apply} \quad u = \begin{cases} 1 & \text{if } \sigma_{on} > 0 \\ 0 & \text{otherwise} \end{cases} \\ &\text{when} \quad i_{Ln} > \frac{v_{on}}{R_{Ln}}, \quad \text{apply} \quad u = \begin{cases} 0 & \text{if } \sigma_{off} > 0 \\ 1 & \text{otherwise.} \end{cases} \end{aligned} \tag{3.40}$$

If the states are above $i_{Ln} = \frac{v_{on}}{R_{Ln}}$ line at any time instant, the σ_{off} equation is evaluated for the current values of the states. According to the control law, the switch is turned off if the states are above σ_{off} and turned on if they are below. The same is applied for the σ_{on} curve when the states are below $i_{Ln} = \frac{v_{on}}{R_{Ln}}$ line.

Figure 3.4 shows the resultant phase plane when the control law (3.40) is applied to a buck converter. Note that the red curve in Figure 3.4 corresponds to the part of the red curve in Figure 3.3 for $i_{Ln} > i_{Ln,target}$, and likewise, the green curve in Figure 3.4 corresponds to the part of the green curve in Figure 3.2 for $i_{Ln} < i_{Ln,target}$. These two curves combined form a natural switching curve for the

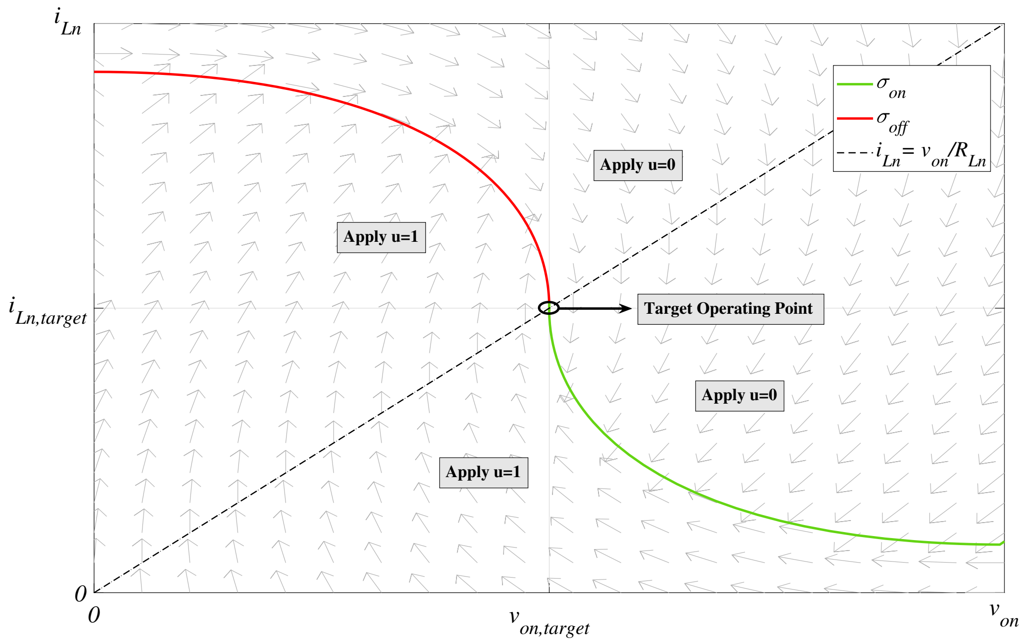

Figure 3.4: Buck converter control law operation

system. The gray arrows in Figure 3.4 correspond to the vector field evaluated by using (3.3) for on-state ($u = 1$) and by using (3.28) for off-state ($u = 0$). They indicate the direction of the solutions at the location of their tails. Since they do not carry meaning about the solutions at the location of their heads, the length of these arrows can be considered infinitesimal. As can be seen from Figure 3.4, when an initial condition is below the switching curve, the control input is $u = 1$, i.e., the switch is in on position and when the initial condition is above the switching curve, the control input is $u = 0$, i.e., the switch is in off position. The vector field in Figure 3.4 shows that independent of the initial condition, the switching control rule in (3.40) will force the solutions to hit the switching curve in finite time. When the solutions hit the switching curve, the switch is turned on ($u = 1$) on the green curve and off ($u = 0$) on the red curve. This way, the solutions will converge to the target operating point by using only one switching action. Since we have analytic formulas for the trajectories, this control law can be given analytically as well. Also, note that the target operating point is not an equilibrium point of the system. Hence it is not possible for the trajectories to stay at this point unless a special control action is employed. One possibility is to use on-off switching with infinite frequency, which is not practical. The other option is to allow a small variation around this point and apply a finite frequency switching control law. This will be explained in Section 3.4

3.3 Transient Analysis

3.3.1 Start-Up Transients

Phase plane trajectories of a resistive loaded buck converter during its start-up when controlled by the control law (3.40) are shown in Figure 3.5. Initially, at time $t = 0$, the operating point starts from $(0, 0)$ and follows the on-state trajectory $\lambda_{on,startup}$ crossing there until it hits the off-state trajectory passing from the target operating point, σ_{off}. At the intersection, normalized inductor current reaches its peak value, called $i_{Ln,peak}$. Then, the switch turns off, and the operating point reaches the target by following the σ_{off} trajectory. Thus, the converter completes the start-up with zero overshoot in the output voltage.

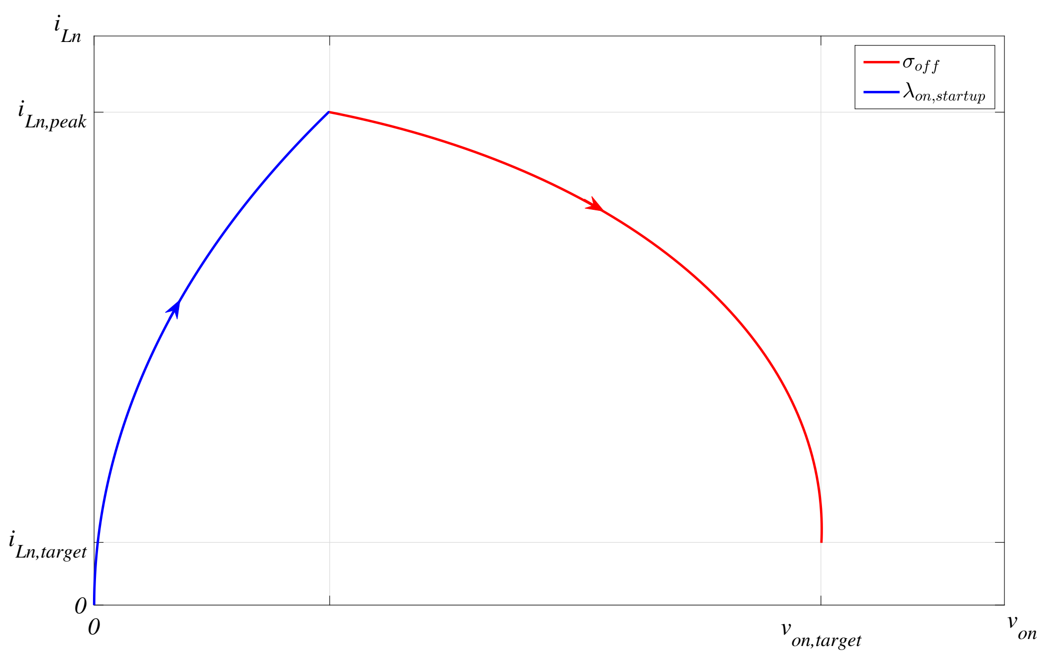

Figure 3.5: Buck converter start-up trajectories

The normalized peak inductor current, $i_{Ln,peak}$ can be calculated by solving the on-state equation (λ_{on}) and the off-state equation (σ_{off}) simultaneously as follows:

$$\underbrace{\lambda_{on}\left(\hat{v}_{on}(0) = -V_{ccn}, \hat{i}_{Ln}(0) = -\frac{V_{ccn}}{R_{Ln}}\right)}_{\lambda_{on,startup}} = \sigma_{off}, \tag{3.41}$$

where λ_{on} and σ_{off} are given by (3.27) and (3.39), respectively. Note that ($v_{on} = 0, i_{Ln} = 0$) is used in (3.5) to get the initial condition for λ_{on}.

Once $i_{Ln,peak}$ value is known, normalized time for which the switch is kept on during start-up can be calculated by using the inductor current equation in (3.3). If we isolate the dt term in this equation and integrate the rest from $i_{Ln} = 0$ to $i_{Ln} = i_{Ln,peak}$, we get the switch on time as follows:

$$t_{n,startup(on)} = \int_{0}^{i_{Ln,peak}} \frac{1}{2\pi(V_{ccn} - v_{on})}\, di_{Ln}. \tag{3.42}$$

Similarly, the inductor current equation in (3.28) can be manipulated so that the dt term is left alone. Then, it can be integrated between $i_{Ln} = i_{Ln,target}$ and $i_{Ln} = i_{Ln,peak}$ in order to get the switch off time during start-up transient as follows:

$$t_{n,startup(off)} = \int_{i_{Ln,target}}^{i_{Ln,peak}} \frac{1}{2\pi v_{on}}\, di_{Ln}. \tag{3.43}$$

For evaluating the integrals in (3.42) and (3.43), the relation between v_{on} and i_{Ln} given in equations (3.23) and (3.29) are used, respectively. Note that, initial conditions must be the ones in (3.41). First, the range of i_{Ln} values defined by the integration limits is divided into small parts. Then, v_{on} values satisfying the corresponding equation for each i_{Ln} value in these ranges are calculated. Using these v_{on} values, integrals are evaluated by a numerical integration method called the trapezoidal rule.

Finally, the total normalized start-up time can be obtained by summing switch on and off times as given below:

$$t_{n,startup} = t_{n,startup(on)} + t_{n,startup(off)}. \tag{3.44}$$

3.3.2 Resistive Load Transients

There are two types of load transients for DC/DC converters, namely loading and unloading. A loading transient is an increase in load of the converter in terms of power, meaning a decrease in load resistance value. An unloading transient is the opposite. Two main concerns about both of these transients are how much the output voltage deviates from its reference value and how much time it takes for the converter to recover.

The response of the buck converter to a loading transient is illustrated in Figure 3.6. When load increases, the controller first determines the new target operating point satisfying (3.37). Then, it checks the states at that instant and according to the control law, turns the switch on. The operating point starts from $(v_{on,target}, i_{Ln,initial})$ and follows the on-state trajectory until it hits the off-state trajectory that passes from the new target. Afterward, the switch is turned off, and states are driven to the new target operating point. Thus the load transient is recovered from with only one switching action. Note that, $i_{Ln,initial}$ is the normalized inductor current at the target operating point before the occurrence of the load transient. Normalized load resistance value before the transient is called $R_{Ln,initial}$. Equating the expressions of on-state and off-state trajectories that are followed during loading transient gives the intersection where the inductor current is at its maximum, $i_{Ln,max}$. To find the latter, first let us define the trajectory corresponding to the loading effect, $\lambda_{on,loading}$, as follows:

$$\lambda_{on,loading}(\hat{v}_{on}, \hat{i}_{Ln}) = \lambda_{on}\left(\hat{v}_{on}, \hat{i}_{Ln}, \hat{v}_{on}(0) = 1 - V_{ccn}, \hat{i}_{Ln}(0) = \frac{1 - V_{ccn}}{R_{Ln,initial}}\right), \tag{3.45}$$

where λ_{on} is given by (3.27). Then, $i_{Ln,max}$ can be found by solving the following equation:

$$\lambda_{on,loading} = \sigma_{off}, \tag{3.46}$$

where σ_{off} is given by (3.39).

Minimum output voltage during loading event can be found as:

$$v_{on,min} = \min_{\lambda_{on,loading}=0} v_{on} \quad s.t. \quad i_{Ln,initial} < i_{Ln} < i_{Ln,max}, \tag{3.47}$$

where

$$i_{Ln,initial} = \frac{1}{R_{Ln,initial}}. \tag{3.48}$$

Since we have the analytic expression for $\lambda_{on,loading}$ defined in (3.45), we can find the minimum value of v_{on} in (3.47) by using the bisection search method for the given i_{Ln} range. Note that, $\lambda_{on,loading} = 0$ equation must be solved numerically at each iteration of the search algorithm.

Then, the output voltage drop due to loading can be found as follows:

$$\Delta v_{on,loading} = 1 - v_{on,min}. \tag{3.49}$$

The normalized time for which the switch is on during loading transient can be calculated by using (3.3) as follows:

$$t_{n,loading(on)} = \int_{i_{Ln,initial}}^{i_{Ln,max}} \frac{1}{2\pi(V_{ccn} - v_{on})}\, di_{Ln}, \tag{3.50}$$

which is derived as described for (3.42). Likewise, the switch off time during loading event can be calculated by taking the integration in (3.43) from $i_{Ln} = i_{Ln,target}$ to $i_{Ln} = i_{Ln,max}$ as follows:

$$t_{n,loading(off)} = \int_{i_{Ln,target}}^{i_{Ln,max}} \frac{1}{2\pi v_{on}}\, di_{Ln}. \tag{3.51}$$

Note that the dependence of v_{on} on i_{Ln} in (3.50) and (3.51) are established by $\lambda_{on,loading} = 0$, where $\lambda_{on,loading}$ is given in (3.45) and $\sigma_{off} = 0$, where σ_{off} is given in (3.39), respectively. Analytical expressions can be given in (3.50) and (3.51). However, they will not be integrable due to the highly non-linear nature of the equations. Therefore, the integrals must be evaluated numerically. This can be done by using the trapezoidal rule as described for the start-up transient case.

Then, the normalized recovery time of the loading transient can be written as the sum of the switch on and off times as follows:

$$t_{n,loading} = t_{n,loading(on)} + t_{n,loading(off)}. \tag{3.52}$$

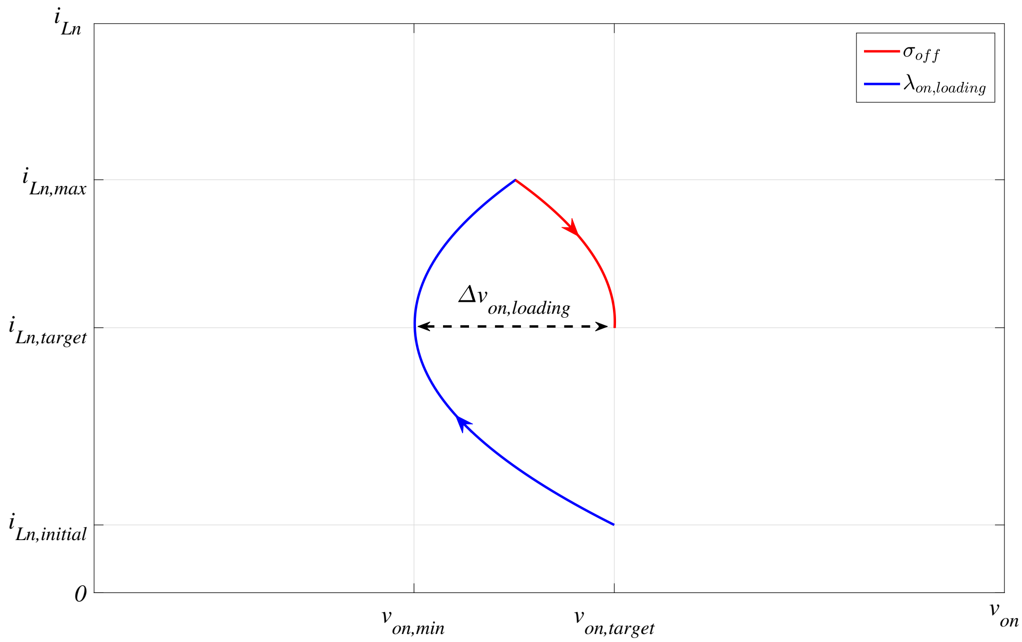

Figure 3.6: Buck converter loading trajectories

Figure 3.7 shows the response of the converter to the unloading event. Similar behaviour is observed as in the loading case. Only this time, the switch is kept off initially when the sudden load decrease occurs. Then, it is on until the new target operating point is reached. The off-state trajectory during unloading is called $\lambda_{off,unloading}$. It can be described as

$$\lambda_{off,unloading}(v_{on}, i_{Ln}) = \lambda_{off}\left(v_{on}, i_{Ln}, v_{on}(0) = 1,\ i_{Ln}(0) = \frac{1}{R_{Ln,initial}}\right), \quad (3.53)$$

where λ_{off} is given by (3.33). Then the minimum normalized inductor current value during unloading, called $i_{Ln,min}$ can be found by equating $\lambda_{off,unloading}$ to the σ_{on} as:

$$\lambda_{off,unloading} = \sigma_{on}, \quad (3.54)$$

where σ_{on} is given in (3.38).

Using the $i_{Ln,min}$ value, maximum output voltage caused by unloading transient can be found as:

$$v_{on,max} = \max_{\lambda_{off,unloading}=0} v_{on} \quad s.t. \quad i_{Ln,min} < i_{Ln} < i_{Ln,initial}, \quad (3.55)$$

where

$$i_{Ln,initial} = \frac{1}{R_{Ln,initial}}.$$

The $v_{on,max}$ in (3.55) can be found via the bisection search method in a similar manner to the loading case. During this search, $\lambda_{off,unloading} = 0$ equation must be solved by a numerical method. Then the $v_{on,max}$ value can be used to obtain the amount of voltage rise due to unloading in the normalized domain as follows:

$$\Delta v_{on,unloading} = v_{on,max} - 1. \tag{3.56}$$

Normalized times spent while the switch is on and off during unloading transient can be calculated by the following two equations:

$$t_{n,unloading(on)} = \int_{i_{Ln,min}}^{i_{Ln,target}} \frac{1}{2\pi(V_{ccn} - v_{on})} \, di_{Ln} \tag{3.57}$$

$$t_{n,unloading(off)} = \int_{i_{Ln,min}}^{i_{Ln,initial}} \frac{1}{2\pi v_{on}} \, di_{Ln}, \tag{3.58}$$

which have the same integrals in (3.42) and (3.43). Their derivations are explained in the case of start-up transients. The integral limits are changed according to unloading trajectories. Also, $\sigma_{on} = 0$, where σ_{on} is given in (3.38) and $\lambda_{off,unloading} = 0$, where $\lambda_{off,unloading}$ is given in (3.53) must be utilized for numerically evaluating the integrals in (3.57) and (3.58), respectively.

After calculating the switch on and off times, the normalized recovery time of the unloading transient can be written as sum of the two as follows:

$$t_{n,unloading} = t_{n,unloading(on)} + t_{n,unloading(off)}. \tag{3.59}$$

3.4 Steady State Analysis

The control law defined previously with σ_{on} and σ_{off} that cross right through the target operating point results in a steady state operation with theoretically

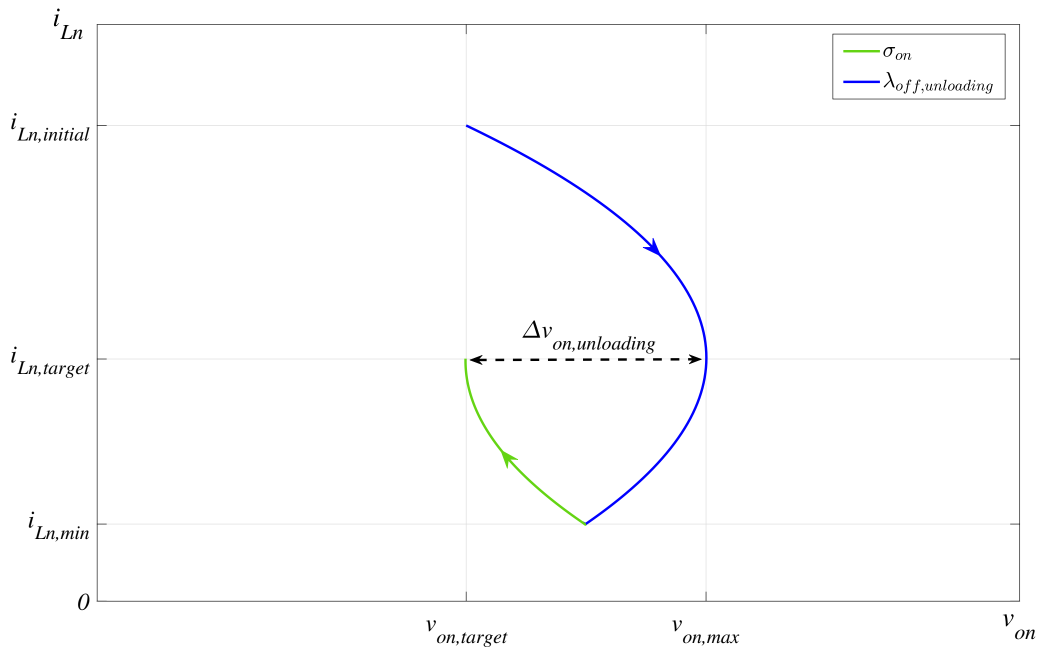

Figure 3.7: Buck converter unloading trajectories

infinite switching frequency. Since this is not practically possible, the switching frequency would be uncertain and as high as physical limitations of components and bandwidth of the controller permit, leading to adverse effects like overheating and electromagnetic interference. In order to avoid this, an operation with controllable and finite frequency should be provided by the controller. For this purpose, a modification in the control law is made, which is a small increment of Δr^2 in the initial radii of spiral equations, σ_{on} and σ_{off}. By this modification, $\sigma_{on\Delta}$ and $\sigma_{off\Delta}$ are defined as

$$\sigma_{on\Delta}(\hat{v}_{on}, \hat{i}_{Ln}, \Delta r) = \sigma_{on}\left(r_0^2 = \frac{(1-V_{ccn})^2}{4\pi^2 R_{Ln}^2} + \left(\frac{\alpha(1-V_{ccn})}{2\pi\beta R_{Ln}} - \frac{1-V_{ccn}}{\beta}\right)^2 + \Delta r^2\right) \tag{3.60}$$

$$\sigma_{off\Delta}(v_{on}, i_{Ln}, \Delta r) = \sigma_{off}\left(r_0^2 = \frac{1}{4\pi^2 R_{Ln}^2} + \left(\frac{\alpha}{2\pi\beta R_{Ln}} - \frac{1}{\beta}\right)^2 + \Delta r^2\right), \tag{3.61}$$

where σ_{on} is given by (3.38) and σ_{off} is given by (3.39).

When $\sigma_{on\Delta}$ and $\sigma_{off\Delta}$ are used in the control law, the resultant steady state operation is as shown in Figure 3.8. When the switch is off in steady state, the

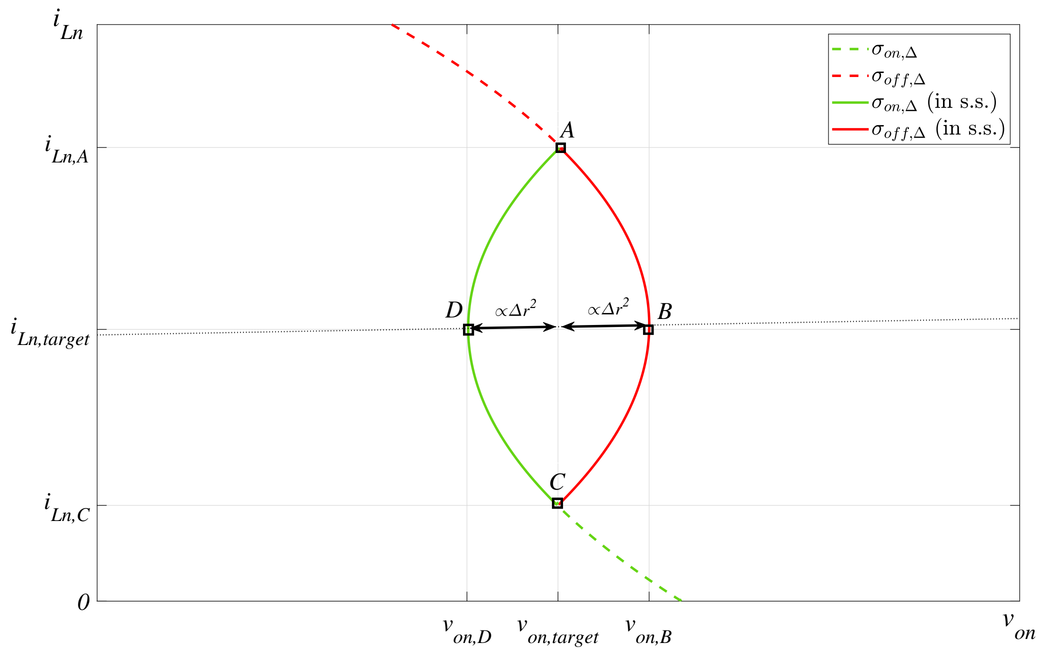

Figure 3.8: Buck converter steady state trajectories

operating point goes from point A to C. At point C, the switch is turned on, and the system goes back to A, completing one full switching cycle. The points A, B, C, D, as well as the switching frequency and peak-to-peak ripples are determined by the amount of Δr^2 added. For fixed L and C filter element values, increasing Δr^2 results in an increase in steady state ripples and a decrease in switching frequency. Meaning a controlled switching frequency operation comes with a cost of an AC ripple around the target operating point for both states.

3.4.1 Ripple Calculations

The steady state peak-to-peak ripples of output voltage and inductor current in normalized domain are called $\Delta v_{on,ss}$ and$\Delta i_{Ln,ss}$, respectively. In order to calculate the ripples, points A, B, C and D that are shown in Figure 3.8 are used. The normalized inductor currents at point A, called $i_{Ln,A}$ and at point C, called $i_{Ln,C}$ can be found by solving the following two equations, respectively:

$$\sigma_{on\Delta} = \sigma_{off\Delta} \quad s.t. \quad i_{Ln} > i_{Ln,target} \tag{3.62}$$

$$\sigma_{on\Delta} = \sigma_{off\Delta} \quad s.t. \quad i_{Ln} < i_{Ln,target}, \tag{3.63}$$

where σ_{on} is given by (3.38) and σ_{off} is given by (3.39). The equations can be solved numerically by using an iterative method such as Newton-Raphson. Solutions can be searched around $v_{on} \approx 1$ for fast convergence.

Then, $i_{Ln,A}$ and $i_{Ln,C}$ can be used to obtain the normalized output voltage at points B and D as follows:

$$v_{on,B} = \max_{\sigma_{off\Delta}=0} v_{on} \quad s.t. \quad i_{Ln,C} < i_{Ln} < i_{Ln,A} \tag{3.64}$$

$$v_{on,D} = \min_{\sigma_{on\Delta}=0} v_{on} \quad s.t. \quad i_{Ln,C} < i_{Ln} < i_{Ln,A}, \tag{3.65}$$

where $\sigma_{on\Delta}$ and $\sigma_{off\Delta}$ are given by (3.60) and (3.61), respectively. Solutions of these equations can be searched in the given i_{Ln} ranges via the bisection search method until the error is below an acceptable tolerance. During this search, $\sigma_{on\Delta} = 0$ and $\sigma_{off\Delta} = 0$ equations must be solved numerically.

After calculating the states at points A, B, C and D, normalized peak-to-peak ripples can be found as follows:

$$\Delta i_{Ln} = i_{Ln,A} - i_{Ln,C} \tag{3.66}$$

$$\Delta v_{on} = v_{on,B} - v_{on,D}. \tag{3.67}$$

3.4.2 Frequency Calculation

The operating point of the buck converter in steady state is cycled between points A and C in Figure 3.8, as mentioned before. When it goes from A to C, the switch is turned off for a normalized time, called $t_{n,ss(on)}$. The system trajectory during this time is described by $\sigma_{on\Delta}$. Likewise, the path from C to A is covered in $t_{n,ss(off)}$. The trajectory that is followed is given by $\sigma_{off\Delta}$. The normalized on-state and off-state times for one switching cycle in steady state are calculated as follows:

$$t_{n,ss(on)} = \int_{i_{Ln,A}}^{i_{Ln,C}} \frac{1}{2\pi(V_{ccn} - v_{on})}\, di_{Ln} \tag{3.68}$$

$$t_{n,ss(off)} = \int_{i_{Ln,A}}^{i_{Ln,C}} \frac{1}{2\pi v_{on}}\, di_{Ln}, \tag{3.69}$$

which are derived from the inductor current differential equations in (3.3) and (3.28). As explained before, the dt terms in these equations are isolated first. Then both sides of the equations are integrated. The integral limits are determined according to the corresponding trajectories. When evaluating the integral in (3.68), It must be considered that v_{on} depends on i_{Ln} by $\sigma_{on\Delta} = 0$ equation, where $\sigma_{on\Delta}$ is as in (3.60). Likewise, for the evaluation of the integral in (3.69), v_{on} depends on i_{Ln} by $\sigma_{off\Delta} = 0$ equation, where $\sigma_{off\Delta}$ is given in (3.61).

By using the switch on and off times in a single cycle, the normalized steady state switching frequency, called f_n can be obtained as follows:

$$f_n = \frac{1}{t_{n,ss(on)} + t_{n,ss(off)}}. \tag{3.70}$$

Note that f_n depends on the Δr^2 term employed in the equations of $\sigma_{on\Delta}$ and $\sigma_{off\Delta}$. So, the operating frequency can be adjusted by changing this term. However, there is an important trade-off to be considered in the selection of Δr^2. Selecting a smaller Δr^2 brings the points A, B, C, D closer to each other, resulting in the steady state ripples (Δi_{Ln} and Δv_{on}) being lower for fixed inductor and capacitor values. This is desired since the output of the converter must be purely DC in an ideal case. If we look from another point of view, small Δr^2 enables the use of smaller filter elements for fixed ripples; thereby, the total circuit size can be kept low. On the other hand, a small Δr^2 also means that it takes less time for the system to complete one switching cycle in steady state, which leads to a higher switching frequency. A high frequency operation is not desired because it causes the conversion efficiency to be low by increasing the switching losses in the semiconductors. Moreover, it requires the controller bandwidth to be high. Otherwise, the control accuracy deteriorates. More details on this topic will be provided in Section 3.7.

3.5 Controller Design

In order to perform an example controller design for a buck converter of $25W$ output power, the design requirements given in Table 3.1 are used. In the design process, the aim is to determine the parameters L, C and Δr^2 so that the design requirements are satisfied when the buck converter circuit implemented with these L and C values is controlled by the proposed controller utilizing this Δr^2 in the equations of $\sigma_{on\Delta}$ and $\sigma_{off\Delta}$. For this purpose, the bisection search algorithm is used, which is given in Appendix A. It takes the design requirements as inputs and outputs the design parameters, L, C and Δr^2. This algorithm is composed of two nested loops, called inner and outer. The outer loop searches for the Δr^2 value in a given range to meet the Δv_o requirement. It solves (3.64), (3.65) and (3.67) to get Δv_o at each iteration by changing the Δr^2 value employed in these equations and keeping the other parameters fixed until the error between two consecutive Δr^2 values is below a certain tolerance. The inner loop does a similar thing to find Z_0 value that gives the required Δi_L for each Δr^2 updated in the outer loop. For this purpose, equations (3.62), (3.63) and (3.66) are solved in the inner loop at each iteration. Normalized frequency, f_n is also calculated in the outer loop by solving equations (3.68)-(3.70). When the algorithm converges, Δr^2 value found in the last iteration is given as one of the outputs. The other two design parameters, L and C are easily calculated at the end of the algorithm by reverting from the normalized domain, using the Z_0 and f_n values together with the desired operating frequency, f as follows:

$$\begin{aligned} C &= \frac{f_n}{2\pi f Z_0} \\ L &= Z_0^2 C. \end{aligned} \tag{3.71}$$

Note that (3.71) is derived from normalization equations in (3.1) and (3.2).

For the example design, the steady state output voltage ripple requirement is selected to be

$$\frac{\Delta v_o}{V_{ref}} \times 100 = 2\% \tag{3.72}$$

of the reference voltage, and the inductor current ripple requirement is selected as

$$\frac{\Delta i_L R_L}{V_{ref}} \times 100 = 60\% \tag{3.73}$$

of its target DC value. A high inductor current ripple percentage as in (3.73) is generally desired in converters so that a smaller inductor can be selected. Since i_L waveform is not an output of the converter, unlike v_o, it is not expected to be close to pure DC.

Table 3.1: Buck converter design requirements

Parameter	**Value**
Vcc	12 V
V_{ref}	5 V
R_L	$1\,\Omega$
Δv_o	0.1 V
Δi_L	3 A
f	10 kHz

Algorithm 1 given in Appendix A is used to solve for the buck converter design parameters. The requirements in Table 3.1 are given to this algorithm as inputs. As a result, L, C and Δr^2 values that satisfy these requirements are obtained as:

$$\begin{aligned}
&\Delta r^2 = 6.362 \times 10^{-4} \\
&C = 374.5\,\mu\text{F} \\
&L = 97.9\,\mu\text{H}.
\end{aligned} \tag{3.74}$$

3.6 Simulation Results

Simulation of the resistive loaded buck converter is done via LTspice. The circuit diagram is provided in Figure 3.9. As can be seen, the hierarchical block feature of the software is used for the controller. The control law (3.40) is implemented inside the block as an analytical expression. Netlist of the controller circuit is provided in Appendix B.1. The feedback signals from the circuit as well as the reference voltage are connected to the controller as inputs. Both switches are driven by the controller output signal u. However, one of them is in active-high while the other is in active-low configurations. Therefore, they are never simultaneously on or off. Note that the simulation is performed by using almost ideal components and switch models because the purpose of this simulation is to verify the theory, which is built upon ideal components. The effects of non-ideal properties of the components will be discussed in the next section.

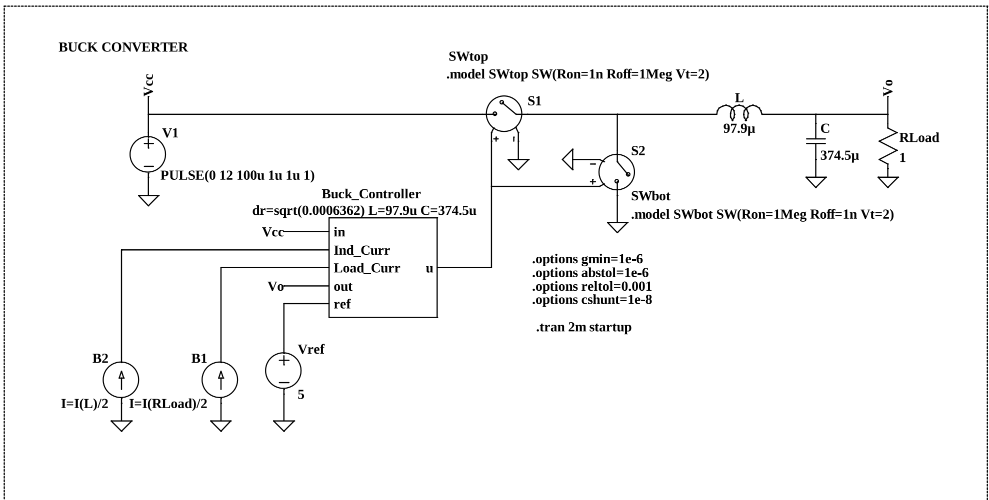

Figure 3.9: Buck converter simulation circuit diagram with ideal components

Note that the simulation is executed with the input voltage, output voltage and load resistance values given in Table 3.1. Also, outputs of the design algorithm given in (3.74) are used as the design parameters L, C and Δr^2 in the simulation. Figure 3.10 shows the simulation results for v_o and i_L waveforms of the buck converter in steady state. Using the data marked on the plot, Δv_o, Δi_L and f parameters are determined as follows:

$$\begin{aligned}
\Delta v_o &= 5.058 - 4.958 = 0.1\,\mathrm{V} \\
\Delta i_L &= 6.510 - 3.515 = 2.995\,\mathrm{A} \\
f &= \frac{1}{(892.178 - 792.102)} \times 10^3 = 9.992\,\mathrm{kHz}.
\end{aligned} \tag{3.75}$$

Since these results match the Δv_o, Δi_L and switching frequency requirements given in Table 3.1, it can be said that design algorithm 1 given in appendix A works successfully.

The start-up transient simulation results for the buck converter is presented

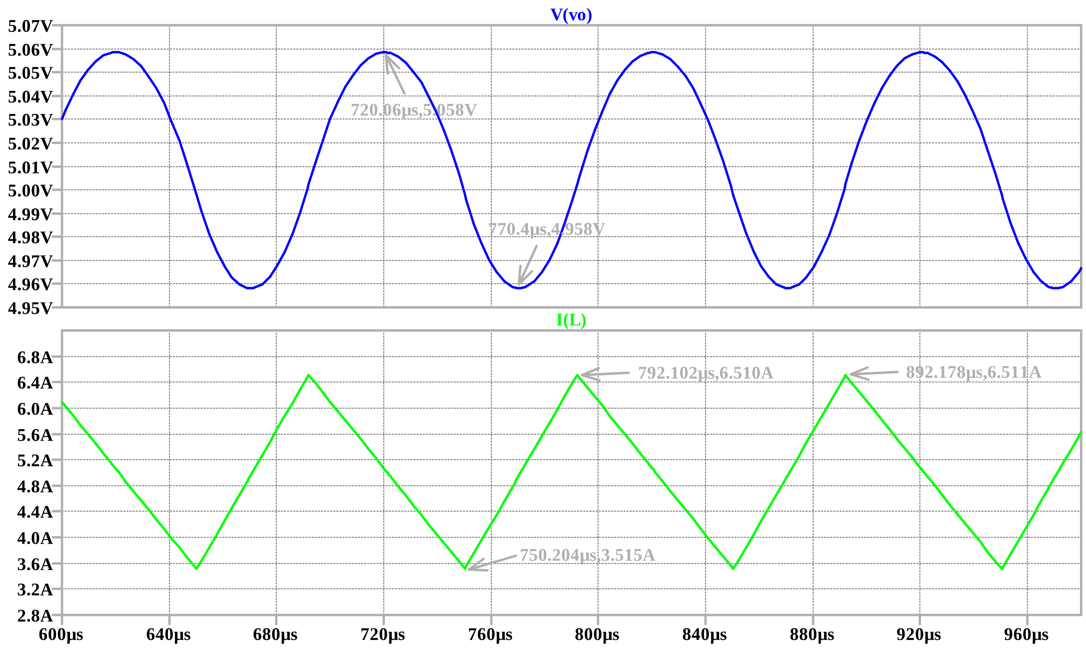

Figure 3.10: Ideal buck converter steady state simulation results, Δv_o, Δi_L and f

in Figure 3.11. The converter is started by applying the input voltage at time $t = 0.1ms$. It is observed that the output voltage is regulated to its reference value with no overshoot. The peak inductor current and the total start-up time are recorded as

$$\begin{aligned} i_{L,peak} &= 13.418\,\text{A} \\ t_{startup} &= 420.933 - 100 = 320.933\,\mu\text{s}. \end{aligned} \tag{3.76}$$

It is observed that the peak inductor current during the start-up is high compared to its steady state value. That limits the design in terms of the physical sizes of the inductor and switches since they must be large enough to handle the peak current. However, that is a price that must be paid if a fast start-up is desired.

Lastly, load transient simulations are performed for the buck converter. Unloading and loading transients are investigated by changing the load resistance from $1\,\Omega$ to $2\,\Omega$ at time $t = 591\mu s$, and changing it back to $1\,\Omega$ at time $t = 1.05ms$, respectively. Figure 3.12 shows the dynamic response of the converter to load transients. Output voltage deviation and recovery time for both transients are calculated using the data marked on the figure.

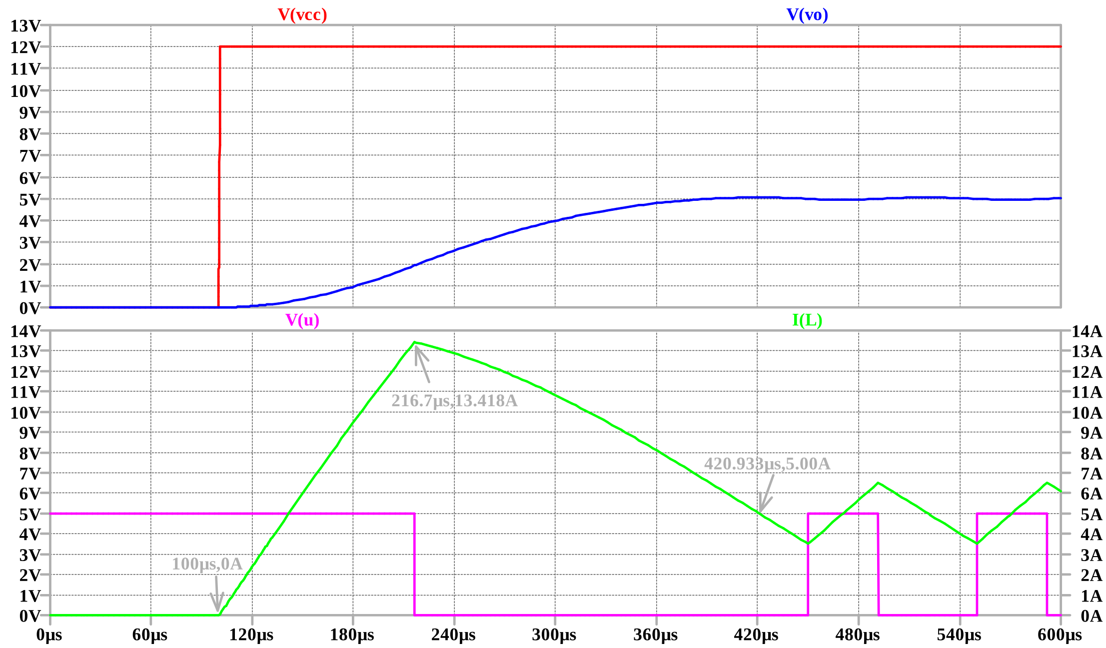

Figure 3.11: Ideal buck converter start-up simulation results, $i_{L,peak}$ and $t_{startup}$

For loading transient:

$$\begin{aligned} \Delta v_{o,loading} &= 5000 - 4733 = 267\,\text{mV} \\ t_{loading} &= 1161 - 1050 = 111\,\mu\text{s}. \end{aligned} \tag{3.77}$$

For unloading transient:

$$\begin{aligned} \Delta v_{o,unloading} &= 5377 - 5000 = 377\,\text{mV} \\ t_{unloading} &= 742.4 - 591.3 = 151.1\,\mu\text{s}. \end{aligned} \tag{3.78}$$

The control signal u is illustrated in Figures 3.11 and 3.12 with purple color. It can be verified by observing the control signal that the target operating point is reached with only one switching action as claimed for both start-up and load transients.

Ideal simulation results given in (3.75)-(3.78) are gathered in Table 3.2. Note that the results of theoretical calculations are also added to this table, which are calculated for the same conditions in the simulations by using various equations

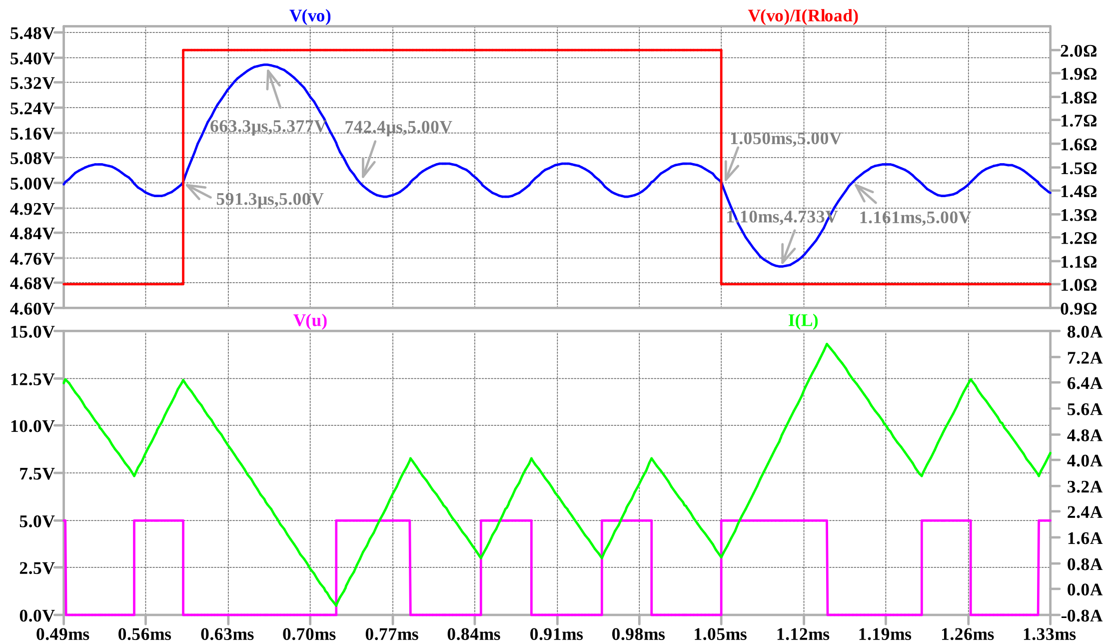

Figure 3.12: Ideal buck converter unloading and loading transients simulation results

given throughout this chapter. The error between theoretical calculations and ideal simulation results are provided in the table as well. It can be seen that the results are equal to each other, with negligible errors for all performance criteria. This consistency supports the correctness of the theory. The small discrepancies between simulation and theoretical results can be due to the difference between tolerances of numerical solution methods.

3.7 Practical Considerations

When it comes to the implementation of a buck converter with the proposed controller, there are some practical concerns that are worth mentioning. A widely used technique in power electronics for current measurement is to place a small valued resistor to the line and measure the voltage on it with an analog to digital converter. Then, the current flowing through the line is obtained as the ratio of voltage to resistance. Since the proposed controller needs inductor and load

Table 3.2: Comparison of ideal simulation results and theoretical calculations for buck converter performance criteria

Parameters	**Ideal Simulation Results**	**Theoretical Values**	**Errors**
Δv_o	0.1 V	0.1 V	0%
Δi_L	3 A	3 A	0%
f	9.99 kHz	10 kHz	0.1%
$i_{L,peak}$	13.42 A	13.44 A	0.15%
$\Delta v_{o,loading}$	267 mV	264.5 mV	0.95%
$\Delta v_{o,unloading}$	377 mV	380 mV	0.79%
$t_{startup}$	321 µs	321.2 µs	0.06%
$t_{loading}$	111 µs	110.2 µs	0.73%
$t_{unloading}$	151.1 µs	151.23 µs	0.09%

current measurements, two sense resistors must be added to the circuit. Also, inductors, capacitors and transistors have parasitic resistances that are neglected in theory. These resistances bring additional damping, causing λ_{on} and λ_{off} spiral trajectories to decay faster.

Another important concern is the tolerances of components. Fortunately, sense resistors with very low tolerances (down to ±0.1%) can be found for accurate current measurements. However, inductors and capacitors usually have ±10% tolerance which can cause significant discrepancies. Besides, inductance and capacitance values decrease with increasing current and voltage, respectively. Meaning they are non-linear as opposed to what is assumed in theory. Although it increases the size, a solution for this problem can be selecting the rated currents and voltages of components above enough the operating conditions. Also, the capacitor value may decrease with aging, especially for aluminum electrolytic capacitors. Ceramic capacitors can be utilized in order to reduce the effect of aging. The last factor that affects the component values is the temperature which must be taken into account during the design stage.

The last practical concern is about the implementation of the controller. In theory, it is assumed that the controller has infinite bandwidth. But in reality, the bandwidth is limited by the time it takes for the controller to solve the $\sigma_{on\Delta}$

and $\sigma_{off\Delta}$ equations and to apply the control law accordingly. Depending on how the controller is implemented, measurements may take some time and further decrease the bandwidth. Due to the limited controller bandwidth, switching action will be taken with a delay.

Effects of non-ideal characteristics of components on the performance of proposed controller are investigated by repeating the simulation with realistic models of components selected from the market. Everything else is kept the same for a fair comparison. The circuit diagram used for realistic buck converter simulations is provided in Figure 3.13. Differences between this circuit and the one with ideal components in Figure 3.9 are:

- Two sense resistors, $R5$ and $R6$ are added. To increase current measurement accuracy, their values are selected as high as possible provided that the voltage does not exceed the 3.3 V analog to digital converter (ADC) input limit at peak current when amplified by a 20 V/V gain amplifier.
- 97.9 µH ideal inductor is replaced with a 100 µH. Because it was the closest value available in the market. Although it is not visible on the diagram, 32 mΩ DC resistance is added to the inductor model.
- Ceramic capacitor models of 47 µF are used as output capacitors. 4.5 mΩ of equivalent series resistance (ESR) is added to the model. Also, capacitance is derated for target DC output voltage. Eight units of capacitors are used in parallel instead of one bulky capacitor. This is a common practice used in power electronics applications in order to reduce the effects of ESR.
- Top and bottom switches in the ideal circuit are replaced with $M1$ and $M2$ NMOS transistor models. Their on-state resistance ($R_{DS(on)}$) value is approximately 1.2 mΩ
- A half-bridge driver integrated circuit (IC) model $U1$ is used to drive the transistors in accordance with the control signal u. This is necessary in practice because the controller may not be strong enough to turn the transistors on and off quickly.

- The control law in (3.40) is implemented using a floating-point 32-bit Arm®-based microcontroller unit (MCU) with a clock frequency of 480 MHz. In order not to lose time with voltage and current measurements, they are transferred from ADC peripheral using direct memory access. In addition, the arctangent function is approximated with a maximum absolute error of 0.0015 rad by using the 9th approximation presented in [53]. This sped up the process significantly since the arctangent function was one of the most time-taking parts of the control law equations. All in all, it is measured via an oscilloscope that it takes 5 µs for the microcontroller to solve the equations and generate the control signal accordingly. For this reason, controller bandwidth is limited in the realistic simulations by means of applying the control signal to the driver IC every 5 µs, not continuously.

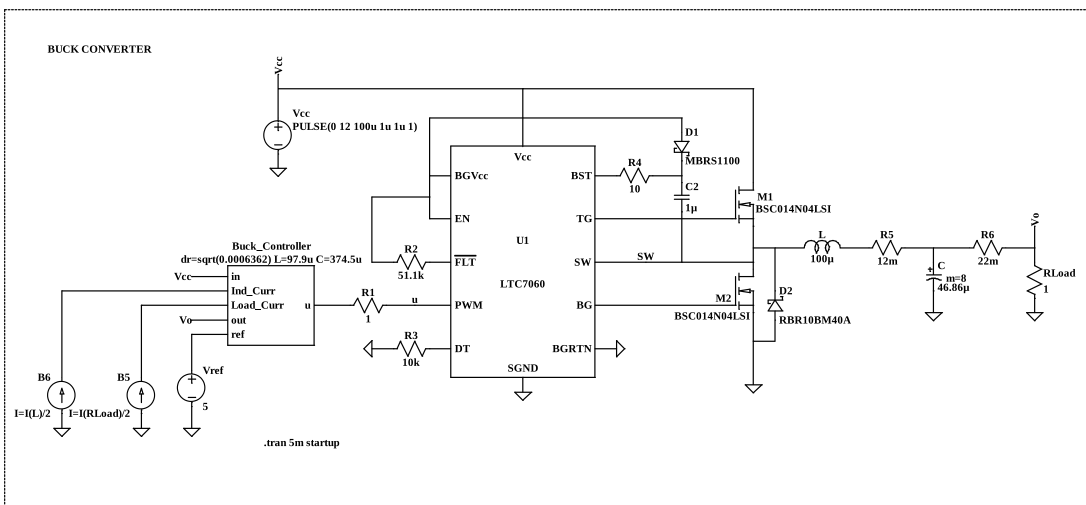

Figure 3.13: Buck converter simulation circuit diagram with realistic component models

Simulation results for steady state, start-up and load transient responses of a realistic buck converter are presented in Figures 3.14, 3.15 and 3.16, respectively. Note that these three figures have counterparts in the ideal simulation case. Performance measures are calculated using the data on the plots and given in Table 3.3 along with their theoretical values. Percentage errors between the realistic simulations results and theoretical values are added to this table as well. Also, the efficiency (η) of the converter is obtained from the realistic simulations and presented in the table.

Table 3.3: Comparison of theoretical values and realistic simulation results for buck converter performance criteria

Parameters	**Realistic Simulation Results**	**Theoretical Values**	**Errors**
Δv_o	0.15 V	0.1 V	50%
Δi_L	3.63 A	3 A	21%
f	8.7 kHz	10 kHz	13%
$i_{L,peak}$	13.46 A	13.44 A	0.15%
$\Delta v_{o,loading}$	391 mV	264.5 mV	47.83%
$\Delta v_{o,unloading}$	453 mV	380 mV	19.21%
$t_{startup}$	377.5 µs	321.2 µs	17.53%
$t_{loading}$	135 µs	110.2 µs	22.5%
$t_{unloading}$	157.6 µs	151.23 µs	4.21%
η	93.15%	100%	6.85%

Simulations are repeated many times by changing one non-ideal characteristic at a time in a controlled manner. As a result, it is observed that the errors other than efficiency error shown in Table 3.3 are caused mainly by the low bandwidth of the controller rather than lossy elements. Especially the effects of output capacitor ESR and MOSFET $R_{DS(on)}$ are negligible compared to sense resistors and the DC resistance of the inductor. Hence, care must be taken to guarantee that the natural frequency of L and C is much lower than the bandwidth of the controller so that the errors are minimized. It must be noted that the comparison in Table 3.3 is only made to give an idea about the magnitude of error between theory and practice. The data can not be treated as exact numbers because most of the simulation results depend on from which switching cycle the data is taken. Nevertheless, the worst case scenario is tried to be reflected in the table.

In practice, Δv_o and Δi_L ripples will not be the same for all cycles in steady state because of the limited controller bandwidth. This behavior can be observed in Figure 3.14. Another important issue is that the extra damping in the system due to losses causes the operating point to drop below $\sigma_{off,\Delta}$ trajectory during the switch-off state before the target operating point is reached. So, the controller

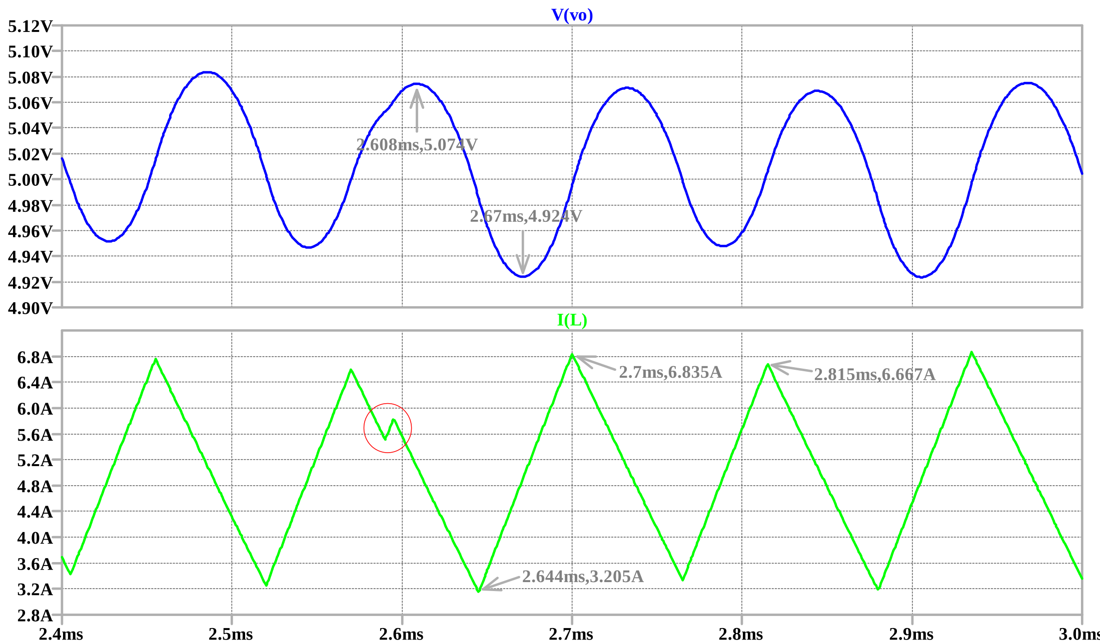

Figure 3.14: Realistic buck converter steady state simulation results, Δv_o, Δi_L and f

must toggle the switch twice in order to drive the operating point above the trajectory. As a result, some chattering may occur during the switch-off state, as shown with red circles placed on the inductor current waveform in Figure 3.14 and Figure 3.15. It can be said that the higher the losses in the system, the higher the chattering frequency. Moreover, increasing the controller bandwidth results in more chattering since the states are checked more frequently. It is interesting to note that the finite bandwidth of a practical controller helps reduce the chattering effect at the expense of a small performance drop.

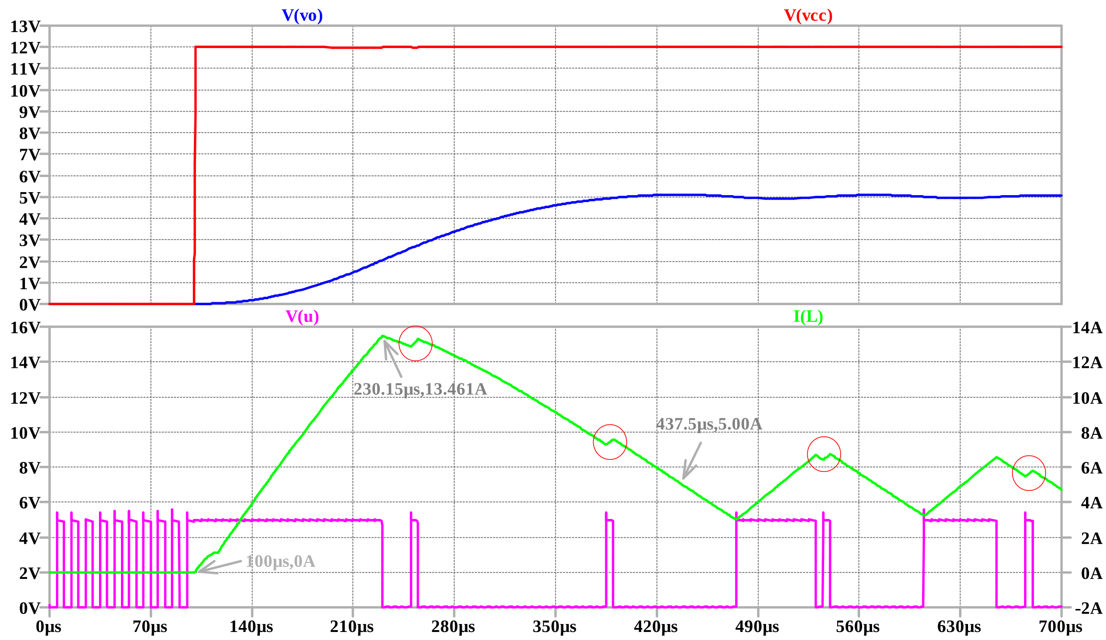

Figure 3.15: Realistic buck converter start-up simulation results, $i_{L,peak}$ and $t_{startup}$

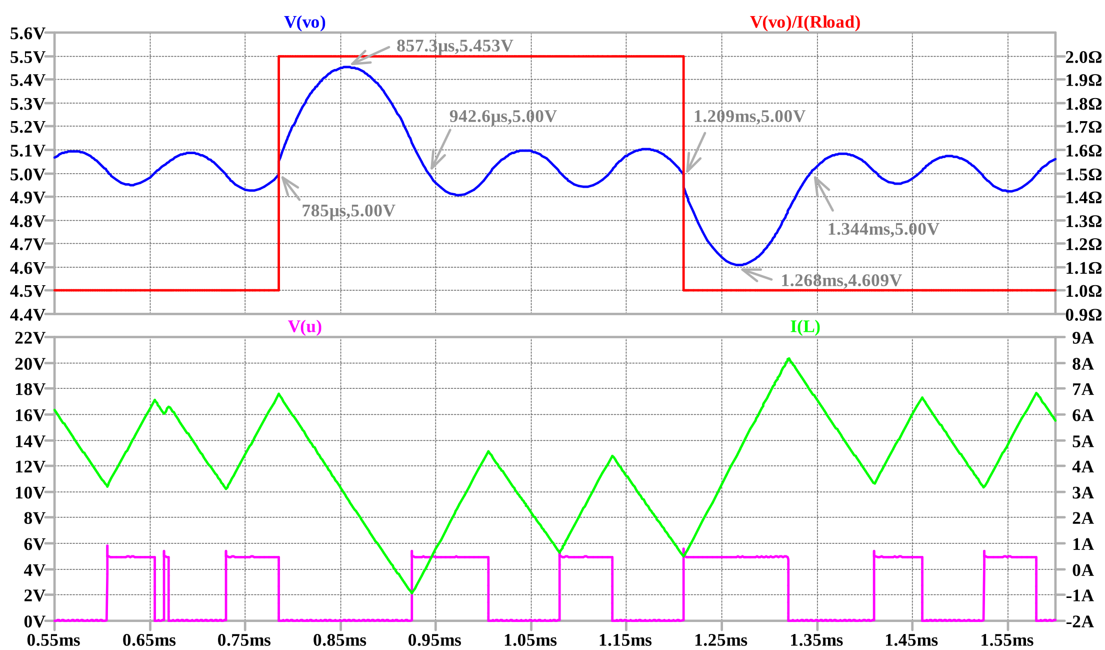

Figure 3.16: Realistic buck converter unloading and loading transients simulation results

Chapter 4

Boundary Control of DC-DC Boost Converter

4.1 Normalization and Modelling

Application of the control method described in the previous chapter is studied for resistive loaded DC-DC boost converter topology. The transistor in the circuit is represented by a switch. The circuit configuration is called on-state when the switch is closed and off-state when it is open. Figure 4.1 shows the simplified boost converter circuit diagram along with the direction of inductor current i_L and polarity of output voltage v_o. On and off states of the boost converter are examined separately. The system is analyzed by considering that the components are lossless and their values are constant. For modelling, the normalization technique explained in Chapter 3 is utilized without any change. Hence, normalization constants in (3.1) and equalities in (3.2) apply for the boost converter too.

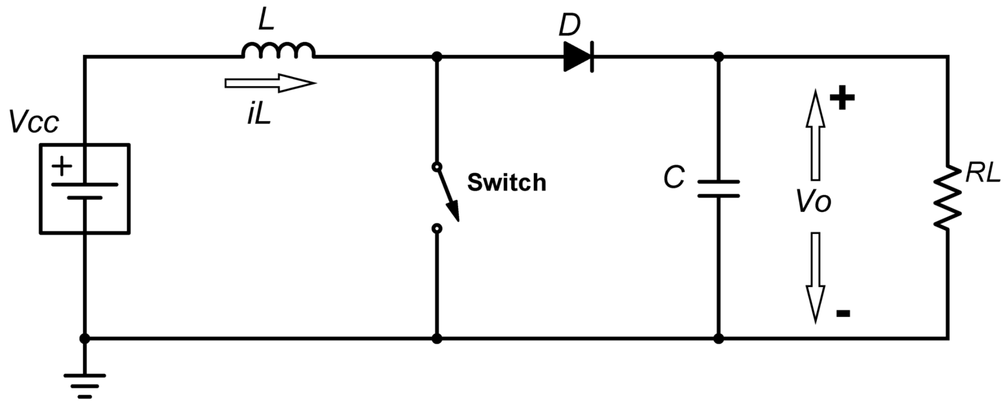

Figure 4.1: Simplified boost converter circuit diagram

4.1.1 Switch On-state Model

When the switch is closed ($u = 1$), the diode turns off, separating the circuit into two. In this case, the following two differential equations can be written for the resistive loaded boost converter in the normalized domain:

$$\begin{aligned} \frac{dv_{on}}{dt_n} &= -2\pi \frac{v_{on}}{R_{Ln}} \\ \frac{di_{Ln}}{dt_n} &= 2\pi V_{ccn}. \end{aligned} \tag{4.1}$$

The inductor current, i_{Ln} and the output voltage, v_{on} are selected as two states of the system. Solving the equations in (4.1) simultaneously by eliminating time t_n yields

$$i_{Ln} = V_{ccn} R_{Ln} \ \ln\left(\frac{v_{on}(0)}{v_{on}}\right) + i_{Ln}(0), \tag{4.2}$$

which defines the on-state natural trajectories of the boost converter.

The family of on-state trajectories is represented by λ_{on}, which is given below:

$$\lambda_{on}(v_{on}, i_{Ln}, v_{on}(0), i_{Ln}(0)) = \ i_{Ln} - i_{Ln}(0) - V_{ccn} R_{Ln} \ \ln\left(\frac{v_{on}(0)}{v_{on}}\right). \tag{4.3}$$

Note that $\lambda_{on} = 0$ gives the solution trajectory of (4.1) corresponding to a given initial condition $i_{Ln}(0)$ and $v_{on}(0)$. Some of infinitely many on-state trajectories are plotted in Figure 4.2 for randomly selected initial conditions. A member of this trajectory family is distinguished from the rest with the name σ_{on}, which is shown by green color in this figure. It is a unique trajectory that passes through the target operating point.

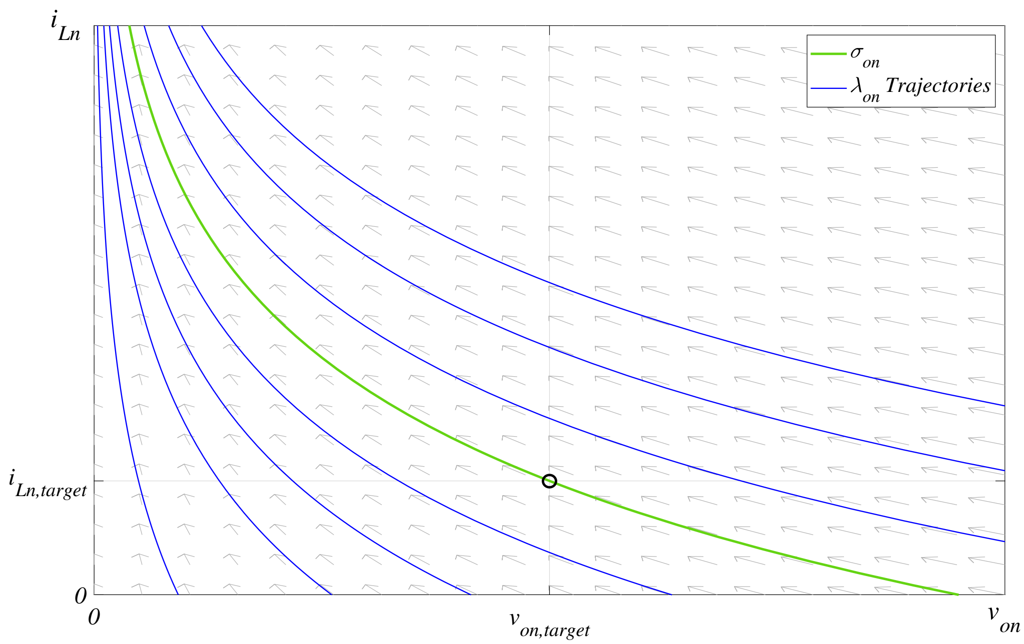

Figure 4.2: Boost converter on-state natural trajectories

4.1.2 Switch Off-state Model

When the switch is open ($u = 0$), the diode turns on because the inductor current that is built during the on-state must be continuous. In this state, the two differential equations describing the behaviour of the system can be given as follows:

$$\begin{aligned} \frac{dv_{on}}{dt_n} &= 2\pi\left(i_{Ln} - \frac{v_{on}}{R_{Ln}}\right) \\ \frac{di_{Ln}}{dt_n} &= 2\pi(V_{ccn} - v_{on}). \end{aligned} \tag{4.4}$$

Note that the off-state equations of boost converter given in (4.4) are exactly the same as on-state equations of buck converter in (3.3). Therefore, the solution in (3.23) applies here. Of course, this time the family of trajectories is denoted by λ_{off}, which is given below:

$$\lambda_{off}(\hat{v}_{on}, \hat{i}_{Ln}, \hat{v}_{on}(0), \hat{i}_{Ln}(0)) = \frac{\hat{i}_{Ln}^2}{4\pi^2} + \left(\frac{\alpha \hat{i}_{Ln}}{2\pi\beta} - \frac{\hat{v}_{on}}{\beta}\right)^2 - r_0^2\, e^{-\frac{2\alpha}{\beta}(\theta(0)-\theta)}, \quad (4.5)$$

where $\hat{i}_{Ln}$ and $\hat{v}_{on}$ are given in (3.4); α and β parameters are given in (3.9); r_0^2, $\theta(0)$ and θ are given in (3.24)-(3.26). By using (4.5), the solution trajectory of (4.4) for a given initial condition $\hat{i}_{Ln}(0)$ and $\hat{v}_{on}(0)$ can be obtained as $\lambda_{off} = 0$.

The natural trajectories followed by the resistive loaded boost converter when the switch is off are presented in Figure 4.3. As in the buck converter case, the λ_{off} trajectory that crosses through the target point is shown in red color and specially named σ_{off}. Since the solutions of (4.4) are unique, so is σ_{off} trajectory.

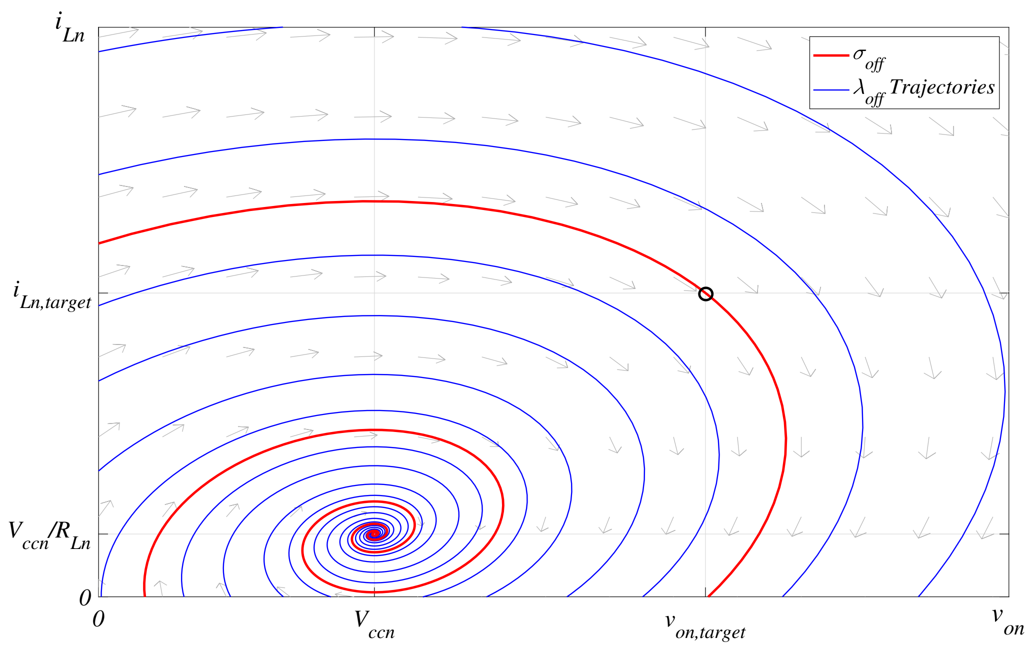

Figure 4.3: Boost converter off-state natural trajectories

It is important to note that the inductor current decreases only in switch off-state, and it can not decrease below zero because the diode blocks the current in the reverse direction. Clearly, the output voltage can not be negative either. These two physical limitations can be stated as:

$$v_{on} \geq 0 \quad \& \quad i_{Ln} \geq 0, \quad (4.6)$$

which confine the operation to the first quadrant of the state plane.

4.2 Control Law Definition

Objectives in the boost converter control are the same as in the buck counterpart. The first one is to keep the output voltage equal to its reference, and the second one is maximizing conversion efficiency. A target operating point for the controller of the boost converter can be derived from these objectives. The first condition, which is $v_o = V_{ref}$ can be written in the normalized domain as follows:

$$v_{on} = 1. \tag{4.7}$$

For the second objective, $P_{out} = P_{in}$ equality must be satisfied. For steady state operation, this can be expanded as follows:

$$\frac{v_o^2}{R_L} = V_{cc}\, i_L. \tag{4.8}$$

In normalized domain, (4.8) becomes

$$i_{Ln} = \frac{v_{on}^2}{V_{ccn} R_{Ln}}. \tag{4.9}$$

Target operating point for boost converter can be obtained from (4.7) and (4.9) as follows:

$$\begin{aligned} v_{on,target} &= 1 \\ i_{Ln,target} &= \frac{1}{V_{ccn} R_{Ln}}. \end{aligned} \tag{4.10}$$

Since the controller design depends on the natural dynamics of the system to drive the states to the target operating point on the phase plane, trajectories passing through that point are of special importance. These are on-state switching curve labeled as $\sigma_{on} \in \lambda_{on}$ and off-state switching curve labeled as $\sigma_{off} \in \lambda_{off}$.

These switching curves are emphasized in Figures 4.2 and 4.3 with green and red colors, respectively. It is worth noting that, off-state phase portrait of the boost converter in Figure 4.3 is essentially the same as the on-state portrait of buck converter in Figure 3.2. However, from the controller point of view, the regions of interest are different for the two converters due to the difference in position of the target operating point with respect to the equilibrium. By substituting the target point given in (4.10) into λ_{on} given in (4.3) as an initial condition, we define the σ_{on} trajectory as follows:

$$\begin{aligned}\sigma_{on}(v_{on}, i_{Ln}) &= \lambda_{on}\left(v_{on}, i_{Ln}, v_{on}(0) = 1\ ,\ i_{Ln}(0) = \frac{1}{V_{ccn}R_{Ln}}\right)\\ &= i_{Ln} + V_{ccn}R_{Ln}\ \ln(v_{on}) - \frac{1}{V_{ccn}R_{Ln}}.\end{aligned} \tag{4.11}$$

In a similar manner, we obtain the σ_{off} trajectory by using the target point as shown below:

$$\sigma_{off}(\hat{v}_{on}, \hat{i}_{Ln}) = \lambda_{off}\left(\hat{v}_{on}, \hat{i}_{Ln}, \hat{v}_{on}(0) = 1 - V_{ccn},\ \hat{i}_{Ln}(0) = \frac{1}{V_{ccn}R_{Ln}} - \frac{V_{ccn}}{R_{Ln}}\right), \tag{4.12}$$

where λ_{off} is given by (4.5).

Using the two switching curves σ_{on} and σ_{off}, a control law that makes the system reach from any starting point to the target operating point is defined as follows:

$$\begin{aligned}&\text{when}\quad v_{on} < 1\ ,\quad \text{apply}\quad u = \begin{cases}0 & \text{if } \sigma_{off} > 0\\ 1 & \text{otherwise}\end{cases}\\ &\text{when}\quad v_{on} > 1\ ,\quad \text{apply}\quad u = \begin{cases}0 & \text{if } \sigma_{on} > 0\\ 1 & \text{otherwise.}\end{cases}\end{aligned} \tag{4.13}$$

According to the control law, if the output voltage is greater than its reference at any time instant, the σ_{on} equation given in (4.11) is evaluated for the states at that time. The switch is turned off if the states are above σ_{on}. Otherwise, it is turned on. The control law makes the same decision by evaluating σ_{off} equation given in (4.12) when the output voltage is less than the reference.

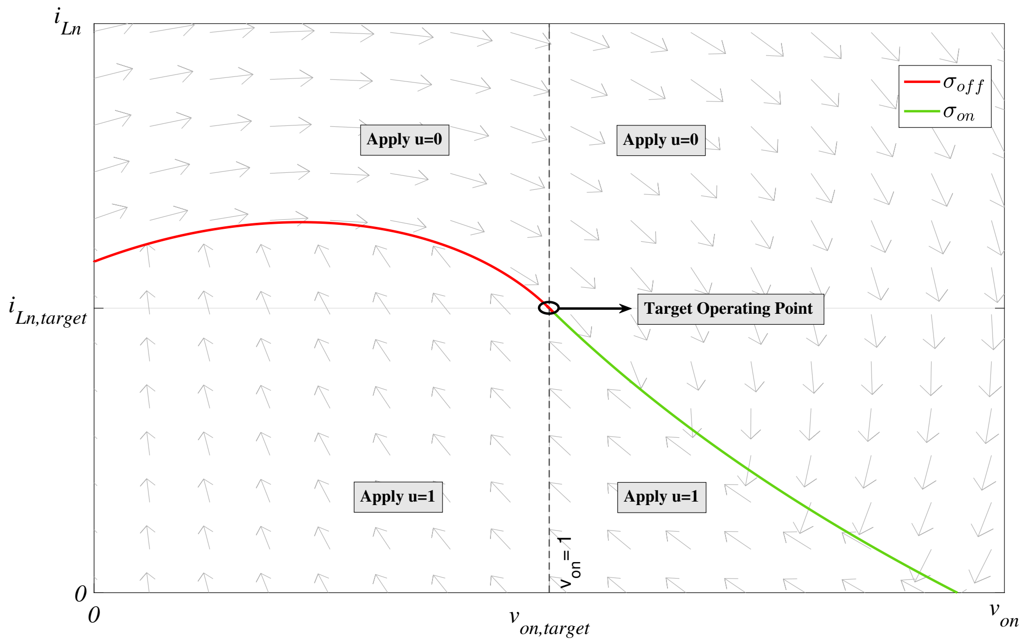

Figure 4.4: Boost converter control law operation

The phase portrait of the boost converter under the control law given by (4.13) is presented in Figure 4.4. Note that the red curve in this figure is the part of the red curve in Figure 4.3 for $v_{on} < 1$, and the green curve is the part of the green curve in Figure 4.2 for $v_{on} > 1$. A natural switching curve is obtained as the combination of these parts of σ_{on} and σ_{off} curves. The operating principle of the controller is quite similar to the buck converter counterpart. Basically, what the controller does is check if the current states of the system are above or below this combined switching curve on the normalized state plane. The switch is turned off ($u = 0$) if the states are above the curve, and it is turned on ($u = 1$) if they are below, thereby forming the vector field as shown by gray arrows in Figure 4.4. These arrows indicate the direction of the solutions at the location of their tails. By following them, it can be seen that the solutions are forced by the control law (4.13) to reach the switching curve in finite time regardless of the initial condition. At this point, the switch is immediately toggled so that the solutions converge to the target operating point. Thus, starting from any point on the state plane, the states are driven to the target by switching only once. An analytical expression for the control law can be written since the on-state and off-state trajectories are analytically derived. In order to keep the system trajectories around the target in steady state while providing a finite switching frequency operation, the control law is slightly altered as in the buck converter case. This needs to be done because the target point is not a natural equilibrium point of the system. Section 4.4 includes further details about this topic.

4.3 Transient Analysis

4.3.1 Start-Up Transients

When the boost converter is energized for the first time, the controller keeps the switch on. The inductor current ramps up starting from zero state, while the output voltage remains at zero. The inductor current continues to increase until its normalized value reaches $i_{Ln,int}$ at which point the σ_{off} trajectory intersected by $v_{on} = 0$ line. Afterward, the switch is turned off, and the system follows its natural off-state trajectory to reach its target operating point defined in (4.10). In this way, the start-up transient of the boost converter is completed. The trajectories followed during this process are presented in Figure 4.5. As can be seen in the figure, the inductor current reaches its peak value, called $i_{Ln,peak}$ during the switch off time interval. This value requires extra attention when designing a boost converter because it may saturate the inductor. When $i_{Ln} = i_{Ln,peak}$, we have $v_{on} = V_{ccn}$. This can be substituted into The σ_{off} equation given in (4.12) to calculate $i_{Ln,peak}$ as follows:

$$\sigma_{off}\left(v_{on} = V_{ccn}\right) = 0. \tag{4.14}$$

Similarly, the inductor current value at which the two start-up trajectories intersect, which is called $i_{Ln,int}$ can be found by solving the following equation:

$$\sigma_{off}\left(v_{on} = 0\right) = 0. \tag{4.15}$$

In order to find the total time of start-up transient, the times spent while the switch is on and off must be calculated separately. The switch on time can be

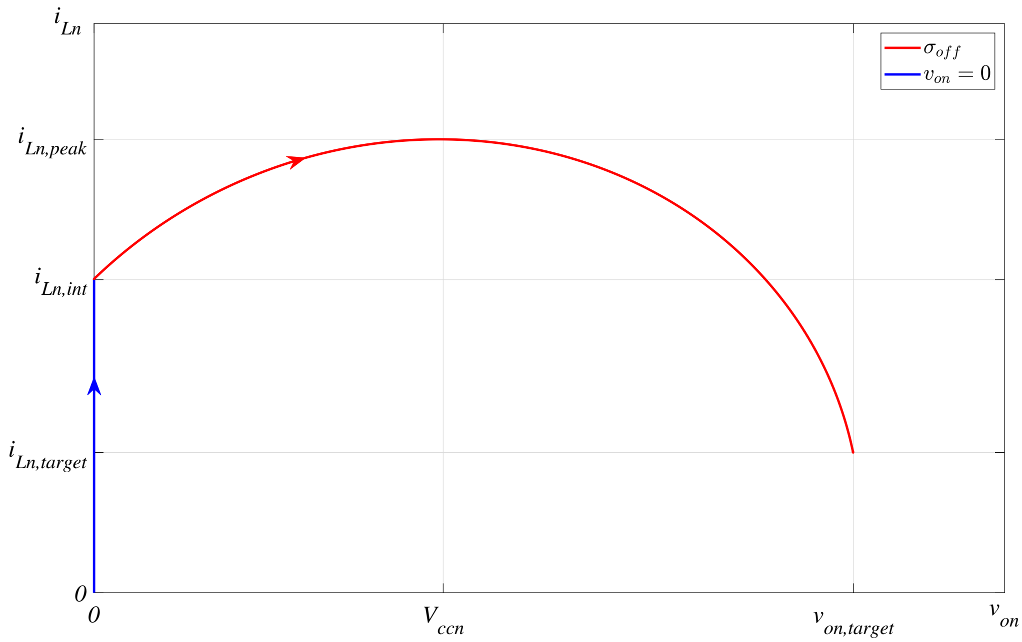

Figure 4.5: Boost converter start-up trajectories

found by isolating the dt term in the inductor current equation given in (4.1) and then integrating along the on-state start-up trajectory shown in Figure 4.5 as follows:

$$t_{n,startup(on)} = \int_0^{i_{Ln,int}} \frac{1}{2\pi V_{ccn}}\, di_{Ln} = \frac{i_{Ln,int}}{2\pi V_{ccn}}, \tag{4.16}$$

where the $i_{Ln,int}$ is the solution of (4.15).

Similarly, if we isolate the dt term in the v_{on} equation given in (4.4) and integrate from $v_{on} = 0$ to $v_{on} = v_{on,target}$, we obtain the switch off time during start-up as:

$$t_{n,startup(off)} = \int_0^{v_{on,target}} \frac{1}{2\pi(i_{Ln} - \frac{v_{on}}{R_{Ln}})}\, dv_{on}. \tag{4.17}$$

For evaluating the integral in (4.17), the relation between i_{Ln} and v_{on} established by $\sigma_{off} = 0$ equation where σ_{off} is given in (4.5) is used. First, the range of v_{on} values defined by the integration limits is discretized into small parts. Then, i_{Ln} values satisfying the $\sigma_{off} = 0$ for each v_{on} value in the range are calculated. These i_{Ln} values are utilized to evaluate the integral numerically via the trapezoidal rule. Note that (4.17) can be further expanded analytically. However, it will not be integrable due to the highly non-linear terms in σ_{off} expression.

Finally, the total start-up time can be calculated by summing the results of (4.16) and (4.17) as follows:

$$t_{n,startup} = t_{n,startup(on)} + t_{n,startup(off)}. \tag{4.18}$$

4.3.2 Resistive Load Transients

When a boost converter is exposed to a loading transient, meaning a step increase in load, a new target operating point that satisfies (4.10) with the new R_{Ln} is set by the controller. Then it turns on the switch in accordance with the control rule (4.13). As depicted in Figure 4.6, the states follow the λ_{on} trajectory that passes through $(v_{on,target}, i_{Ln,initial})$ point until they reach the σ_{off} curve formed by substituting the new target operating point into (4.12). At the junction of two trajectories, the inductor has its normalized maximum current, $i_{Ln,max}$. To calculate this value, first we define the on-state trajectory corresponding to loading event, $\lambda_{on,loading}$, as follows:

$$\begin{aligned}\lambda_{on,loading}(v_{on}, i_{Ln}) &= \lambda_{on}\left(v_{on}, i_{Ln}, v_{on}(0) = 1, i_{Ln}(0) = \frac{1}{V_{ccn}R_{Ln,initial}}\right) \\ &= i_{Ln} + V_{ccn}R_{Ln}\ \ln(v_{on}) - \frac{1}{V_{ccn}R_{Ln,initial}},\end{aligned} \tag{4.19}$$

where λ_{on} is given in (4.3) and the $R_{Ln,initial}$ is the normalized load resistance value before the loading transient occurs. Also note that the initial condition employed in λ_{on} is the target operating point defined by (4.10) prior to the transient.

Then $i_{Ln.max}$ can be found by solving the following equation:

$$\lambda_{on,loading} = \sigma_{off}, \tag{4.20}$$

where σ_{off} is given by 4.12.

When $i_{Ln} = i_{Ln,max}$ point is reached, the switch turns off and stays off, obeying the control law (4.13) until the solutions converge to the new target operating point as shown in Figure 4.6. As mentioned before, the converter manages to make through the loading transient by single switching action.

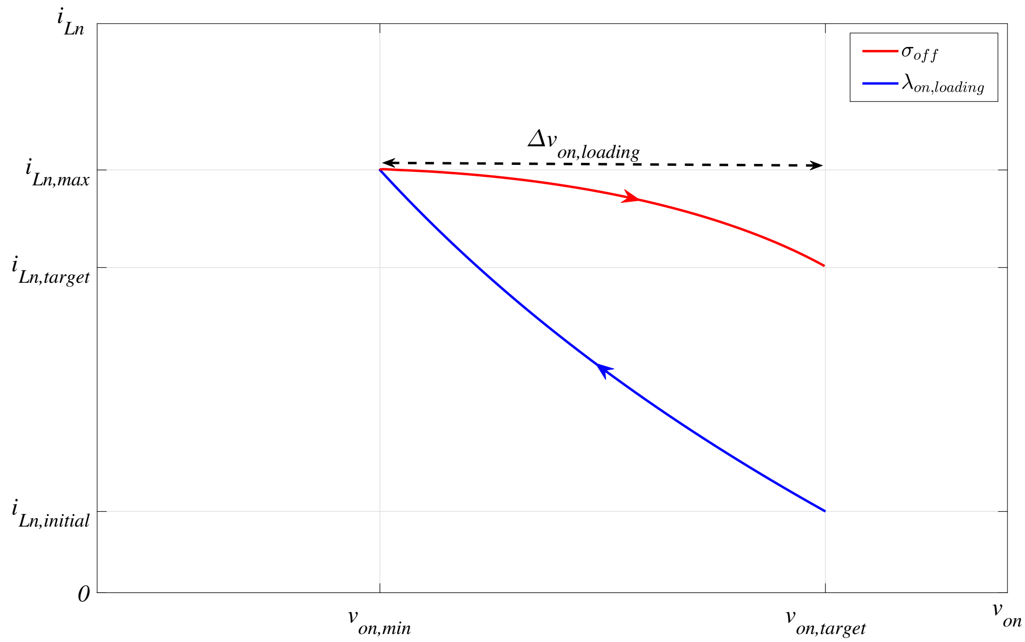

Figure 4.6: Boost converter loading trajectories

The minimum value of normalized output voltage during loading transient of the boost converter is called $v_{on,min}$. It can be calculated by using (4.2) as follows:

$$i_{Ln,max} - i_{Ln,initial} - V_{ccn}R_{Ln} \ \ln\left(\frac{v_{on,target}}{v_{on,min}}\right) = 0, \tag{4.21}$$

where $i_{Ln,max}$ is the solution of (4.20).

Since $i_{Ln,initial}$ and $v_{on,target}$ expressions in (4.21) are the coordinates of the target point before the loading, (4.10) equations can be used to replace them with $\frac{1}{V_{ccn}R_{Ln,initial}}$ and 1, respectively. Then, $v_{on,min}$ can be found as follows:

$$v_{on,min} = e^{\frac{1}{V_{ccn}R_{Ln}}\left(\frac{1}{V_{ccn}R_{Ln,initial}} - i_{Ln,max}\right)}. \tag{4.22}$$

Using the $v_{on,min}$ value, we obtain the normalized voltage deviation from reference caused by loading as:

$$\Delta v_{on,loading} = 1 - v_{on,min}. \tag{4.23}$$

In order to compute the normalized time for which the switch is on during loading, the integral given in (4.16) can be evaluated from $i_{Ln} = i_{Ln,initial}$ to

$i_{Ln} = i_{Ln,max}$ as follows:

$$t_{n,loading(on)} = \int_{i_{Ln,initial}}^{i_{Ln,max}} \frac{1}{2\pi V_{ccn}}\, di_{Ln} = \frac{i_{Ln,max}}{2\pi V_{ccn}} - \frac{1}{2\pi R_{Ln,initial} V_{ccn}^2}. \tag{4.24}$$

The normalized time to complete the loading transient after the switch is turned off can be calculated by evaluating the integral given in (4.17) along off-state loading trajectory as follows:

$$t_{n,loading(off)} = \int_{v_{on,min}}^{v_{on,target}} \frac{1}{2\pi(i_{Ln} - \frac{v_{on}}{R_{Ln}})}\, dv_{on}, \tag{4.25}$$

where i_{Ln} depends on v_{on} by $\sigma_{off} = 0$ equation. Note that derivation and evaluation methods for the integral in (4.25) is as explained for the (4.17) equation in the start-up transient case.

Once we have the $t_{n,loading(on)}$ and $t_{n,loading(off)}$ values, the total elapsed time during the loading transient can be found by adding the two as:

$$t_{n,loading} = t_{n,loading(on)} + t_{n,loading(off)}. \tag{4.26}$$

Let us remember that we can always revert back from the normalized domain by using the corresponding normalization equation given in (3.2). For example, the loading transient duration in the regular time domain can be calculated as:

$$t_{loading} = 2\pi\sqrt{LC}\; t_{n,loading}. \tag{4.27}$$

The boost converter response in the case of unloading transient, meaning a sudden load decrease, is illustrated in Figure 4.7. Explanation of the controller response is quite similar to that in the loading case. First, a new target point is determined with the new load resistance value. Then, the switch is kept off until the solutions hit the σ_{on} curve on the state plane, then it is toggled so that the states converge to the target by following the natural on-state trajectory. The trajectory followed by the system during switch off time during unloading transient, called $\lambda_{off,unloading}$ can be described as:

$$\lambda_{off,unloading}(\hat{v}_{on}, \hat{i}_{Ln}) = \lambda_{off}\left(\hat{v}_{on}(0) = 1 - V_{ccn}, \hat{i}_{Ln}(0) = \frac{1}{V_{ccn} R_{Ln,initial}} - \frac{V_{ccn}}{R_{Ln}}\right), \tag{4.28}$$

where λ_{off} is given by (4.5) and $R_{Ln,initial}$ is the normalized load resistance before the transient. Note that the initial condition used in (4.28) is the target point prior to the transient, which is obtained by substituting (4.10) into (3.4).

As can be seen in Figure 4.7 that the inductor current reaches its minimum value, called $i_{Ln,min}$, during unloading transient at the intersection of $\lambda_{off,unloading}$ and σ_{on} trajectories. This value can be calculated by the following equation:

$$\lambda_{off,unloading} = \sigma_{on} \quad s.t. \quad v_{on} > 1, \tag{4.29}$$

where $\lambda_{off,unloading}$ and σ_{on} are defined in (4.28) and (4.11), respectively.

Note that unloading transient causes the output voltage to rise above its reference. The maximum normalized value of the voltage is named as $v_{on,max}$. It can be calculated by the following equation:

$$v_{on,max} = \max_{\lambda_{off,unloading}=0} v_{on} \quad s.t. \quad i_{Ln,min} \leq i_{Ln} < i_{Ln,initial}, \tag{4.30}$$

where

$$i_{Ln,initial} = \frac{1}{V_{ccn} R_{Ln,initial}} \tag{4.31}$$

and $\lambda_{off,unloading}$ is given in (4.28). An iterative algorithm such as bisection search can be used to find the $v_{on,max}$. $\lambda_{off,unloading} = 0$ equation must be solved in each iteration for the given i_{Ln} range.

Then we obtain the normalized voltage rise caused by the unloading event as:

$$\Delta v_{on,unloading} = v_{on,max} - 1. \tag{4.32}$$

To find the total required time for the boost converter to recover from an unloading transient, first, we need to calculate the switch on and switch off times as done in the loading and start-up transient cases. The former can be found as follows:

$$t_{n,unloading(on)} = \int_{i_{Ln,min}}^{i_{Ln,target}} \frac{1}{2\pi V_{ccn}} \, di_{Ln} = \frac{1}{2\pi V_{ccn}} \left(\frac{1}{R_{Ln} V_{ccn}} - i_{Ln,min} \right), \tag{4.33}$$

where $i_{Ln,min}$ is the solution of (4.29). The integral in (4.33) is derived from the i_{Ln} equation given in (4.1) by isolating the dt term as explained before.

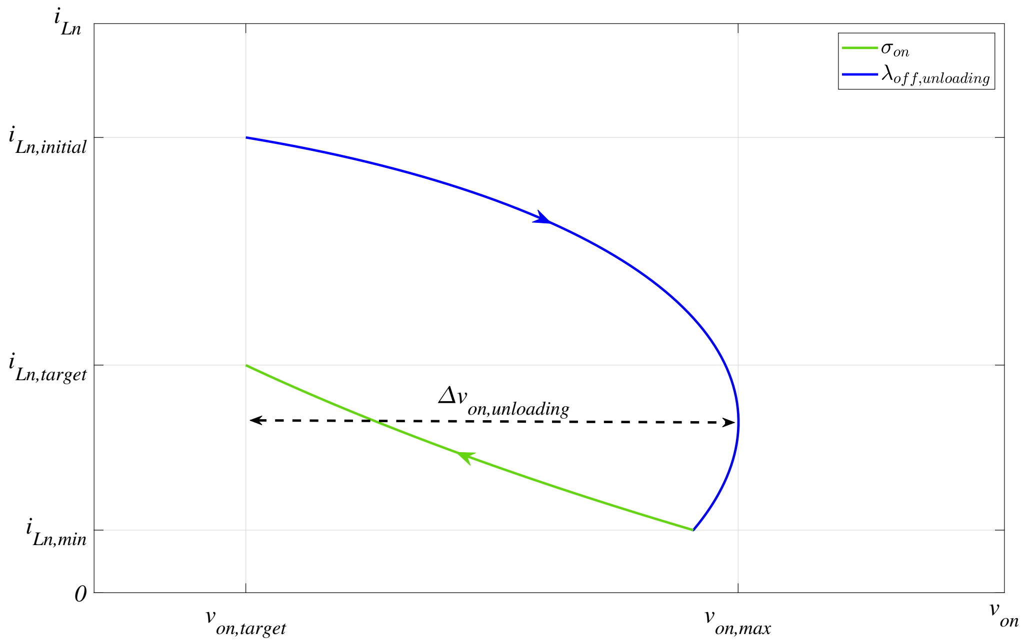

Figure 4.7: Boost converter unloading trajectories

Similarly, the switch off time during unloading transient of boost converter can be calculated by using the integral given in (4.17) as follows:

$$t_{n,unloading(off)} = \int_{i_{Ln,initial}}^{i_{Ln,min}} \frac{1}{2\pi(V_{ccn} - v_{on})} \, di_{Ln} \tag{4.34}$$

Clearly, the relation between v_{on} and i_{Ln} defined by $\lambda_{off,unloading} = 0$ equation where $\lambda_{off,unloading}$ is given in (4.5) applies for the integration in (4.34). The integral is evaluated numerically via the trapezoidal rule as explained in the start-up transient case.

Finally, the results of (4.33) and (4.34) are added to get the total unloading transient recovery time for the boost converter as follows:

$$t_{n,unloading} = t_{n,unloading(on)} + t_{n,unloading(of)}. \tag{4.35}$$

4.4 Steady State Analysis

The problem of uncontrolled switching frequency operation in steady state, which is analyzed for the buck converter in Section 3.4, arises in control of boost converter as well. Since the system does not have an equilibrium at the target point, using the σ_{on} and σ_{off} switching curves as they are defined in (4.11) and (4.12) leads to an uncontrolled switching in steady state at a very high frequency. In order to avoid this, a small modification must be applied to at least one of the switching curves employed in (4.13). Unlike the buck converter, only the σ_{off} curve is altered in the boost converter case. By this modification, which is a small increase in the initial radius of the off-state switching curve, a new switching curve, called $\sigma_{off\Delta}$ is obtained as:

$$\sigma_{off\Delta}(\hat{v}_{on}, \hat{i}_{Ln}, \Delta r) = \sigma_{off}\left(r_0^2 = \frac{\hat{i}_{Ln}(0)^2}{4\pi^2} + \left(\frac{\alpha\hat{i}_{Ln}(0)}{2\pi\beta} - \frac{\hat{V}_{on}(0)}{\beta}\right)^2 + \Delta r^2\right), \tag{4.36}$$

where σ_{off} is given by (4.12) and

$$\begin{aligned}\hat{i}_{Ln}(0) &= \frac{1}{V_{ccn}R_{Ln}} - \frac{V_{ccn}}{R_{Ln}} \\ \hat{v}_{on}(0) &= 1 - V_{ccn}.\end{aligned} \tag{4.37}$$

Controlling the amount of Δr^2 added to the switching curve enables the controller to determine the switching frequency and peak-to-peak ripples in steady state.

System trajectories of the boost converter in steady state are illustrated in Figure 4.8 with solid red and green lines. The operating point travels between points A and B at which the switch is toggled. Normalized peak-to-peak ripples of the output voltage and the inductor current are equal to the distance between A and B points on the horizontal axis and on the vertical axis, respectively. Figure 4.8 shows that as Δr^2 grows, points A and B get away from each other, causing an increase in the ripple magnitudes. Another important note is that increasing Δr^2 leads to an increase in the travel times of the states between points A and B. Consequently, the switching frequency decreases.

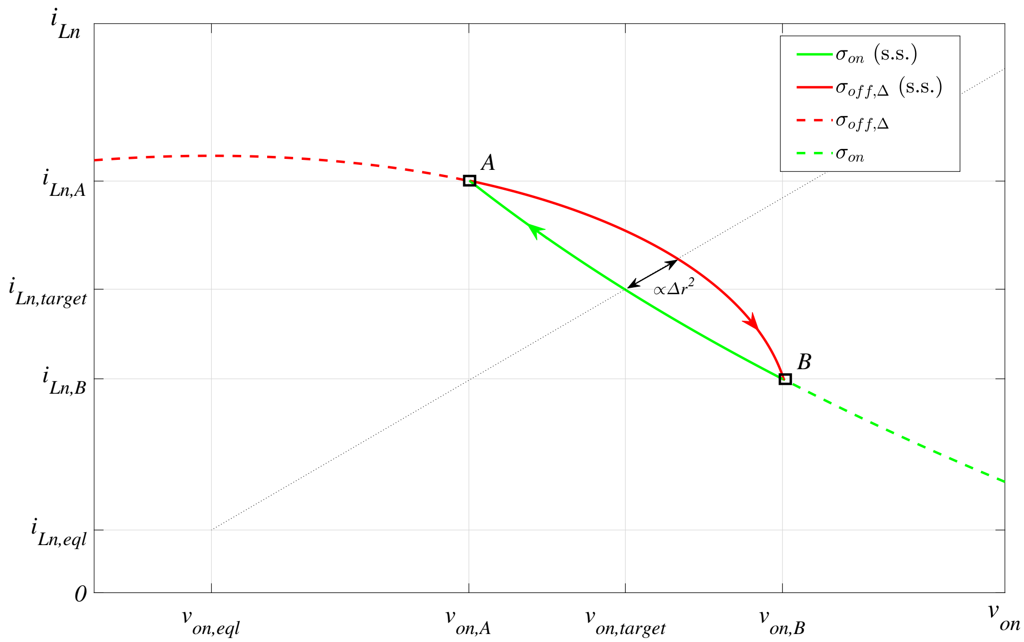

Figure 4.8: Boost converter steady state trajectories

4.4.1 Ripple Calculations

The normalized peak-to-peak ripples of the output voltage and the inductor current in steady state operation of the boost converter are found by calculating the intersection points of steady state trajectories. Coordinates of the intersection point A $(v_{on,A}, i_{Ln,A})$ in Figure 4.8 can be obtained by solving the following equation:

$$\sigma_{off\Delta} = \sigma_{on} \quad s.t. \quad i_{Ln} > \frac{1}{V_{ccn}R_{Ln}} \ \& \ v_{on} < 1, \tag{4.38}$$

where $\sigma_{off\Delta}$ is given in (4.36), and σ_{on} is given in (4.11).

Similarly, by solving the equation (4.38) for

$$i_{Ln} < \frac{1}{V_{ccn}R_{Ln}} \ \& \ v_{on} > 1,$$

we obtain the coordinates of point B $(v_{on,B}, i_{Ln,B})$ on the state plane. Note that the equation (4.38) can be expressed analytically. However, an analytical solution can not be given. Hence, it is solved numerically via the Newton-Raphson method.

Once the states at the intersection points are known, the steady state peak-to-peak ripples of the output voltage (Δv_{on}) and the inductor current (Δi_{Ln}) can be found as follows:

$$\Delta v_{on} = v_{on,B} - v_{on,A} \tag{4.39}$$

$$\Delta i_{Ln} = i_{Ln,A} - i_{Ln,B}. \tag{4.40}$$

4.4.2 Frequency Calculation

The switching frequency of the boost converter can be calculated with the help of Figure 4.8. As mentioned before, steady state operation of the converter is trapped between A and B points on the state plane, obeying the control law given in (4.13). The switch turns on and off repeatedly at the switching frequency, f. The normalized time it takes for the system states to go from point A to B is called $t_{n,ss(off)}$. Since the switch is off during this time, $t_{n,ss(off)}$ can be calculated by integrating the off-state inductor current equation given in (4.4) as follows:

$$t_{n,ss(off)} = \int_{i_{Ln,A}}^{i_{Ln,B}} \frac{1}{2\pi(V_{ccn} - v_{on})} \, di_{Ln} \tag{4.41}$$

where the integration limits are the two solutions of equation (4.38), and the relation between two states can be obtained from (4.36) as $\sigma_{off\Delta} = 0$. To evaluate the integral, the i_{Ln} range given by the limits of the integral is discretized first. Then for each i_{Ln} value in this range, the corresponding v_{on} is calculated by solving the $\sigma_{off\Delta} = 0$ equation. Finally, these v_{on} values are used in the Trapezoidal Rule to calculate the integral numerically.

The amount of normalized time required for the system states to travel from point B back to A is called $t_{n,ss(on)}$. it can be calculated by changing the limits of the integration given in (4.16) according to steady state trajectory as follows:

$$t_{n,ss(on)} = \int_{i_{Ln,B}}^{i_{Ln,A}} \frac{1}{2\pi V_{ccn}} \, di_{Ln} = \frac{i_{Ln,A} - i_{Ln,B}}{2\pi V_{ccn}}. \tag{4.42}$$

Results of (4.41) and (4.42) can be used to calculate the normalized steady state switching frequency, called f_n, as given below:

$$f_n = \frac{1}{t_{n,ss(on)} + t_{n,ss(off)}}. \tag{4.43}$$

Note that the switching frequency of the boost converter can be set to the desired value by selecting the Δr^2 parameter employed in the $\sigma_{off\Delta}$ equation accordingly. When selecting this parameter, it must be considered that the trade-off between the steady state ripples and the frequency, which is explained for buck converter in Section 3.4.2, applies for boost converter as well.

4.5 Controller Design

When designing a boost converter to be controlled by the proposed controller, the three design parameters to be determined are the same as those in the buck converter. Two of them are L, C values to be used in the power stage of the converter, and the third one is Δr^2 value that must be inserted into the off-state switching curve expression as shown in (4.36) to make it pass through slightly above the target operating point. It is important to determine these three parameters correctly so that the design requirements such as maximum output voltage ripple and switching frequency are satisfied.

Table 4.1: Boost converter design requirements

Parameter	**Value**
Vcc	12 V
V_{ref}	24 V
R_L	9.6 Ω
Δv_o	0.24 V
Δi_L	2.78 A
f	12 kHz

An example controller design is carried out for a boost converter of $60W$ output power with the design requirements given in Table 4.1. The output voltage ripple requirement of this example design is selected as:

$$\frac{\Delta v_o}{V_{ref}} \times 100 = 1\% \tag{4.44}$$

of its reference, V_{ref}.

For the inductor current, percentage ripple is selected as:

$$\frac{\Delta i_L V_{cc} R_L}{V_{ref}^2} \times 100 = 55.6\% \tag{4.45}$$

of target DC inductor current.

Boost converter design parameters are calculated by using Algorithm 2 given in Appendix A. This algorithm is almost the same as the one used for buck converter design. The only difference is that the calculations of parameters are done with the equations given for the boost converter in this chapter. Since the working principles of the design algorithm are explained in Section 3.5, it is not repeated here. References to the equations utilized in the process are given in Algorithm 2 itself. When the design requirements given in 4.1 are inputted to the algorithm, the characteristic impedance (Z_0), normalized switching frequency (f_n) and Δr^2 values that satisfy these requirements are obtained as outputs. Using Z_0 and f_n values, two circuit parameters, L and C, are calculated by using the equations given in (3.71). All in all, the design parameters are determined as follows:

$$\begin{aligned} \Delta r^2 &= 3.65 \times 10^{-5} \\ C &= 434.5\,\mu\text{F} \\ L &= 180\,\mu\text{H}. \end{aligned} \tag{4.46}$$

4.6 Simulation Results

A boost converter circuit built with the design parameters in (4.46) is simulated via LTspice software. Input voltage, output voltage reference and load resistance values given in Table 4.1 are used as the design requirements. As in the case of the buck converter, simulations are first done with ideal component models in order to check the correctness of the theory. Then they are repeated with non-ideal components to see the discrepancies.

The circuit diagram used for ideal boost converter simulations is given in Figure 4.9. As can be seen in the figure, the controller takes four inputs from the circuit as well as the reference voltage. It drives a low-side switch according to the control law, which is implemented inside the controller block. The netlist of the controller circuit is provided in Appendix B.2. The simulation results for the steady state v_o and i_L waveforms are obtained as shown in Figure 4.10. By using the data marked on this figure, peak-to-peak ripples and switching frequency are calculated as:

$$\begin{aligned}
\Delta v_o &= 24.12 - 23.879 = 241\,\text{mV} \\
\Delta i_L &= 6.398 - 3.613 = 2.785\,\text{A} \\
f &= \frac{1}{(1.348 - 1.265)} \times 10^3 = 12.05\,\text{kHz}
\end{aligned} \tag{4.47}$$

Based on the fact that the results are almost equal to the design requirements in Table 4.1, it can be said that the simulation and the theory are in good agreement.

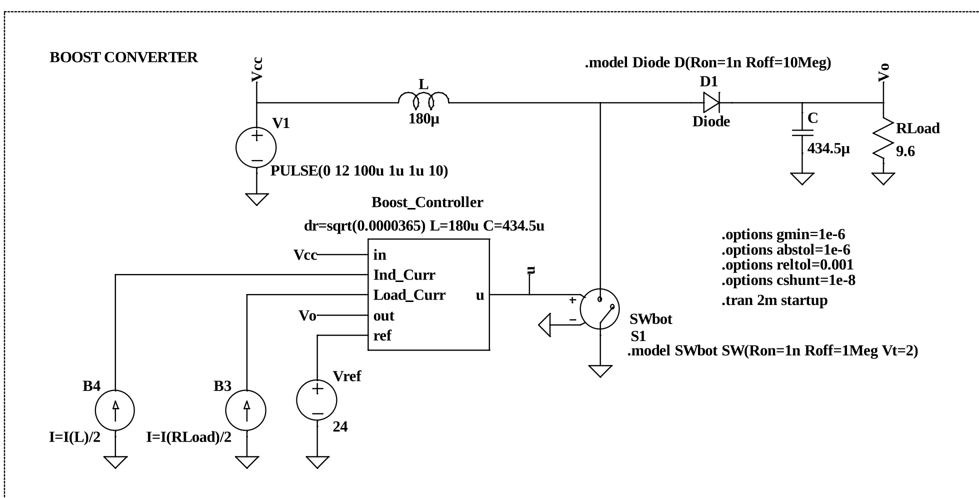

Figure 4.9: Boost converter simulation circuit diagram with ideal components

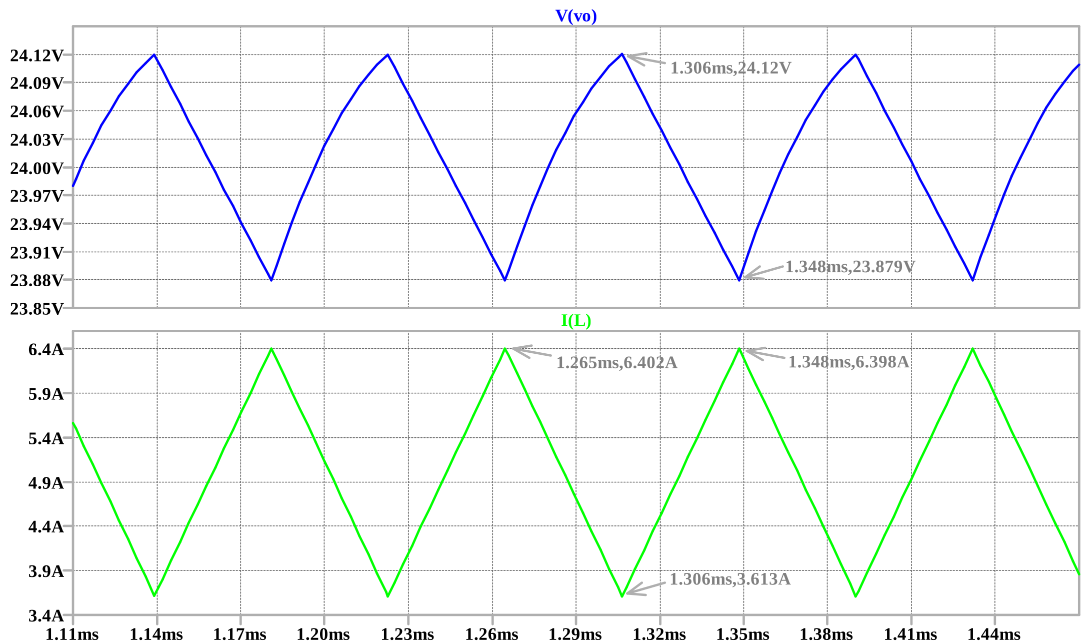

Figure 4.10: Ideal boost converter steady state simulation results, Δv_o, Δi_L and f

Start-up transient simulation results for the ideal boost converter are presented in Figure 4.11. Starting at $t = 0.1\,\text{ms}$, the operating point follows the trajectories shown in Figure 4.5 and reaches the target with one switching action. No overshoot is observed in output voltage as expected. The peak inductor current and total start-up transient times are recorded as:

$$\begin{aligned} i_{L,peak} &= 21.111\,\text{A} \\ t_{startup} &= 851.276\,\mu\text{s}. \end{aligned} \tag{4.48}$$

Note that the trade-off between the high inductor current and low start-up time explained in the buck converter case applies to the boost converter.

The response of the boost converter to load transients are simulated by changing the load resistance from $9.6\,\Omega$ to $12\,\Omega$ and then back to $9.6\,\Omega$ for unloading and loading transients, respectively. Waveforms during these events are presented in Figure 4.12. For the loading transient, voltage drop and recovery time

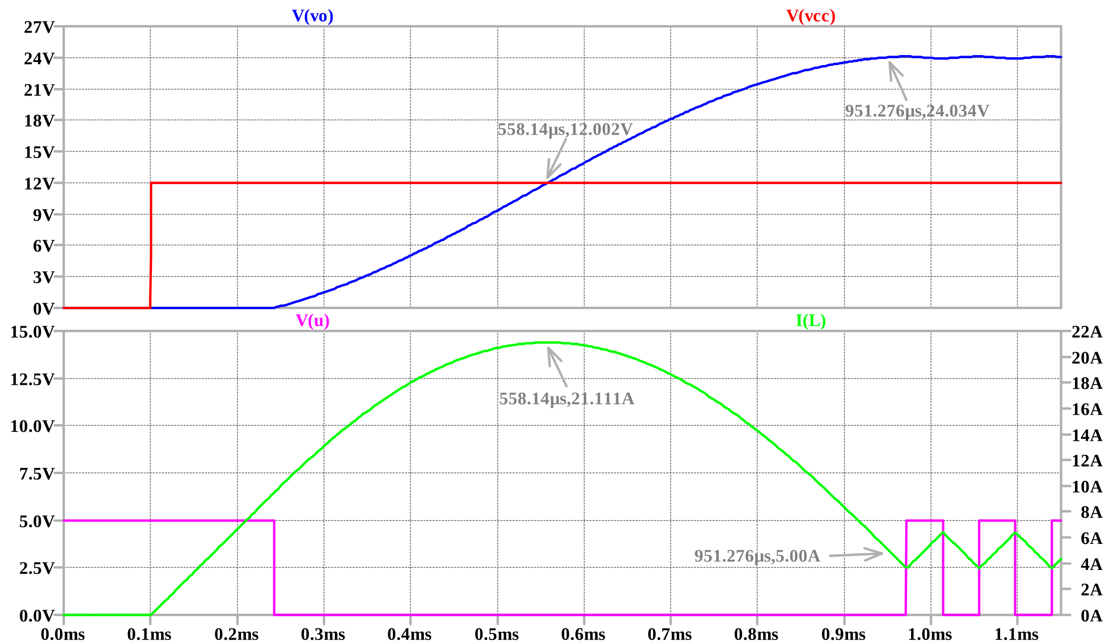

Figure 4.11: Ideal boost converter start-up simulation results, $i_{L,peak}$ and $t_{startup}$

are recorded as:

$$\begin{aligned} \Delta v_{o,loading} &= 24000 - 23694 = 306\,\text{mV} \\ t_{loading} &= 1636 - 1549 = 87\,\mu\text{s}. \end{aligned} \tag{4.49}$$

Output voltage rise and recovery time for unloading transient are obtained from Figure 4.12 as follows:

$$\begin{aligned} \Delta v_{o,unloading} &= 24194 - 24000 = 194\,\text{mV} \\ t_{unloading} &= 1381 - 1280 = 101\,\mu\text{s}. \end{aligned} \tag{4.50}$$

Simulation results in (4.47)-(4.50), which are the main performance criteria of a boost converter control, are presented in Table 4.2 for the purpose of comparison with the results of theoretical calculations. The theoretical values given in this table are calculated for the same conditions used in the simulations. Percentage errors between the theory and simulation are also added to this table. Note that for all parameters, the error is negligibly small, which shows the correctness of the theory. It is expected to obtain very small errors in this comparison since

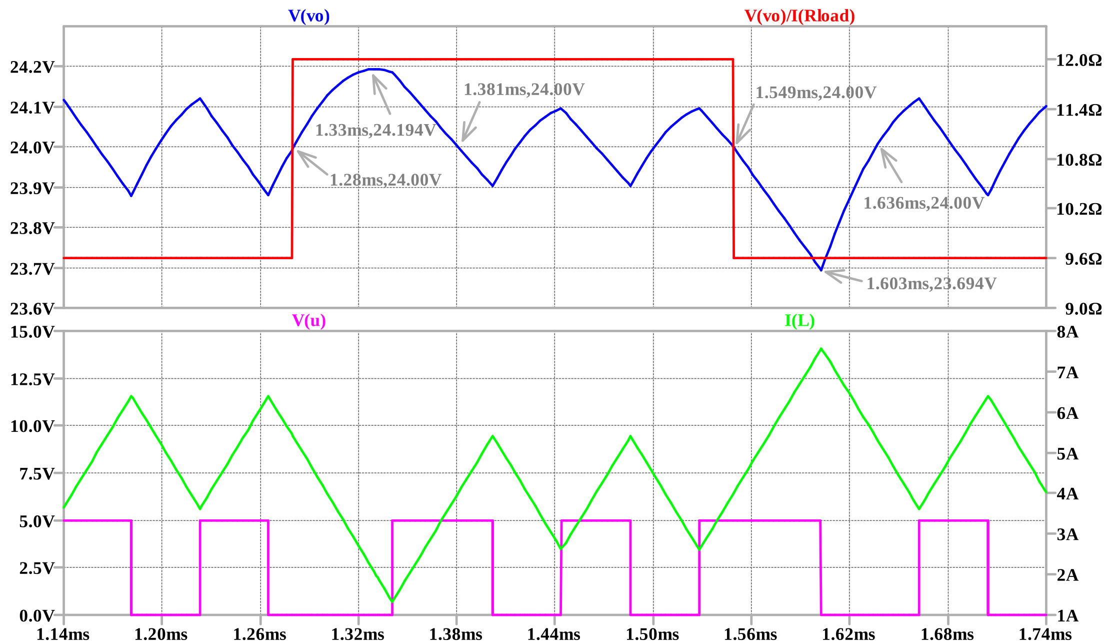

Figure 4.12: Ideal boost converter unloading and loading transients simulation results

simulations are performed with ideal component models. In the next section, non-ideal components will be employed in order to make the simulations more realistic. Potential deviations from the theory in real implementations will be examined in detail.

Table 4.2: Comparison of theoretical values and ideal simulation results for boost converter performance criteria

Parameters	Ideal Simulation Results	Theoretical Values	Errors
Δv_o	0.241 V	0.240 V	0.42%
Δi_L	2.785 A	2.78 A	0.18%
f	12.05 kHz	12 kHz	0.42%
$i_{L,peak}$	21.111 A	21.113 A	0.01%
$\Delta v_{o,loading}$	306 mV	305 mV	0.33%
$\Delta v_{o,unloading}$	194 mV	192 mV	1.04%
$t_{startup}$	851 µs	847.6 µs	0.4%
$t_{loading}$	87 µs	87.2 µs	0.23%
$t_{unloading}$	101 µs	100.4 µs	0.6%

4.7 Practical Considerations

There are mainly three causes of potential differences between theory and practice for the boost converter. The first one is the additional damping effect due to resistances in the circuit. The second one is related to the variability of real component values due to tolerances and operating conditions. The final one is the limited controller bandwidth. Detailed explanations are not given here since these concerns are the same as in the buck converter case, and they are already explained in Section 3.7.

Boost converter simulations are improved by using realistic component models, as shown in Figure 4.13. Components are selected from the market, and their models are built in accordance with their datasheets provided by manufacturers. The main features that distinguish realistic simulations from ideal ones are listed below.

- Two sense resistors of $40\,\mathrm{m\Omega}$ ($R4$) and $7.5\,\mathrm{m\Omega}$ ($R5$) are added to the circuit for load and inductor current measurements, respectively. Their values are optimized for high accuracy.

- DC resistance of $52\,\mathrm{m\Omega}$ is added to the $180\,\mathrm{\mu H}$ inductor model.

- Fourteen units of $47\,\mathrm{\mu F}$ and two units of $10\,\mathrm{\mu F}$ ceramic capacitor models are used as output capacitors so that the total capacitance is close to the calculated value when derated with respect to the operating conditions. Note that the capacitance values seen on the circuit diagram are derated values. Their ESR value at the operating frequency is around $4\,\mathrm{m\Omega}$.

- A transistor ($Q2$) model with drain to source on-state resistance ($R_{DS(on)}$) value of $1.2\,\mathrm{m\Omega}$ is used as the main switch. Also, a second transistor ($Q1$) with the same model is connected in parallel with the diode ($D4$). This transistor will be turned on by the driver IC whenever the diode must be on. In this way, the forward voltage drop on the diode, which is approximately $0.7\,\mathrm{V}$ for the realistic model, is significantly reduced.

- A half-bridge driver IC model ($U1$) is added in order to take the possible delays in driving the transistors into account.

- Controller bandwidth is limited by setting the control signal update rate to 200 kHz. This value is selected based on an experiment that is made on a microcontroller, as explained in Section 3.7.

Boost converter simulation results for inductor current and output voltage waveforms in steady state are plotted in Figure 4.14. As can be seen in this figure, peak-to-peak ripples are varying at each cycle due to the limited controller bandwidth. Moreover, chattering is observed in some of the cycles, as emphasized by red circles. This is caused by resistive elements, as mentioned earlier. This effect is more frequent for start-up transient of boost converter as can be seen in Figure 4.15. Components with minimum parasitic resistances must be selected in the design process in order to mitigate the chattering effect. As expected, the output voltage reaches its 24 V reference value without any overshoot at the end of the start-up transient.

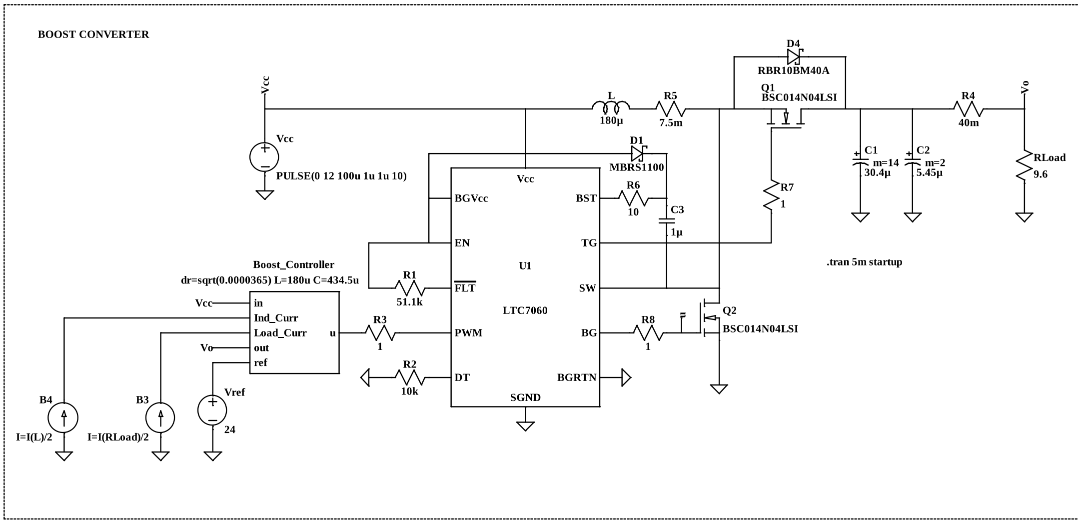

Figure 4.13: Boost converter simulation circuit diagram with realistic component models

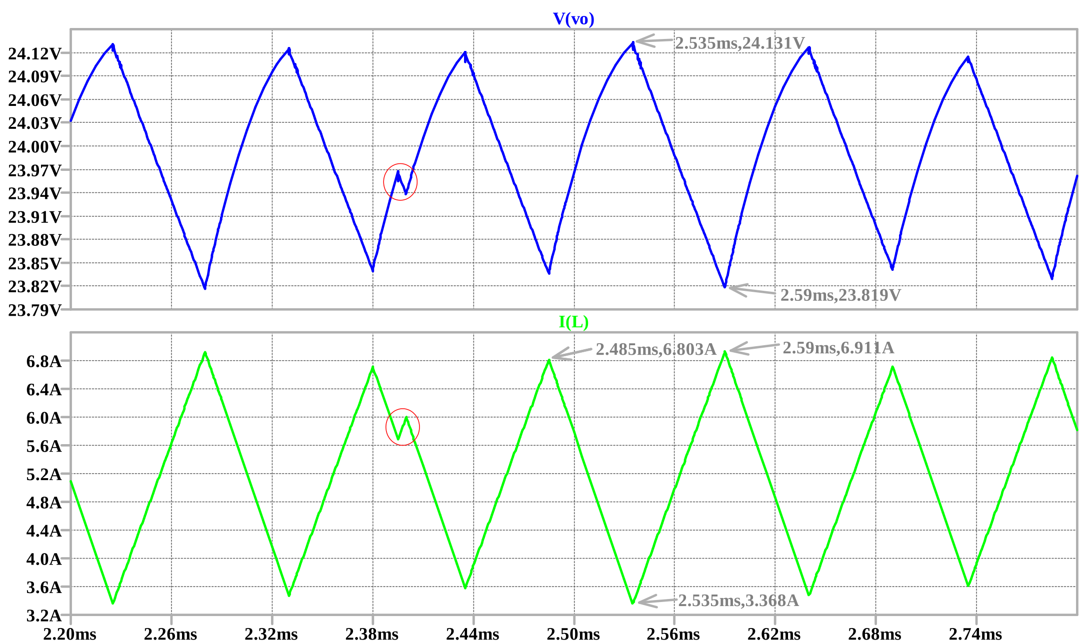

Figure 4.14: Realistic boost converter steady state simulation results, Δv_o, Δi_L and f

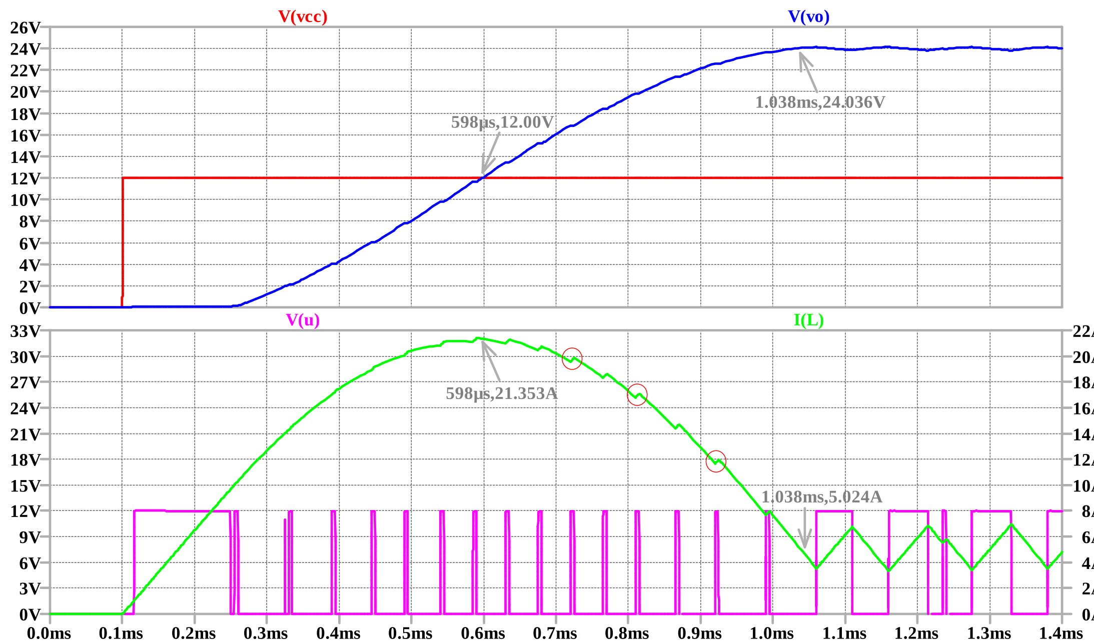

Figure 4.15: Realistic boost converter start-up simulation results, $i_{L,peak}$ and $t_{startup}$

Loading and unloading transient responses of realistic boost converter are examined by simulating the circuit shown in Figure 4.13. To do this, first, a step change in load resistance from $9.6\,\Omega$ to $12\,\Omega$, then another step change from $12\,\Omega$ to $9.6\,\Omega$ are applied. As shown in Figure 4.16, these load steps coincide with reference crossing of the output voltage. Using the data gathered from Figures 4.14-4.16 along with the theoretically calculated values given in Table 4.2, a comparison between practical and theoretical results for the key performance criteria is presented in Table 4.3. Simulation result for the efficiency (η) of the converter is also given in the last row of this table.

Since DC/DC converters are used as voltage sources, the inductor current related parameters like Δi_L and $i_{L,peak}$ can be regarded irrelevant as far as performance is concerned. However, they are important for determining the saturation and root-mean-square (RMS) current ratings of the inductor. The size of the component to be selected depends on these parameters.

Table 4.3: Comparison of theoretical values and realistic simulation results for boost converter performance criteria

Parameters	**Realistic Simulation Results**	**Theoretical Values**	**Errors**
Δv_o	0.312 V	0.24 V	30%
Δi_L	3.543 A	2.78 A	27.45%
f	9.524 kHz	12 kHz	20.63%
$i_{L,peak}$	21.353 A	21.113 A	1.14%
$\Delta v_{o,loading}$	374 mV	305 mV	22.62%
$\Delta v_{o,unloading}$	205 mV	192 mV	6.77%
$t_{startup}$	938 µs	847.6 µs	10.67%
$t_{loading}$	110 µs	87.2 µs	26.15%
$t_{unloading}$	104 µs	100.4 µs	3.59%
η	96.77%	100%	3.23%

The same comments made for the effects of non-ideal components and controller characteristics in the case of the buck converter (see section 3.7) can be made for the boost converter too. Therefore, discussions on the errors given in Table 4.3 are omitted here. The key to mitigating the errors is, again, keeping the controller bandwidth as high as possible compared to the natural frequency of L and C. Some ideas on how to do this will be shared in the next chapter.

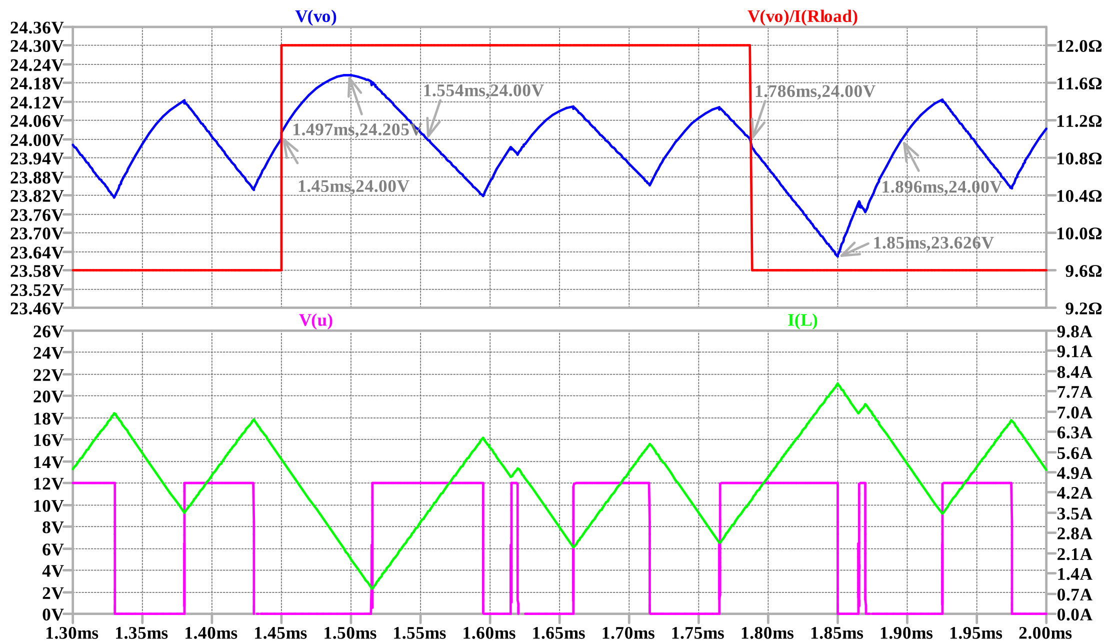

Figure 4.16: Realistic boost converter unloading and loading transients simulation results

Chapter 5

Conclusions and Future Work

Since DC-DC converters are non-linear and variable structure systems, boundary control is very suitable for them. The proposed boundary control method is an excellent alternative for buck and boost converters when a fast transient response is prioritized. It manages to recover from sudden load changes only in one switch toggle action thanks to the natural switching surfaces employed in the control laws. Start-up transients are also handled in the same way without any overshoot or steady state error. The geometrical representation of system trajectories and the control laws on the state-plane makes the method easily comprehensible. In addition, the utilization of the normalization technique enables a parameter-independent generalized analysis. Modification of switching surface in steady state operation provides controlled voltage and current ripple magnitudes. The proposed controller also renders a chattering-free and fixed-frequency operation for converters, which is important in practice for mitigating EMI problems and heat losses. Besides these advantages, there are certain drawbacks too as all control methods have. For example, the trade-off between control effort and response speed must be taken into consideration. Also, solving control law equations requires a high-speed processor, so that controller bandwidth is high. Otherwise, obtained results can differ from theoretical ones. The chattering effect is completely eliminated in theory. Nonetheless, small chattering can be observed in practice due to additional losses and variations in component values. This problem can be minimized in the design stage by careful component selection. Altogether, the use of natural switching surfaces in boundary control of buck and boost converters provide great performance improvements, especially for the systems where large-signal uncertainties are frequently encountered. The superior performance of the proposed control method is verified via simulations. It can be assessed in many energy conversion applications such as electric vehicles, PV systems or wind turbines.

In summary, the main contributions of this thesis are as follows:

- The equations describing the dynamics of buck and boost converters under resistive load are solved in the normalized domain. By eliminating the time, natural state-plane trajectories are obtained for both switch ON and OFF cases. These trajectories are graphically presented to provide valuable insight into the behaviours of the converters.
- Boundary control laws are proposed for both buck and boost converters by using natural switching. These control laws provide excellent start-up and load transient performances, which are limited only by the physical properties of filter components in theory. Also, other goals such as steady state operation with fixed and controlled frequency, zero chattering and zero output voltage overshoot are achieved.
- A theoretical basis for calculating the durations of loading, unloading and start-up transients together with peak voltage and current variations is provided. Besides, the calculations are independent of the circuit parameters and operating conditions thanks to the normalization.
- Finally, procedures for designing buck and boost converters to be controlled by the proposed method are given as pseudocodes. For the given input-output voltages and load resistance, these procedures yield a design that satisfies pre-determined performance requirements.

In the near future, we are planning to test the proposed controllers on an experimental setup for both buck and boost converters. For this setup, control laws are already implemented and tested on a microcontroller, as explained in Chapter 3. As a possible future work, control bandwidth can be tested by using a digital signal processor (DSP) instead of a microcontroller. This could speed up the computations, thereby increase the performance of the controller. Another improvement could be achieved by storing pre-calculated arctangent values in the digital memory as a look-up table rather than evaluating an approximate function each time it is needed. As mentioned before, series parasitic resistances inherent in the components are excluded from the analysis in this work. Their adverse effects are discussed with the help of simulations in Chapter 3 and 4. These effects can be alleviated if the system trajectories are derived by taking these resistances into account. Also, reactive planning techniques such as the sequential composition of controllers can be applied to provide robustness against parameter uncertainties and reach the target operating point faster. Moreover, the system constraints can be included in the control problem by integrating the proposed controllers with a reference governor-type add-on control scheme. Finally, the method presented herein can be applied to other DC-DC converter topologies, for instance, flyback, Cuk, single-ended primary-inductor converter (SEPIC) or buck-boost so that new boundary control strategies can be developed to optimize their dynamics.

Bibliography

[1] D. Pikulin, "Subharmonic oscillations and chaos in DC-DC switching converters," *Elektronika ir Elektrotechnika*, vol. 19, no. 4, pp. 33–36, 2013.

[2] W. Li and X. He, "Review of nonisolated high-step-up DC/DC converters in photovoltaic grid-connected applications," *IEEE Transactions on Industrial Electronics*, vol. 58, no. 4, pp. 1239–1250, 2011.

[3] M. Taghvaee, M. Radzi, S. M. Moosavain, H. Hizam, and M. Marhaban, "A current and future study on non-isolated DC–DC converters for photovoltaic applications," *Renewable & Sustainable Energy Reviews*, vol. 17, pp. 216–227, 2013.

[4] L. R. Shahida and T. M. George, "Implementation of sliding mode control for a buck converter in a photovoltaic system," *2014 International Conference on Advances in Green Energy, ICAGE 2014*, pp. 245–250, 2014.

[5] L. M. Fernandez, P. Garcia, C. A. Garcia, and F. Jurado, "Hybrid electric system based on fuel cell and battery and integrating a single DC/DC converter for a tramway," *Energy Conversion and Management*, vol. 52, no. 5, pp. 2183–2192, 2011.

[6] O. Ellabban, O. Hegazy, J. V. Mierlo, and P. Lataire, "Dual loop digital control design and implementation of a DSP based high power boost converter in fuel cell electric vehicle," *2010 12th International Conference on Optimization of Electrical and Electronic Equipment*, pp. 610–617, 2010.

[7] W. Chen, A. Q. Huang, C. Li, G. Wang, and W. Gu, "Analysis and comparison of medium voltage high power DC/DC converters for offshore wind

energy systems," *IEEE Transactions on Power Electronics*, vol. 28, no. 4, pp. 2014–2023, 2013.

[8] B. Labbe, B. Allard, X. Lin-Shi, and D. Chesneau, "An integrated sliding-mode buck converter with switching frequency control for battery-powered applications," *IEEE Transactions on Power Electronics*, vol. 28, no. 9, pp. 4318–4326, 2013.

[9] A. Rauf, S. Li, R. Madonski, and J. Yang, "Continuous dynamic sliding mode control of converter-fed DC motor system with high order mismatched disturbance compensation," *Transactions of the Institute of Measurement and Control*, vol. 42, no. 14, pp. 2812–2821, 2020.

[10] L. Ardhenta and R. K. Subroto, "Feedback Control for Buck Converter - DC Motor Using Observer," *2020 12th International Conference on Electrical Engineering, ICEENG 2020*, pp. 30–33, 2020.

[11] R. Silva-Ortigoza, V. M. Hernández-Guzmán, M. Antonio-Cruz, and D. Muñoz-Carrillo, "DC/DC buck power converter as a smooth starter for a DC motor based on a hierarchical control," *IEEE Transactions on Power Electronics*, vol. 30, no. 2, pp. 1076–1084, 2015.

[12] I. G. Zurbriggen, M. Ordonez, and M. Anun, "Dynamic physical limits of buck converters: The T0/4 transient benchmark rule," *Conference Proceedings - IEEE Applied Power Electronics Conference and Exposition - APEC*, pp. 421–428, 2013.

[13] J. M. Galvez, M. Ordonez, F. Luchino, and J. E. Quaicoe, "Improvements in boundary control of boost converters using the natural switching surface," *IEEE Transactions on Power Electronics*, vol. 26, no. 11, pp. 3367–3376, 2011.

[14] S. Verma, S. K. Singh, and A. G. Rao, "Overview of control Techniques for DC-DC converters," *Research Journal of Engineering Sciences*, vol. 2, no. 8, pp. 18–21, 2013.

[15] L. Guo, J. Y. Hung, and R. M. Nelms, "Evaluation of DSP-based PID and fuzzy controllers for DC-DC converters," *IEEE Transactions on Industrial Electronics*, vol. 56, no. 6, pp. 2237–2248, 2009.

[16] A. Forsyth and S. Mollov, "Modelling and control of DC-DC converters," *Power engineering journal*, vol. 12, no. 5, pp. 229–236, 1998.

[17] R. D. Middlebrook and S. Cuk, "A general unified approach to modelling switching-converter power stages," in *1976 IEEE Power Electronics Specialists Conference*, pp. 18–34, June 1976.

[18] D. M. Mitchell, *DC-DC switching regulator analysis.* McGraw-Hill Companies, 1988.

[19] J. G. Kassakian, M. F. Schlecht, and G. C. Verghese, *Principles of power electronics*, vol. 1991. Addison-Wesley Reading, MA, 1991.

[20] S. Saggini, P. Mattavelli, and M. Ghioni, "High-performance mixed-signal voltage-mode control for DC-DC converters with inherent analog derivative action," *Conference Proceedings - IEEE Applied Power Electronics Conference and Exposition - APEC*, vol. 23, no. 3, pp. 28–33, 2007.

[21] B. Bryant and M. K. Kazimierczuk, "Modeling the closed-current loop of PWM boost DC-DC converters operating in CCM with peak current-mode control," *IEEE Transactions on Circuits and Systems I: Regular Papers*, vol. 52, no. 11, pp. 2404–2412, 2005.

[22] O. Trescases, A. Prodić, and W. T. Ng, "Digitally Controlled Current-Mode DC–DC Converter IC," *IEEE Transactions on Circuits and Systems I: Regular Papers*, vol. 58, no. 1, pp. 219–231, 2011.

[23] M. Lešo, J. Žilková, M. Biroš, and P. Talian, "Survey of Control Methods for DC-DC Converters," *Acta Electrotechnica et Informatica*, vol. 18, no. 3, pp. 41–46, 2018.

[24] V. Paduvalli, R. J. Taylor, and P. T. Balsara, "Analysis of Zeros in a Boost DC-DC Converter: State Diagram Approach," *IEEE Transactions on Circuits and Systems II: Express Briefs*, vol. 64, no. 5, pp. 550–554, 2017.

[25] V. I. Utkin, "Sliding Mode Control Design Principles and Applications to Electric Drives," *IEEE Transactions on Industrial Electronics*, vol. 40, no. 1, pp. 23–36, 1993.

[26] R. Venkataramanan, "Sliding mode control of power converters," *Journal of the Indian Institute of Science*, vol. 69, p. 193, 1986.

[27] S. C. Tan, Y. M. Lai, and C. K. Tse, "General design issues of sliding-mode controllers in DC-DC converters," *IEEE Transactions on Industrial Electronics*, vol. 55, no. 3, pp. 1160–1174, 2008.

[28] Z. Chen, W. Gao, J. Hu, and X. Ye, "Closed-loop analysis and cascade control of a nonminimum phase boost converter," *IEEE Transactions on Power Electronics*, vol. 26, no. 4, pp. 1237–1252, 2011.

[29] K. Leung and H. Chung, "A Comparative Study of the Boundary Control of Buck Converters Using First- and Second-Order Switching Surfaces -Part I: Continuous Conduction Mode," in *2005 IEEE 36th Power Electronics Specialists Conference*, pp. 2133–2139, 2005.

[30] K. Leung and H. Chung, "Derivation of a second-order switching surface in the boundary control of buck converters," *IEEE Power Electronics Letters*, vol. 2, pp. 63–67, 2004.

[31] T. T. Song and H. S. Chung, "Boundary control of boost converters using state-energy plane," *PESC Record - IEEE Annual Power Electronics Specialists Conference*, vol. 23, no. 2, pp. 551–563, 2006.

[32] G. E. Pitel and P. T. Krein, "Minimum-time transient recovery for DC-DC converters using raster control surfaces," *IEEE Transactions on Power Electronics*, vol. 24, no. 12, pp. 2692–2703, 2009.

[33] I. G. Zurbriggen, M. Anun, and M. Ordonez, "Dynamic physical limits of boost converters: A benchmarking tool for transient performance," *2014 IEEE Energy Conversion Congress and Exposition, ECCE 2014*, pp. 4118–4124, 2014.

[34] K. Young, V. Utkin, and U. Ozguner, "A control engineer's guide to sliding mode control," *IEEE Transactions on Control Systems Technology*, vol. 7, no. 3, pp. 328–342, 1999.

[35] I. Boiko and L. Fridman, "Analysis of chattering in continuous sliding-mode controllers," *IEEE Transactions on Automatic Control*, vol. 50, no. 9, pp. 1442–1446, 2005.

[36] V. Utkin, "Chattering problem," *IFAC Proceedings Volumes*, vol. 44, no. 1, pp. 13374–13379, 2011.

[37] M. Agostinelli, R. Priewasser, S. Marsili, and M. Huemer, "Constant switching frequency techniques for sliding mode control in DC-DC converters," *Proceedings of the Joint 3rd International Workshop on Nonlinear Dynamics and Synchronization, INDS'11 and 16th International Symposium on Theoretical Electrical Engineering, ISTET'11*, no. 1, pp. 318–322, 2011.

[38] S. Ding, W. X. Zheng, J. Sun, and J. Wang, "Second-order sliding-mode controller design and its implementation for buck converters," *IEEE Transactions on Industrial Informatics*, vol. 14, no. 5, pp. 1990–2000, 2018.

[39] A. Sferlazza, C. Albea-Sanchez, L. Martinez-Salamero, G. Garcia, and C. Alonso, "Min-type control strategy of a DC-DC synchronous boost converter," *IEEE Transactions on Industrial Electronics*, vol. 67, no. 4, pp. 3167–3179, 2020.

[40] R. Ling, R. Hu, Q. Hu, J. Liu, and F. Wang, "Fixed-frequency second-order sliding-mode control of buck DC-DC converter," in *2018 Chinese Control And Decision Conference (CCDC)*, pp. 655–660, IEEE, 2018.

[41] Y. Feng, F. Han, and X. Yu, "Chattering free full-order sliding-mode control," *Autom.*, vol. 50, pp. 1310–1314, 2014.

[42] Z. Zhao, S. Li, and J. Yang, "Continuous Finite-Time Sliding Mode Control for Uncertain Nonlinear Systems with Applications to DC-DC Buck Converters," *Asian Journal of Control*, vol. 21, no. 1, pp. 312–322, 2019.

[43] S. K. Pandey, S. L. Patil, U. M. Chaskar, and S. B. Phadke, "Direct duty ratio control of buck DC-DC converters using disturbance observer based integral sliding mode control," *Proceedings: IECON 2018 - 44th Annual Conference of the IEEE Industrial Electronics Society*, pp. 5507–5512, 2018.

[44] S. K. Pandey, S. L. Patil, and S. B. Phadke, "Regulation of Nonminimum Phase DC-DC Converters Using Integral Sliding Mode Control Combined with a Disturbance Observer," *IEEE Transactions on Circuits and Systems II: Express Briefs*, vol. 65, no. 11, pp. 1649–1653, 2018.

[45] Z. Tian, Z. Lyu, J. Yuan, and C. Wang, "UDE-based sliding mode control of DC–DC power converters with uncertainties," *Control Engineering Practice*, vol. 83, no. March 2018, pp. 116–128, 2019.

[46] O. Kirshenboim and M. M. Peretz, "Minimum-time within a deviation-constrained hybrid controller for boost converters," *2015 IEEE 16th Workshop on Control and Modeling for Power Electronics, COMPEL 2015*, pp. 1–6, 2015.

[47] M. K. Al-Nussairi, R. Bayindir, and E. Hossain, "Fuzzy logic controller for DC-DC buck converter with constant power load," in *2017 IEEE 6th International Conference on Renewable Energy Research and Applications (ICRERA)*, pp. 1175–1179, 2017.

[48] F. Taeed, K. H. Andersen, and M. Nymand, "Adaptive digital current mode controller for DC-DC converters," *2015 17th European Conference on Power Electronics and Applications, EPE-ECCE Europe 2015*, 2015.

[49] K. Z. Liu, Y. Yokozawa, T. Katane, and T. Nakagawa, "An MPC-PI approach for buck DC-DC converters and its implementation," *IEEJ Transactions on Industry Applications*, vol. 133, no. 8, pp. 171–176, 2013.

[50] H. Maruta, M. Motomura, K. Ueno, and F. Kurokawa, "Reference modification control DC-DC converter with neural network predictor," *2012 IEEE 13th Workshop on Control and Modeling for Power Electronics, COMPEL 2012*, pp. 1–4, 2012.

[51] H. Maruta, M. Motomura, and F. Kurokawa, "An evaluation study on circuit parameter conditions of neural network controlled DC-DC converter," *Proceedings - 2013 12th International Conference on Machine Learning and Applications, ICMLA 2013*, vol. 2, pp. 249–254, 2013.

[52] N. Jiteurtragool, C. Wannaboon, and W. San-Um, "A power control system in DC-DC boost converter integrated with photovoltaic arrays using optimized back propagation Artificial Neural Network," in *2013 5th International Conference on Knowledge and Smart Technology (KST)*, pp. 107–112, 2013.

[53] S. Rajan, S. Wang, and R. Inkol, "Efficient approximations for the four-quadrant arctangent function," *Canadian Conference on Electrical and Computer Engineering*, no. May, pp. 1043–1046, 2006.

Appendix A

Converter Design Algorithms

Algorithm 1 Buck Converter Design Algorithm

procedure BuckDesign($\Delta v_{o\_desired}$, $\Delta i_{L\_desired}$, Vcc, V_{ref}, R_L, f)
  set A search range (Δr^2_{lower},Δr^2_{upper}) and a tolerance Δr^2_{tol} for Δr^2 parameter
  repeat
    $\Delta r^2 \leftarrow \frac{\Delta r^2_{upper}+\Delta r^2_{lower}}{2}$
    set A search range (Z_{0_lower},Z_{0_upper}) and a tolerance Z_{0_tol} for Z_0 parameter
    repeat
      $Z_0 \leftarrow \frac{Z_{0\_upper}+Z_{0\_lower}}{2}$
      Calculate inductor current ripple, Δi_L (see equation 3.66)
      if $\Delta i_L < \Delta i_{L\_desired}$ **then**
        $Z_{0\_upper} \leftarrow Z_0$
      else
        $Z_{0\_lower} \leftarrow Z_0$
      end if
    until Error between Z_0 values in two consecutive iterations is less than Z_{0_tol}
    Calculate normalized switching frequency, f_n (see equation 3.70)
    Calculate output voltage ripple, Δv_o (see equation 3.67)
    if $\Delta v_o > \Delta v_{o\_desired}$ **then**
      $\Delta r^2_{upper} \leftarrow \Delta r^2$
    else
      $\Delta r^2_{lower} \leftarrow \Delta r^2$
    end if
  until Error between Δr^2 values in two consecutive iterations is less than Δr^2_{tol}
  print Δr^2
  Calculate capacitance C and inductance L according to (3.71)
  print C and L
end procedure

Algorithm 2 Boost Converter Design Algorithm

procedure BOOSTDESIGN($\Delta v_{o\_desired}$, $\Delta i_{L\_desired}$, Vcc, V_{ref}, R_L, f)
  set A search range (Δr^2_{lower},Δr^2_{upper}) and a tolerance Δr^2_{tol} for Δr^2 parameter
  repeat
    $\Delta r^2 \leftarrow \frac{\Delta r^2_{upper} + \Delta r^2_{lower}}{2}$
    set A search range (Z_{0_lower},Z_{0_upper}) and a tolerance Z_{0_tol} for Z_0 parameter
    repeat
      $Z_0 \leftarrow \frac{Z_{0\_upper} + Z_{0\_lower}}{2}$
      Calculate inductor current ripple, Δi_L (see equation 4.40)
      if $\Delta i_L < \Delta i_{L\_desired}$ **then**
        $Z_{0\_upper} \leftarrow Z_0$
      else
        $Z_{0\_lower} \leftarrow Z_0$
      end if
    until Error between Z_0 values in two consecutive iterations is less than Z_{0_tol}
    Calculate normalized switching frequency, f_n (see equation 4.43)
    Calculate output voltage ripple, Δv_o (see equation 4.39)
    if $\Delta v_o > \Delta v_{o\_desired}$ **then**
      $\Delta r^2_{upper} \leftarrow \Delta r^2$
    else
      $\Delta r^2_{lower} \leftarrow \Delta r^2$
    end if
  until Error between Δr^2 values in two consecutive iterations is less than Δr^2_{tol}
  print Δr^2
  Calculate capacitance C and inductance L according to (3.71)
  print C and L
end procedure

Appendix B

Controller Circuit Netlists

B.1 Netlist of the Buck Converter Controller

```
"ExpressPCB Netlist"
"LTspice XVII"
1
0
0
""
""
""
"Part IDs Table"
```

```
"B1" "V= (((i(Rsense)*sqrt(L/C))/V(ref)) - (V(in)/V(ref))/(V(out
    )/(i(Rload)*sqrt(L/C))))**2/(4*pi**2) - exp((2*(pi/(V(out)/(i
    (Rload)*sqrt(L/C))))*(atan((2*pi*(((V(in)/V(ref)) - (V(out)/V
    (ref)))/((pi/(V(out)/(i(Rload)*sqrt(L/C))))*((sqrt(4*(V(out)
    /(i(Rload)*sqrt(L/C)))**2-1)))) + ((pi/(V(out)/(i(Rload)*sqrt
    (L/C))))*(((i(Rsense)*sqrt(L/C))/V(ref)) - (V(in)/V(ref))/(V(
    out)/(i(Rload)*sqrt(L/C)))))/(2*((pi/(V(out)/(i(Rload)*sqrt(L
    /C))))*((sqrt(4*(V(out)/(i(Rload)*sqrt(L/C)))**2-1))))*pi)))
    /(((i(Rsense)*sqrt(L/C))/V(ref)) - (V(in)/V(ref))/(V(out)/(i(
    Rload)*sqrt(L/C))))) + atan((2*pi*(((V(in)/V(ref)) - 1)/((pi
    /(V(out)/(i(Rload)*sqrt(L/C))))*((sqrt(4*(V(out)/(i(Rload)*
    sqrt(L/C)))**2-1)))) - ((pi/(V(out)/(i(Rload)*sqrt(L/C))))*((
    V(in)/V(ref))/(V(out)/(i(Rload)*sqrt(L/C))) - 1/(V(out)/(i(
    Rload)*sqrt(L/C)))))/(2*((pi/(V(out)/(i(Rload)*sqrt(L/C))))
    *((sqrt(4*(V(out)/(i(Rload)*sqrt(L/C)))**2-1))))*pi)))/((V(in
    )/V(ref))/(V(out)/(i(Rload)*sqrt(L/C))) - 1/(V(out)/(i(Rload)
    *sqrt(L/C))))))/((pi/(V(out)/(i(Rload)*sqrt(L/C))))*((sqrt
    (4*(V(out)/(i(Rload)*sqrt(L/C)))**2-1)))))*(((V(in)/V(ref))/(
    V(out)/(i(Rload)*sqrt(L/C))) - 1/(V(out)/(i(Rload)*sqrt(L/C))
    ))**2/(4*pi**2) +(((V(in)/V(ref)) - 1)/((pi/(V(out)/(i(Rload)
    *sqrt(L/C))))*((sqrt(4*(V(out)/(i(Rload)*sqrt(L/C)))**2-1))))
     - ((pi/(V(out)/(i(Rload)*sqrt(L/C))))*((V(in)/V(ref))/(V(out
    )/(i(Rload)*sqrt(L/C))) - 1/(V(out)/(i(Rload)*sqrt(L/C)))))
    /(2*((pi/(V(out)/(i(Rload)*sqrt(L/C))))*((sqrt(4*(V(out)/(i(
    Rload)*sqrt(L/C)))**2-1))))*pi))**2 + dr**2) + (((V(in)/V(ref
    )) - (V(out)/V(ref)))/((pi/(V(out)/(i(Rload)*sqrt(L/C))))*((
    sqrt(4*(V(out)/(i(Rload)*sqrt(L/C)))**2-1)))) + ((pi/(V(out)
    /(i(Rload)*sqrt(L/C))))*(((i(Rsense)*sqrt(L/C))/V(ref)) - (V(
    in)/V(ref))/(V(out)/(i(Rload)*sqrt(L/C)))))/(2*((pi/(V(out)/(
    i(Rload)*sqrt(L/C))))*((sqrt(4*(V(out)/(i(Rload)*sqrt(L/C)))
    **2-1))))*pi))**2" ""
```

```
"B2" "V= ((V(out)/V(ref))/((pi/(V(out)/(i(Rload)*sqrt(L/C))))*((
    sqrt(4*(V(out)/(i(Rload)*sqrt(L/C)))**2-1)))) - ((pi/(V(out)
    /(i(Rload)*sqrt(L/C))))*((i(Rsense)*sqrt(L/C))/V(ref)))/(2*((
    pi/(V(out)/(i(Rload)*sqrt(L/C))))*((sqrt(4*(V(out)/(i(Rload)*
    sqrt(L/C)))**2-1))))*pi))**2 - exp((2*(pi/(V(out)/(i(Rload)*
    sqrt(L/C))))*(atan(2*(V(out)/(i(Rload)*sqrt(L/C)))*pi*(1/((pi
    /(V(out)/(i(Rload)*sqrt(L/C))))*((sqrt(4*(V(out)/(i(Rload)*
    sqrt(L/C)))**2-1)))) - (pi/(V(out)/(i(Rload)*sqrt(L/C))))
    /(2*(V(out)/(i(Rload)*sqrt(L/C)))*((pi/(V(out)/(i(Rload)*sqrt
    (L/C))))*((sqrt(4*(V(out)/(i(Rload)*sqrt(L/C)))**2-1))))*pi))
    ) - atan((2*pi*((V(out)/V(ref))/((pi/(V(out)/(i(Rload)*sqrt(L
    /C))))*((sqrt(4*(V(out)/(i(Rload)*sqrt(L/C)))**2-1)))) - ((pi
    /(V(out)/(i(Rload)*sqrt(L/C))))*((i(Rsense)*sqrt(L/C))/V(ref)
    ))/(2*((pi/(V(out)/(i(Rload)*sqrt(L/C))))*((sqrt(4*(V(out)/(i
    (Rload)*sqrt(L/C)))**2-1))))*pi)))/((i(Rsense)*sqrt(L/C))/V(
    ref)))))/((pi/(V(out)/(i(Rload)*sqrt(L/C))))*((sqrt(4*(V(out)
    /(i(Rload)*sqrt(L/C)))**2-1)))))*((1/((pi/(V(out)/(i(Rload)*
    sqrt(L/C))))*((sqrt(4*(V(out)/(i(Rload)*sqrt(L/C)))**2-1))))
    - (pi/(V(out)/(i(Rload)*sqrt(L/C))))/(2*(V(out)/(i(Rload)*
    sqrt(L/C)))*((pi/(V(out)/(i(Rload)*sqrt(L/C))))*((sqrt(4*(V(
    out)/(i(Rload)*sqrt(L/C)))**2-1))))*pi))**2 + 1/(4*(V(out)/(i
    (Rload)*sqrt(L/C)))**2*pi**2) + dr**2) + ((i(Rsense)*sqrt(L/C
    ))/V(ref))**2/(4*pi**2)" ""
"Control_Law" "V=if(((i(Rsense)*sqrt(L/C))/V(ref))<(V(out)/V(ref
    ))/(V(out)/(i(Rload)*sqrt(L/C))),(if(V(sigma_ON)>0,1,0)),(if(
    V(sigma_OFF)>0,0,1)))*5" ""
"Rload1" "1" ""
"Rsense1" "1" ""
"B3" "I=2*I(Rload1)" ""
"Rload" "1" ""
"B4" "I=2*I(Rsense1)" ""
"Rsense" "1" ""
"S1" "SWinput" ""
"V1" "PULSE(0 1 0 1n 1n 100n 5u)" ""
"C1" "10n" ""
"R1" "1m" ""

"Net Names Table"
"sigma_ON" 1
"0" 2
```

```
"sigma_OFF" 14
"N003" 15
"Load_Curr" 17
"Ind_Curr" 18
"N001" 19
"N002" 21
"u" 23
"N004" 25
"N005" 27

"Net Connections Table"
1 1 1 0
2 1 2 3
2 2 2 4
2 3 2 5
2 4 1 6
2 5 1 7
2 6 1 8
2 7 1 9
2 8 1 10
2 9 1 11
2 10 4 12
2 11 2 13
2 12 2 0
3 2 1 0
4 3 1 16
4 13 2 0
5 4 2 0
6 5 2 0
7 6 2 20
7 7 2 0
8 8 2 22
8 9 2 0
9 10 1 24
9 12 1 0
10 10 2 26
10 13 1 0
11 10 3 28
11 11 1 0
```

B.2 Netlist of the Boost Converter Controller

```
"ExpressPCB Netlist"
"LTspice XVII"
1
0
0
""
""
""
"Part IDs Table"
"B1" "V=((i(Rsense)*sqrt(L/C))/V(ref)) - 1/((V(out)/(i(Rload)*
   sqrt(L/C)))*(V(in)/V(ref))) + (V(out)/(i(Rload)*sqrt(L/C)))*(
   V(in)/V(ref))*ln((V(out)/V(ref)))" ""
"B2" "V= (((i(Rsense)*sqrt(L/C))/V(ref)) - (V(in)/V(ref))/(V(out
   )/(i(Rload)*sqrt(L/C))))**2/(4*pi**2) - exp((2*(pi/(V(out)/(i
   (Rload)*sqrt(L/C))))*(atan((2*pi*(((V(in)/V(ref)) - (V(out)/V
   (ref)))/((pi/(V(out)/(i(Rload)*sqrt(L/C))))*((sqrt(4*(V(out)
   /(i(Rload)*sqrt(L/C)))**2-1)))) + ((pi/(V(out)/(i(Rload)*sqrt
   (L/C))))*(((i(Rsense)*sqrt(L/C))/V(ref)) - (V(in)/V(ref))/(V(
   out)/(i(Rload)*sqrt(L/C)))))/(2*((pi/(V(out)/(i(Rload)*sqrt(L
   /C))))*((sqrt(4*(V(out)/(i(Rload)*sqrt(L/C)))**2-1))))*pi)))
   /(((i(Rsense)*sqrt(L/C))/V(ref)) - (V(in)/V(ref))/(V(out)/(i(
   Rload)*sqrt(L/C))))) + atan((2*pi*(((V(in)/V(ref)) - 1)/((pi
   /(V(out)/(i(Rload)*sqrt(L/C))))*((sqrt(4*(V(out)/(i(Rload)*
   sqrt(L/C)))**2-1)))) - ((pi/(V(out)/(i(Rload)*sqrt(L/C))))*((
   V(in)/V(ref))/(V(out)/(i(Rload)*sqrt(L/C))) - 1/((V(out)/(i(
   Rload)*sqrt(L/C)))*(V(in)/V(ref)))))/(2*((pi/(V(out)/(i(Rload
   )*sqrt(L/C))))*((sqrt(4*(V(out)/(i(Rload)*sqrt(L/C)))**2-1)))
   )*pi)))/((V(in)/V(ref))/(V(out)/(i(Rload)*sqrt(L/C))) - 1/((V
   (out)/(i(Rload)*sqrt(L/C)))*(V(in)/V(ref)))))))/((pi/(V(out)
   /(i(Rload)*sqrt(L/C))))*((sqrt(4*(V(out)/(i(Rload)*sqrt(L/C))
   )**2-1)))))*((((V(in)/V(ref)) - 1)/((pi/(V(out)/(i(Rload)*
```

```
    sqrt(L/C))))*((sqrt(4*(V(out)/(i(Rload)*sqrt(L/C)))**2-1))))
    - ((pi/(V(out)/(i(Rload)*sqrt(L/C))))*((V(in)/V(ref))/(V(out)
    /(i(Rload)*sqrt(L/C))) - 1/((V(out)/(i(Rload)*sqrt(L/C)))*(V(
    in)/V(ref)))))/(2*((pi/(V(out)/(i(Rload)*sqrt(L/C))))*((sqrt
    (4*(V(out)/(i(Rload)*sqrt(L/C)))**2-1))))*pi))**2 + dr**2 +
    ((V(in)/V(ref))/(V(out)/(i(Rload)*sqrt(L/C))) - 1/((V(out)/(i
    (Rload)*sqrt(L/C)))*(V(in)/V(ref))))**2/(4*pi**2)) + (((V(in)
    /V(ref)) - (V(out)/V(ref)))/((pi/(V(out)/(i(Rload)*sqrt(L/C))
    ))*((sqrt(4*(V(out)/(i(Rload)*sqrt(L/C)))**2-1)))) + ((pi/(V(
    out)/(i(Rload)*sqrt(L/C))))*(((i(Rsense)*sqrt(L/C))/V(ref)) -
     (V(in)/V(ref))/(V(out)/(i(Rload)*sqrt(L/C)))))/(2*((pi/(V(
    out)/(i(Rload)*sqrt(L/C))))*((sqrt(4*(V(out)/(i(Rload)*sqrt(L
    /C)))**2-1))))*pi))**2" ""
"Control_Law" "V=if((V(out)/V(ref))>1,(if(V(sigma_ON)>0,1,0)),(
    if(V(sigma_OFF)>0,1,0)))*5" ""
"Rload1" "1" ""
"Rsense1" "1" ""
"B3" "I=2*I(Rload1)" ""
"Rload" "1" ""
"B4" "I=2*I(Rsense1)" ""
"Rsense" "1" ""
"S1" "SWinput" ""
"V1" "PULSE(0 1 0 1n 1n 100n 5u)" ""
"C1" "10n" ""
"R1" "1m" ""

"Net Names Table"
"sigma_ON" 1
"0" 2
"sigma_OFF" 14
"N003" 15
"Load_Curr" 17
"Ind_Curr" 18
"N001" 19
"N002" 21
"u" 23
"N004" 25
"N005" 27
```

```
"Net Connections Table"
1 1 1 0
2 1 2 3
2 2 2 4
2 3 2 5
2 4 1 6
2 5 1 7
2 6 1 8
2 7 1 9
2 8 1 10
2 9 1 11
2 10 4 12
2 11 2 13
2 12 2 0
3 2 1 0
4 3 1 16
4 13 2 0
5 4 2 0
6 5 2 0
7 6 2 20
7 7 2 0
8 8 2 22
8 9 2 0
9 10 1 24
9 12 1 0
10 10 2 26
10 13 1 0
11 10 3 28
11 11 1 0
```